ANL-6270

Argonne National Laboratory

STUDY OF THE NUCLEAR ENERGY LEVELS ASSOCIATED WITH THE DECAY OF $_{66}Dy^{166}$, $_{69}Tm^{172}$, AND $_{68}Er^{172}$

by

R. G. Helmer and S. B. Burson

DISCLAIMER

LEGAL NOTICE

This report was prepared as an account of Government sponsored work. Neither the United States, nor the Commission, nor any person acting on behalf of the Commission:

A. Makes any warranty or representation, expressed or implied, with respect to the accuracy, completeness, or usefulness of the information contained in this report, or that the use of any information, apparatus, method, or process disclosed in this report may not infringe privately owned rights; or

B. Assumes any liabilities with respect to the use of, or for damages resulting from the use of any information, apparatus, method, or process disclosed in this report.

As used in the above, "person acting on behalf of the Commission" includes any employee or contractor of the Commission, or employee of such contractor, to the extent that such employee or contractor of the Commission, or employee of such contractor prepares, disseminates, or provides access to, any information pursuant to his employment or contract with the Commission, or his employment with such contractor.

Price $2.50 . Available from the Office of Technical Services, Department of Commerce, Washington 25, D.C.

ANL-6270
Physics
(TID-4500, 16th Ed.)
AEC Research and
Development Report

ARGONNE NATIONAL LABORATORY
9700 South Cass Avenue
Argonne, Illinois

STUDY OF THE NUCLEAR ENERGY LEVELS ASSOCIATED WITH THE DECAY OF $_{66}Dy^{166}$, $_{69}Tm^{172}$, AND $_{68}Er^{172}$

by

R. G. Helmer and S. B. Burson

January 1961

Operated by The University of Chicago
under
Contract W-31-109-eng-38

Abstract

The primary purpose of the investigation was to study the energy levels of odd-odd nuclei, specifically those populated by the decay of Dy^{166} and Er^{172}. The decay of $_{69}Tm^{172}$, the daughter of Er^{172}, was also studied. These radionuclides were produced by the successive capture of two neutrons in the stable isotopes Dy^{164} and Er^{170}. As an introduction to the experimental work, a survey of the pertinent features of the theory of beta decay and gamma-ray transitions is presented. Also the single-particle model and the unified model are discussed. Measurements were made with internal-conversion-electron spectrographs, a beta-ray spectrometer, and a multichannel scintillation coincidence spectrometer. Energy levels in $_{67}Ho^{166}_{99}$ are established at 0, 54.2, 82.5, 370, and 428 kev. The first three levels have spins 0, 2, and 1 and are interpreted as members of a rotational band with K = 0. From the decay of Tm^{172} a level scheme was constructed for the even-even nucleus $_{70}Yb^{172}_{102}$. The energies and the corresponding spin and parity assignments are 0 (0^+), 0.079 (2^+), 0.260 (4^+), 1.17 (3), 1.46 (2), 1.54 (3), 1.60 (1), 1.64 (?), and 1.73 Mev (3). It is also concluded that the spin of the thulium ground state is I = K = 2 with negative parity. Interpretations in terms of the collective model are discussed. From the decay of Er^{172}, the energy levels and the corresponding spin and parity assignments in $_{69}Tm^{172}_{103}$ are 0 (2^-), 408, 450 or 160, 475 ± 15, 530 (0^+ or 1^+), and 610 kev (0^+ or 1^+).

PREFACE

This research was conducted at the Argonne National Laboratory under the Participating Institutions Program in conjunction with the University of Michigan. The studies were carried out under the supervision of Prof. M. L. Wiedenbeck of the University of Michigan and Dr. S. B. Burson of Argonne National Laboratory. This relationship is the continuation of a long standing arrangement originated by the late Prof. J. M. Cork of the University of Michigan in cooperation with Dr. S. B. Burson.

The author wishes to acknowledge his debt to Prof. J. M. Cork for the opportunities and guidance he provided before the beginning of the present research, and to Prof. M. L. Wiedenbeck for his guidance during the course of this investigation.

The author also desires to express his gratitude to several members of the staff of the Argonne National Laboratory. Dr. S. B. Burson has kindly made available all of the instruments and materials with which the experiments were performed, and has rendered valuable assistance in planning the experiments and in the interpretation of the experimental data.

The advice of Dr. J. Milsted and Dr. D. C. Stewart of the Argonne Chemistry Division concerning the chemical separation of the rare-earth elements has been greatly appreciated, as have the many courtesies extended by Dr. F. E. Throw.

Thanks are also extended to three Argonne student assistants, J. Gueths, D. Beery, and R. Dilling, who aided in the processing of some of the experimental data.

The patience and encouragement of the author's wife have been an important contribution to the completion of this research. She has also rendered valuable assistance in the preparation of the manuscript.

LIST OF TABLES

LIST OF FIGURES

CHAPTER I. Introduction

The ultimate goal of physics is to attain a quantitative explanation for all natural phenomena in terms of the smallest possible number of independent laws. The progress toward this goal in many branches of physics has been to a large extent independent of the progress in other fields of physics. A quantitative explanation of the phenomena in any one field involves the description of the basic constituents of which complex systems are built, the rules for the interactions of the constituents, and finally the manner in which the fundamental interactions combine to produce those of the complex systems. Ultimately, these descriptions and interactions must be related to the "elementary particles" of which all matter is constructed and the interactions of these elementary particles.

Although nuclear physics deals with the "elementary particles" and interactions from which all matter is constructed, ignorance of the laws of nuclear physics has not been a great impediment to advancement in other fields of science. In many cases laws governing the interactions of electron, atomic, or larger systems have been successfully postulated in spite of the lack of the corresponding laws for nuclear systems. This has been possible primarily because the energies necessary to produce nuclear excitations are usually much higher than those involved in extranuclear phenomena.

The basic goals of nuclear physics have essentially remained unchanged since the discovery of the nucleus. Physicists are still attempting to determine what elementary particles exist and the interactions between them. From the discovery of the electron in 1897 through the observation of the Ξ particle in 1959, a total of twenty five elementary particles have been observed and five more are postulated from the current "theory" which predicts the existence of anti-particle-particle pairs. These particles have been grouped into isotopic-spin multiplets such that each member of a group has a differ-

ent charge but the same spin, the same strangeness, and approximately the same mass. In this manner the twenty particles that are heavier than 200 electron-mass units can be classified as five multiplets plus the corresponding five antiparticle groups. Irrespective of the success in the classification and understanding of some of the properties of the known particles, the question of how many of these are truly elementary particles has not been answered; nor has that of how many more are to be discovered with the higher energy machines of the future.

The problem of the interactions of elementary particles, and especially those involving the nucleons, has been studied extensively by means of scattering experiments. The angular distributions and cross sections for the scattering of nucleons or very light nuclei from very light nuclei should be related directly to the nucleon-nucleon interaction. Although these measurements do indicate that the interaction has a short range and is "charge independent," no quantitative expression for the spatial dependence of the force has been deduced.

Another approach to the nucleon interactions is through the study of nuclear structure. However, in this case the problem is compounded by the inherent difficulties of a many-body system. Because of insufficient knowledge to attack the problem directly, it has been expedient to formulate phenomenological theories or "models" of the nucleus. These models attempt to "explain" the experimental data in terms of a few ad hoc rules. Eventually these rules and models must be derived from physical laws; but in the meantime the models may provide some insight into the physical laws from which they arise.

Currently nuclei are discussed in terms of two complementary models, namely, the shell model or single-particle model and the collective model. The investigations reported here are concerned with nuclei that are in the region of the periodic table in which the collective model has had a great deal of success in interpreting and

predicting nuclear properties. In this region, a vast amount of experimental data on the level structure of even-even and odd-mass nuclei has been accumulated. However, extremely little is known about the levels in odd-odd nuclei. The states of odd-odd nuclei are also of interest because they involve the interaction of a proton and neutron outside of the "core"; this is not true of the other two classes.

The purpose of this investigation is to add a small amount of knowledge in one of the many branches of nuclear physics, namely, to study the energies and characters of the levels in two odd-odd nuclei and one related even-even nucleus. It is hoped that this information will aid in the eventual solution of the basic problems of nuclear physics.

CHAPTER II. Radioactivity

A. CLASSIFICATION OF NUCLEAR STATES

In a theoretical description, the nucleus is treated in general as a quantum mechanical system. Any nuclear state is then classified by the eigenvalues of the operators that correspond to the dynamical variables which are constants of the system (i.e., by the quantum numbers). No general solution of the nuclear problem exists and the "phenomenological" treatments are only valid in certain approximations. Therefore, the set of quantum numbers used to describe a state depends on the model that is assumed to be applicable.

In spite of this dependence of the quantum numbers on the model, there are three quantum numbers that should always be applicable. Two of these correspond to the basic conservation laws of classical physics. The law of conservation of energy implies that the energy E of any level must be well defined. Also the law of conservation of angular momentum requires the existence of a total angular momentum (or spin) I. The third quantum number arises from the law of conservation of parity which has no classical analogue. This law, which holds as far as this study is concerned, implies that each level has a definite parity π. By definition, the parity of a state is positive if the wave function is unchanged under an inversion of the spatial coordinates, negative if the sign is reversed. If parity is conserved, the wave function of a state can be chosen so that it has either positive or negative parity.

In addition to these three quantum numbers, there are others which are applicable only in certain approximations.

B. ELEMENTARY PARTICLES

Although there are many elementary particles (currently about 30), all but nine have lifetimes of less than 10^{-5} sec. These short-lived particles exist only as the products of high-energy nuclear

reactions. Most of the other nine elementary particles are involved in the formation of nuclear states or in the transitions between such states. The properties of the particles of interest here are listed in Table I.

TABLE I

Properties of some elementary particles.

Particle	Symbol	Mass[a]	Charge[b]	Intrinsic spin[c]
Photon	γ	0	0	1
Neutrino	ν	0	0	$\frac{1}{2}$
Antineutrino	$\bar{\nu}$	0	0	$\frac{1}{2}$
Electron	e^- or β^-	1	-1	$\frac{1}{2}$
Positron	e^+ or β^+	1	1	$\frac{1}{2}$
Proton	p	1836	1	$\frac{1}{2}$
Neutron	n	1839	0	$\frac{1}{2}$

[a] In units of the rest mass of the electron.

[b] In units of the proton charge.

[c] In units of $\hbar$.

In terms of the present theory of elementary particles, the electron and positron are considered as a particle-antiparticle pair. The electrons, $e^{\pm}$, and the neutrinos, ν and $\bar{\nu}$, are members of a group of particles known as leptons. The proton and neutron, often called nucleons, are members of a group known as baryons.

C. BETA DECAY

Two types of nuclear instability are found in nature. The first is characterized by the spontaneous emission of one or more nucleons, namely, alpha emission or fission. The second type of instability, known as beta decay, is characterized by the emission of leptons. It is the latter form of radioactive decay that is of interest

in this investigation.

Beta decay is a generic term which applies to the following three modes of decay:

beta emission	$n \rightarrow p + e^- + \bar{\nu}$	(1a)
positron emission	$p \rightarrow n + e^+ + \nu$	(1b)
electron capture	$p + e^- \rightarrow n + \nu$	(1c)

All the nucleons and the electron on the left side of (1c) are in states of definite energy. The leptons on the right side of each reaction are in unbound states; i.e., they are emitted from the nucleus. Henceforth the discussion will be explicitly concerned only with beta emission, the only mode encountered in this study, although the theory applies equally to positron emission. (The electron capture process is basically different in that only one particle is emitted into an unbound state.)

The theory of beta decay was formulated by Fermi,[1] who treated the neutron and proton as two states of the same particle and assumed that electrons and neutrinos could be created and annihilated. This formulation is somewhat analogous to the theory of absorption and emission of light quanta. (The treatment of creation and annihilation operators necessitates the use of field theory. Also both leptons generally have energies large enough to require exact application of the theory of special relativity.)

It can be shown that the interaction energy, or Hamiltonian, is then of the form

$$H = g(\psi_n^* O_H Q \psi_p)(\psi_e^* O_L \psi_\nu) , \qquad (2)$$

where g is a constant that measures the strength of the interaction (analogous to an electric charge e); Q is an operator that transforms a neutron into a proton; O_H and O_L are operators, as yet undetermined, that act on the wave functions of the heavy and light particles, respective-

ly; and ψ_p, ψ_n, ψ_e, ψ_ν are the wave functions of the particles. These wave functions depend not only on space and time, but also on "internal" degrees of freedom resulting from the intrinsic spins of $\frac{1}{2}$. In fact, the functions have four components at each space-time point.

One assumes that H is invariant under both proper and improper Lorentz transformations (i.e., translation, space inversion, and time reversal) and that no derivatives of the wave functions occur. From these conditions it follows that the products $(\psi_n^* \psi_p)$ include 16 independent combinations. These are classified into five groups: scalar (one combination), vector (four), tensor (six), axial vector (four), and pseudoscalar (one). Since H must be a scalar, each product $(\psi_n^* \psi_p)$ must be combined with the complementary $(\psi_e^* \psi_\nu)$ product. This gives five invariants which are denoted by H_i, where i = S,V,T,A, and P. Then the total Hamiltonian is given by $H = g \sum_i C_i H_i$, where all of the C_i are constant and real. The form of each H_i is determined from theory, but the numerical values of the C_i must be found experimentally.

In 1956, Lee and Yang[2] suggested that the assumption of conservation of parity in beta decay (and weak interactions in general) might not be valid. They point out that the types of experiments that had been carried out up to that time (shapes of allowed, first-forbidden, and unique-forbidden spectra, and beta-neutrino and beta-gamma correlations) would not be affected by the nonconservation of parity. In 1957, Wu et al.[3] demonstrated experimentally that parity is not conserved in beta decay. In this case the Hamiltonian has the form

$$H = g(C_V H_V + C_V' H_V' + C_A H_A + C_A' H_A' + \cdots).$$

If one also drops the assumption of invariance under time reversal, the coupling constants, C_i and C_i', can be complex numbers, so that there are twenty arbitrary constants.

Evidence now available greatly reduces the number of

constants. A large number of experiments[4] together indicate that $C_V^2 \approx C_A^2 \gg C_S^2$ and $C_A^2 \gg C_T^2$. The relative magnitude of C_P has not been determined. Other experiments[4] can be interpreted only if $C_V = C_V'$ and $C_A = C_A'$.

In this study only spectral shapes are measured. Therefore, as noted above, the nonconservation of parity or failure of time reversal invariance would have no effect on the pertinent theoretical predictions (except for a trivial redefinition of the coupling constants).

The calculation of the distribution of the electrons emitted as a function of momentum involves an integration of the Hamiltonian. For this integration, it is useful to write the wave functions as series expansions. If Coulomb effects are neglected, the leptons can be treated as free particles. The corresponding wave functions are plane waves which can be expanded in the form

$$e^{i\vec{k}\cdot\vec{r}} = \sum_{\ell=0}^{\infty} (2\ell+1)\, i^{\ell}\, j_{\ell}(kr)\, P_{\ell}(\cos\theta) \quad ,$$

where $\vec{k}$ is the wave vector, $\vec{r}$ is the position vector, j_{ℓ} is the spherical Bessel function, and P_{ℓ} is the Legendre polynomial. Each succeeding term corresponds to a wave of higher angular momentum. For all cases of practical interest, each succeeding term is of smaller magnitude.

Although the leptons must be treated in a completely relativistic manner, the same is not true for the nucleons. Instead it is very useful to expand the operators acting on the nucleon wave functions in powers of v/c.

If only the first term of each expansion is retained, the resulting matrix elements are related to "allowed" beta decay. If, by chance, the probability for this type of decay should vanish, one considers the next term in each expansion. The successive matrix elements formed in this fashion are called "first forbidden," "second

forbidden," etc. The selection rules for the first few "degrees of forbiddenness" are listed in Table II.

TABLE II

Classification of beta-ray transitions: selection rules and range of log ft values.

Class	Spin change	Parity change	Log ft
Allowed	0 or 1	no	3 - 6
Ordinary first forbidden	0 or 1	yes	6 - 8
Unique first forbidden	2	yes	8 - 10
Second forbidden	2 or 3	no	10 - 14

For an allowed transition, the probability of emission for an electron with a momentum between p and p+ dp is

$$N(p)\,dp = \frac{g^2}{2\pi^3} F(Z,p)\, p^2 (W_0 - W)^2 [(C_S^2 + C_V^2)|M_F|^2 + (C_T^2 + C_A^2)|M_{GT}|^2](1 - \frac{b}{W})dp, \quad (3)$$

where W is the electron energy and W_0 is the energy of the transition (both in units of mc^2), and

$$b = 2\gamma \frac{C_S C_V |M_F|^2 + C_T C_A |M_{GT}|^2}{(C_S^2 + C_V^2)|M_F|^2 + (C_T^2 + C_A^2)|M_{GT}|^2} ,$$

$$F(Z,p) = 2(1+\gamma)(2pR)^{2(\gamma-1)} \exp\left[\pi y \frac{|\Gamma(\gamma + i\,y)|^2}{|\Gamma(2\gamma+1)|^2}\right] ,$$

with

$$\gamma = \sqrt{1 - (\alpha Z)^2}, \quad \alpha = \frac{e^2}{\hbar c} \approx \frac{1}{137}, \quad \text{and} \quad y = \frac{\alpha Z W}{p} .$$

The factor F(Z,p) represents the effects of the Coulomb field on the electron, and M_F and M_{GT} are integrals of the nucleon wave functions. Experimentally it is found for most spectra that b = 0 within

experimental error. Using this fact and letting $f(Z,p) = p^2 F(Z,p)$ reduces Eq. (3) to

$$\left[\frac{N}{f}\right]^{\frac{1}{2}} = C(W_0 - W) . \qquad (4)$$

Thus a plot of $(N/f)^{\frac{1}{2}}$ vs W should yield a straight line whose intercept on the abscissa is W_0. Such a plot is called a Kurie or Fermi plot.

For forbidden transitions the matrix elements M_F and M_{GT} both vanish, but new matrix elements are generated by the next terms in the series expansions. The spectral distribution of the electrons for an n-times forbidden transition is given by

$$N(p)\,dp = \frac{g^2}{2\pi^3} F(Z,p)\, p^2 (W_0 - W)^2 S_n(W)$$

The Fermi plot then has the shape

$$\left[\frac{N}{f}\right]^{\frac{1}{2}} = C (W_0 - W) \left[S_n(W) \right]^{\frac{1}{2}} . \qquad (5)$$

General expressions have been derived for the "shape factors" $S_n(W)$.[5]

The transition probability for a particular beta decay is defined as the number of transitions per second per active nucleus. This probability depends strongly on the transition energy. The comparison of different transitions is facilitated by removing this energy dependence and comparing the "reduced" probabilities. The reduced transition probability T is usually expressed in terms of the logarithm of its reciprocal, i.e., $\log(1/T) = \log ft$. In the expansions of the wave functions, each succeeding term is smaller than the preceeding one. It follows that the transition probability should decrease (log ft should increase) with increasing forbiddenness. The ranges of log ft values that have been observed are listed in Table II for the various types of transitions.

So far only the quantum numbers E, I, and π have been

considered. In the case of a specific nuclear model, there may be additional selection rules which will reduce the transition probabilities to be expected. (The ranges of log ft values quoted in Table II do not include transitions which are believed to be hindered by other selection rules.)

D. GAMMA-RAY EMISSION AND INTERNAL CONVERSION

1. Introduction

Generally a beta-ray transition leaves the daughter nucleus in an excited state. The nucleus will de-excite to its ground state by way of one or more gamma-ray transitions. Such a transition can take place either by emission of a gamma-ray (electromagnetic radiation) or by ejection of an electron from an atomic orbit. The latter process is called internal conversion.

It is convenient and useful to classify a gamma-ray transition by its multipole order L, where L is the angular momentum carried off by the quantum. For each multipole order, there are two classes of radiation which differ with respect to parity, namely,

$$\text{electric } 2^L \text{ pole (EL) with } \Delta\pi = (-1)^L, \qquad \text{and}$$

$$\text{magnetic } 2^L \text{ pole (ML) with } \Delta\pi = (-1)^{L-1},$$

where

$$\Delta\pi = \begin{cases} 1 & \text{for no change in parity} \\ -1 & \text{for a change in parity.} \end{cases}$$

The conservation of angular momentum and of parity for the system impose selection rules for the multipolarity (multiple order and class) of a gamma transition between two nuclear states with total angular momenta I_i, I_f and parities π_i, π_f, these are

$$|I_i - I_f| \leq L \leq I_i + I_f \quad \text{and}$$

$$\frac{\pi_i}{\pi_f} = \begin{cases} (-1)^L & \text{for EL} \\ (-1)^{L-1} & \text{for ML} . \end{cases} \tag{6}$$

From the fact that electromagnetic waves are transverse, it follows that no gamma rays of multipole order zero can occur.

It follows from the selection rule $|I_i - I_f| \leq L \leq I_i + I_f$ that mixtures of transitions of different multipole orders are allowed. As will be shown below, the transition probability for gamma rays decreases rapidly with increasing multipole order. Hence, one expects the lowest allowed multipole order ($L = |I_i - I_f|$) to predominate; but in some cases a mixture of the two lowest allowed multipole orders will occur.

Before outlining the theories of these two processes, it is of interest to note the difference in their dependence on nuclear properties. The transition probability for gamma-ray emission between two nuclear states will depend on the wave functions of the two states. This means that these probabilities can only be calculated explicitly for specific nuclear models. In contrast, the probability for internal conversion depends on the energy of the transition, on L, and on the electron wave functions. Thus the internal-conversion probabilities can be calculated to a high degree of accuracy independent of the nuclear structure. This relationship means that internal-conversion data can be compared with theory in order to determine the character of the transition. The character and the data on gamma-ray emission can then be used to obtain information concerning the nuclear wave functions.

2. Gamma-Ray Emission

Electromagnetic transitions are induced by an interaction between the magnetic or electric moments of the nucleus and the radiation field. In quantum mechanics, the transition probability T between the states i and f is given according to perturbation theory by the equation:

$$T_{i \to f} = \frac{2\pi}{\hbar} |\langle f | H | i \rangle|^2 (dN/dE),$$

where H is the perturbation interaction and dN/dE denotes the density of possible final states. In order to carry out complete theoretical calculations, one must make some assumption about the nuclear structure so that the initial and final wave functions can be calculated. However, the basic quantum mechanical theory of multipole radiation indicates that it is reasonable to express the transition probability in the form

$$T_{i \to f} = \frac{8\pi(L+1)}{\hbar L[(2L+1)!!]^2} \left(\frac{\omega}{c}\right)^{2L+1} B(\sigma L, I_i \to I_f) \quad , \qquad (7)$$

where σL stands for an electric or magnetic transition of order L, $\omega = (E_i - E_f)/\hbar$, c is the velocity of light, and B is the reduced transition probability. The energy dependence of the transition probability is expected to be contained in the ω^{2L+1} term, so that the $B(\sigma L, I_i \to I_f)$ is independent of the transition energy. All of the properties of nuclear structure are contained in B which is given by

$$B(\sigma L, I_i \to I_f) = \sum |\langle f | M^{\sigma}_{LM} | i \rangle|^2 \quad ,$$

where the M^{σ}_{LM} are the electric and magnetic multipole operators.

The results of some theoretical calculations for specific nuclear models will be discussed in conjunction with those models.

3. Internal Conversion

As noted previously, the internal-conversion process involves an interaction between a nucleus in an excited state and the atomic electrons. This interaction results in the ejection of an atomic electron from the i th shell or subshell. The ejected electron carries off a kinetic energy of $E-E_i$, where E is the transition energy and E_i is the electron binding energy. Calculations of the theoretical transition probabilities are carried out by means of perturbation theory. The results give values for the internal-conversion coefficients,

$$\alpha_i(\sigma L) \equiv \frac{\text{number of electrons ejected from the } i\text{th subshell}}{\text{number of photons emitted}}$$

$$= 2\pi^3 k \sum |\langle f | H | i \rangle|^2 ,$$

where k is the transition energy in units of mc^2 (and the units are such that $m = c = \hbar = 1$). The last factor is the square of the absolute value of the matrix element between the initial and final electron states for this perturbation. The summation is over all unobserved degrees of freedom, including the initial and final magnetic substates of the electron. This summation removes interference terms when the transition has mixed character (e.g., M1 + E2). Since there is no interference between different multipole orders, the conversion coefficient for a mixed transition is given by

$$\alpha = d\,\alpha(L) + (1 - d)\,\alpha(L') ,$$

where d is a constant, $0 \leq d \leq 1$, and $L' = L \pm 1$. The theoretical values of the conversion coefficients depend on:

1. the multipolarity of the competing gamma-ray transitions,
2. the Z of the emitting nucleus,
3. the subshell of the electron, and
4. the energy of the transition.

Extensive tables of theoretical internal-conversion coefficients have been tabulated by both Rose[6] and Sliv.[7] Both calculations include corrections for the effects of the finite nuclear size, although their methods for making the corrections differ. It should be noted that once the nucleus is allowed to have finite size, it is possible that the nuclear structure will have some effect on the conversion coefficients, but this effect is expected to be very small.

These theoretical calculations are of great value to the experimentalist because they often allow him to deduce the multipolarity (L and π) of a transition from its conversion coefficients. In practice,

it is often difficult to measure the absolute value of a conversion coefficient, but it may be possible to measure the relative intensities of a set of conversion lines from the same transition. Since the rate of photon emission is the same, one can compare these ratios directly with the theoretical ratios of the conversion coefficients, namely,

$$\frac{a_K}{a_L} = \frac{K}{L} = \frac{\text{number of K electrons}}{\text{number of L electrons}} .$$

These values are sometimes sufficient to determine the multipolarity.

The process of internal conversion also provides an excellent tool for measuring transition energies. Since the binding energies of atomic electrons are known accurately, the conversion-line energies together with the binding energies give an accurate value for the transition energy.

CHAPTER III. Nuclear Models

A. NUCLEAR SHELL MODEL

By 1950 a large amount of experimental data indicated the existence of a nuclear shell structure, analogous to the shell structure of atoms. These nuclear shells appeared to be filled at the neutron and proton numbers 2, 8, 20, 50, 82, and 126.[8] (These are often called "magic numbers.")

The nuclear shell model, or single-particle model,[8] successfully accounts for the magic numbers as well as some other properties of low-energy excited states.

The basic assumption of the shell model is: The interactions of any particular nucleon with all the remaining nucleons in the nucleus can, to a satisfactory approximation, be replaced by a single static potential. This potential is in some sense the average of the two-particle (and three-particle) interactions.

It is reasonable to assume that this static potential does not have a singularity at the center of mass, that it decreases rapidly at the nuclear surface, and that it is spherically symmetric. (Relaxation of the last condition is discussed in Sec. B of this chapter.) Two soluble potentials which have these properties are the isotropic harmonic oscillator and the square well with infinite walls. Both potentials have energy levels which are determined by the orbital angular momentum ℓ, and are $2(2\ell+1)$ degenerate. Although both potentials have closed shells for 2, 8, and 20 particles, neither is capable of explaining the magic numbers 50, 82, and 126.

However, it was found[9] that by adding a spin-orbit coupling term of the proper magnitude and sign to a potential intermediate between the two above, all of the magic numbers can be explained. This spin-orbit coupling term [$f(\vec{r})\,\vec{\ell}\cdot\vec{s}$, where $\vec{r}$ is the distance from the center of mass and $\vec{s}$ is the intrinsic or particle spin] splits every ℓ level into two levels with total angular momentum $j = \ell \pm \frac{1}{2}$, each with

a degeneracy of $2j+1$. The sign of the spin-orbit interaction is taken so that the $\ell + \frac{1}{2}$ level becomes the lower one. Figure 1 shows the energy-level sequence for an isotropic harmonic oscillator, for a potential intermediate between that and an infinite square well, and for the intermediate potential with spin-orbit coupling.

This model is analogous to the structure of the atom. In the atomic case, the electron shells become filled at the rare gases (2, 10, 18, 36, 54, and 86 electrons) which are to be compared with the magic number nuclei (2, 8, 20, 50, 82, and 126 protons or neutrons).

For nuclei, these levels are filled in order of increasing energy, proton levels and neutron levels being filled independently. The wave function for each nucleon is characterized by a set of individual quantum numbers, namely, n, j, ℓ, and m, where n is the total oscillator quantum number, j and ℓ are the total and orbital angular momenta, respectively, and m is the projection of j on an axis fixed in space. The properties of the entire nucleus are governed by the appropriate combinations of these wave functions for the individual particles.

Now that a potential which produces the magic numbers has been obtained, it is of interest to see if this level sequence is compatible with the total angular momenta, or spins, of nuclear ground states. In order to make this comparison, it is necessary to specify the coupling rules for obtaining the total angular momentum J of the nucleus from the angular momenta j of the particles. These rules are:

1. For any closed shell or subshell (a subshell is a j level) the particles couple so that $J = 0$.

2(a). A pair of nucleons in an unclosed subshell usually couples so that $J = 0$. Hence, for an odd-A nucleus J is equal to the j

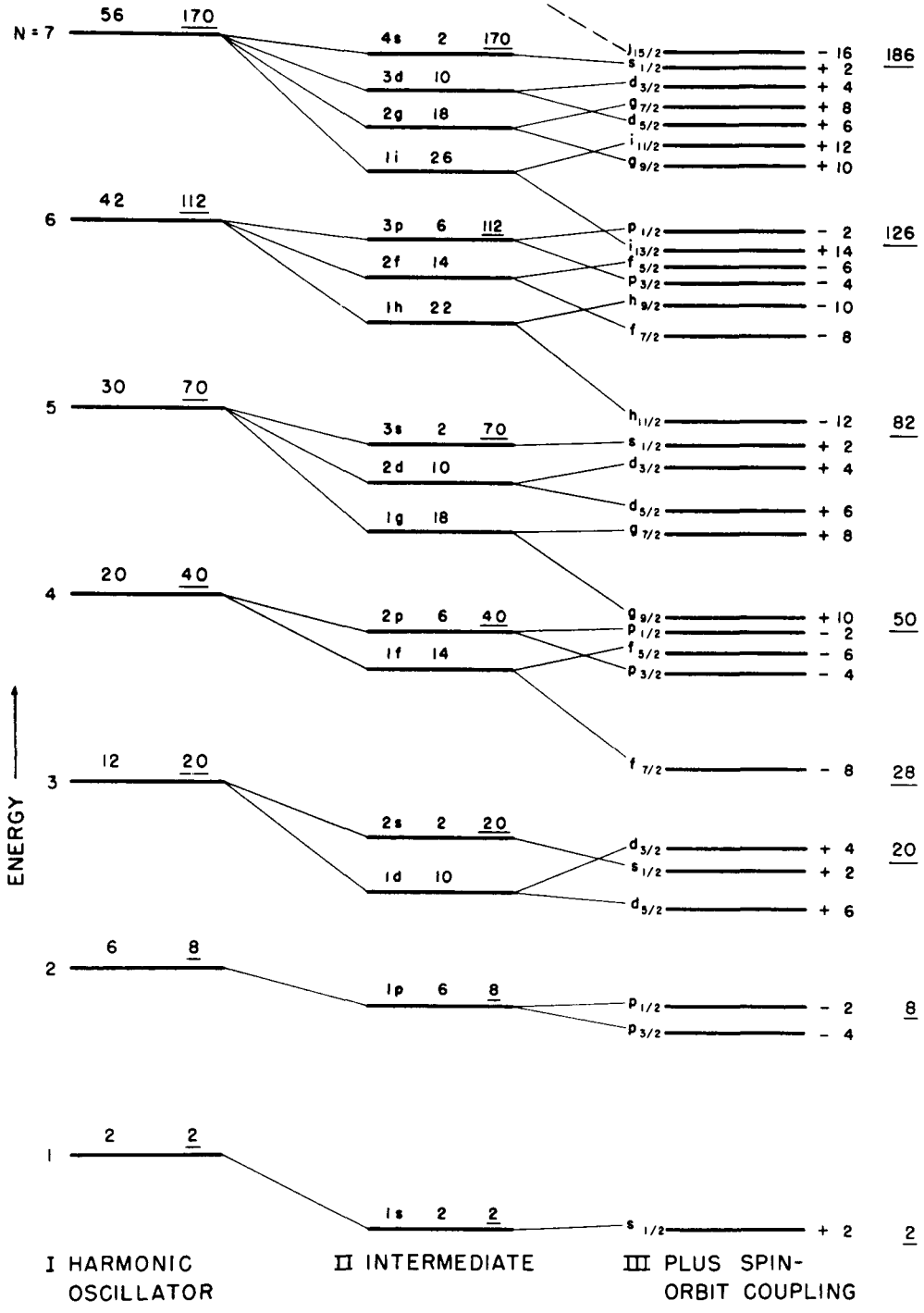

Fig. 1. Energy-level diagrams for the single-particle model.

of the unpaired particle; and for even-even nuclei $J = 0$.

2(b). If there are m particles in a subshell, and m is odd, greater than 2, and less than $2j - 1$, it is possible for the m particles to couple so that $J = j - 1$. (This "anomalous coupling" rule has been discussed theoretically[10] and appears to be justified.)

3. For nuclei with an odd number of both neutrons and protons, the neutrons couple to the spin J_n and likewise the protons to J_p according to rule 2. These two spins then couple to give the total spin J, where $J_n + J_p \geq J \geq |J_n - J_p|$. (Nordheim[11] has proposed a more explicit set of coupling rules.

There is one other empirical phenomenon that must be included in this model before the predicted ground-state spins will agree with experiment. Consider the case of two closely spaced levels with a large difference in spin and with the state with the smaller spin lying lower (e.g., the $g_{9/2}$ and $p_{1/2}$ levels in Fig. 1). The observed ground-state spins indicate that the energy of a configuration with an odd number of nucleons in the $g_{9/2}$ level is always higher than that of the corresponding state with one of the particles in the $p_{1/2}$ level excited to the $g_{9/2}$ level. For example, the configuration $(p_{1/2})^2(g_{9/2})^3$, for which $J = 9/2$, does not occur in a ground state because the state $(p_{1/2})(g_{9/2})^4$, for which $J = 1/2$, has a lower energy. This lower energy is explained by the existence of a pairing energy (i.e., the energy released in the process of coupling two particles so that $\vec{j}_1 + \vec{j}_2 = 0$) which increases rapidly with increasing j.

With the above coupling rules for the angular momenta, the pairing-energy arguments, and the level ordering in Fig. 1, one can assign reasonable configurations that account for most of the observed ground-state spins. The only major exceptions are in the regions $155 \leq A \leq 185$ and $A \geq 225$ where it appears that this restricted shell model does not apply.

For an odd-Z nucleus it has been shown that the sign of the nuclear quadrupole moment is positive (negative) if there is an incompletely filled level that is more than (less than) half full. The shell-model configurations that give the observed ground-state spins also generally predict the measured sign for the quadrupole moment.

By use of the shell-model wave functions, estimates of the gamma-ray transition probabilities have been made for a single-proton transition. Table III gives a partial list of such estimates. Since the theoretical calculations depend critically on the wave functions of the specific nuclear states involved, these estimates cannot be expected to be accurate to better than an order of magnitude.

TABLE III

Estimates of the transition probabilities T for gamma-ray emission for a single-proton transition. E is the gamma-ray energy in Mev and A is the atomic mass. These values are taken from reference 12.

Multipolarity	T in sec^{-1}
E1	$1.5 \times 10^{14} A^{2/3} E^3$
M1	$2.8 \times 10^{13} E^3$
E2	$1.6 \times 10^{8} A^{4/3} E^5$
M2	$1.2 \times 10^{8} A^{2/3} E^5$
E3	$1.1 \times 10^{2} A^{2} E^7$
M3	$1.8 \times 10^{2} A^{4/3} E^7$

B. THE UNIFIED MODEL AND COLLECTIVE MOTIONS

1. Introduction

Although the shell model, or single-particle model,

has been very successful in explaining and predicting many properties of ground states and low-energy excited states, there are several phenomena that it does not explain satisfactorily. In the regions of the periodic table where there is a large number of both neutrons and protons outside of closed shells ($150 \leq A \leq 190$ and $A \geq 225$), properties are observed which are indicative of collective motions of the entire nucleus. More explicitly, some of these nuclei have electric quadrupole moments and electric quadrupole gamma-ray transition probabilities which exceed the shell-model predictions by more than one and two orders of magnitude, respectively.[13] Also the energy levels observed in even-even nuclei show a marked similarity in spite of the great variety of particle configurations that the shell model predicts.

The "unified model" has been developed in order to describe a system that preserves the particle structure of a shell model, but simultaneously can have vibrations and rotations of the nucleus as a whole.[14] The collective motions of the nucleus are described in terms of a hydrodynamical model. Three basic assumptions are made concerning these collective motions. The first is that in the first approximation the nuclear "fluid" is incompressible. Mathematically this means the divergence of the fluid velocity is zero ($\nabla \cdot \vec{v} = 0$) at all points in the nucleus. Second, it is assumed that the fluid motion is irrotational ($\nabla \times \vec{v} = 0$). Lastly, the equation of the nuclear surface is assumed to be

$$R = R_0 \left[1 + \sum_{\mu=-2}^{2} \alpha_\mu Y_\mu^2(\theta,\phi) \right] , \qquad (8)$$

where the α_μ are constants and the Y_μ^2 are spherical harmonics. This surface is an ellipsoid and the length of the radii along the principal axes are given by

$$R_{\lambda} = R_0 \left[1 + (5/4\pi)^{\frac{1}{2}} \beta \cos\left(\gamma - \frac{2\pi\lambda}{3}\right) \right] , \qquad (9)$$

where $\lambda = 1$, 2, and 3, $0^\circ \leq \gamma \leq 60^\circ$, and β is the deformation parameter. From this expression it follows that for $\gamma > 0^\circ$ the surface is a triaxial ellipsoid, while for $\gamma = 0^\circ$ the nucleus has an axis of rotational symmetry. For $\beta = 0$ the surface reduces to a sphere.

For nuclei with all protons and neutrons in closed shells, the equilibrium shape of the nucleus is expected to be spherical. This shape should be very stable and the nucleus should be well described by the single-particle model. Its excited states should be characterized by the excitation of a particle to a higher energy level.

As the number of either neutrons or protons gets a few units away from a magic number, the shape of the nucleus may be expected to vibrate around its spherical equilibrium shape. The nuclear system now has degrees of freedom of a vibrational nature and a set of vibrational energy levels. The interaction between the vibrational and particle excitations presents a very complicated theoretical problem for nuclei in these regions.

For nuclei with a larger number of both protons and neutrons outside of their respective closed shells, the equilibrium shape is no longer expected to be spherical,[15] that is, the equilibrium value of the parameter β is no longer zero. The system now has three distinct possible motions: pseudorotation of the nucleus, vibration of the nuclear surface about its equilibrium shape, and individual particle motions. For "large" deformations the nucleus is expected to be described by the strong-coupling scheme[14] discussed in the following sections.

The studies which are reported herein are of nuclei with proton numbers midway between the magic numbers 50 and 82 and neutron numbers midway between the magic numbers of 82 and 126.

Experimental data indicate that the nuclei of this region are characterized by "large" equilibrium deformations.

2. Total Wave Function

If the energies of the intrinsic or particle excitations are large compared to those of the collective motions, on the basis of the adiabatic approximation, the wave function of the nucleus is the product of wave functions for the separate motions. If the vibrational and rotational motions are similarly decoupled from each other, the wave function takes on the form

$$\psi = \chi \phi \mathcal{D} ,$$

where χ represents the motion of the individual particles in the deformed field, ϕ denotes the vibrations of the nucleus about its equilibrium shape, and $\mathcal{D}$ represents the rotation of the nuclear surface. It follows from Eq. (8) that the nucleus has reflection symmetry with respect to a plane through the center of mass and perpendicular to the symmetry axis. It can be shown that this reflection symmetry implies that the collective motions have even parity. Hence, the parity of the system is determined by that of the particle wave function χ. In this treatment of the collective motion, it is assumed that the equilibrium shape of the deformed nucleus has axial symmetry ($\gamma = 0$). It then follows that for a nucleus in the vibrational ground state the properly symmetrized wave function has the form

$$\psi = \text{constant} \cdot \phi \{ \chi_{\Omega} \mathcal{D}^{I}_{MK}(\theta_i) + (-1)^{I - \Sigma j_p} \chi_{-\Omega} \mathcal{D}^{I}_{M-K}(\theta_i) \} , \qquad (10)$$

where the quantum numbers Ω, I, K, and M, which are valid for the strong-coupling scheme are illustrated in Fig. 2. (The θ_i are the Euler angles.)

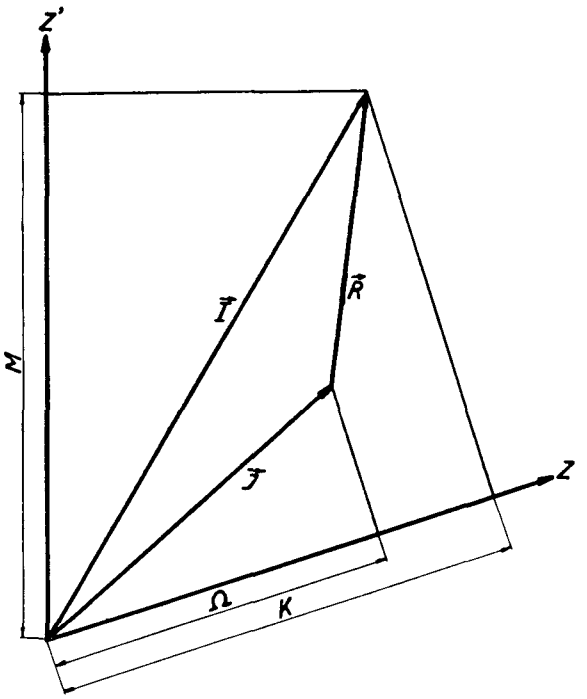

Fig. 2. Angular-momentum coupling scheme for deformed nuclei. The total angular momentum $\vec{I}$ is composed of two parts. One part $\vec{R}$ corresponds to the collective motion of the nucleus, while the other part $\vec{J}$ represents the intrinsic motion of the nucleons. The vector $\vec{J}$ precesses around the nuclear symmetry axis z with a constant projection Ω. The total angular momentum $\vec{I}$ has the component M along the z' axis which is fixed in space and the component K along the symmetry axis. In the ground state, $\vec{R}$ is perpendicular to the z axis so that $\Omega = K$.

3. Intrinsic Wave Function and Energy Levels

The intrinsic wave function χ can be calculated by use of a static potential as in the shell model. Nilsson[16] has carried out the calculations of the energy levels of individual nucleons in deformed nuclei as a function of the deformation. These calculations were carried out by use of the Hamiltonian

$$H = -\frac{\hbar^2}{2M}\Delta + \frac{M}{2}[\omega^2(1+\frac{2}{3}\delta)(x^2+y^2) + \omega^2(1-\frac{4}{3}\delta)z^2] + C\vec{\ell}\cdot\vec{s} + D\vec{\ell}^2, \quad (11)$$

where x, y, and z are the coordinates of a particle in the system fixed in the body and δ is the deformation parameter ($\delta \approx 0.95\beta$). The $\vec{\ell}\cdot\vec{s}$ term is the spin-orbit coupling and the $\vec{\ell}^2$ term has somewhat the same effect as using a potential intermediate between the harmonic oscillator and a square well. The coefficients C and D must be adjusted so that the level structure reduces to that of the shell model as the deformation goes to zero ($\delta \to 0$).

In these calculations the energies of the intrinsic states are calculated by use of a representation in which the states are labeled by the quantum numbers N, ℓ, Λ, and Σ. Here N is the total oscillator quantum number and the operators corresponding to the other three quantum numbers are $\vec{\ell}^2$, ℓ_z, and s_z, respectively, where $\vec{\ell}$ and $\vec{s}$ are the orbital and intrinsic angular momenta of the particle. (The subscript z indicates the projection on the nuclear symmetry axis.) In general, these three operators do not commute with the total Hamiltonian and, therefore, these are not good quantum numbers (i.e., ℓ, Λ, and Σ are not constants for a particular state). However, the operator $j_z = \ell_z + s_z$ does commute with H and the corresponding quantum number $\Omega = \Lambda + \Sigma$ is always a constant of the motion. (Ω is the projection on the symmetry axis of the total angular momentum of the particle.)

In the limit of small deformations ($\delta = 0$), this model

reduces to the shell model description.

In the limit of large deformations, the $\vec{l} \cdot \vec{s}$ and $\vec{l}^2$ terms can be treated as perturbations. The states are then labeled by the "asymptotic" quantum numbers N, n_z, Λ, and Σ. N is the total number of oscillator quanta and n_z is the number of oscillator quanta along the symmetry axis (i.e., the number of nodal planes perpendicular to the symmetry axis.) Experimentally it appears that in the region of deformed nuclei with $155 \leqslant A \leqslant 185$, these asymptotic quantum numbers are applicable.

The level diagrams calculated by Nilsson[17] for $50 \leqslant Z \leqslant 82$ and $82 \leqslant N \leqslant 126$ are shown in Fig. 3. As noted above, the levels are characterized by the component along the symmetry axis of the angular momentum Ω_i of the individual particles. Each level is two-fold degenerate corresponding to the states $\pm\Omega_i$. In the regions of large deformation, the z component of the total nuclear angular momentum is given by $\Omega = \sum\Omega_i$, where z denotes the direction of the symmetry axis. The protons and neutrons fill these levels independently and in the order of increasing energy. Thus for an even number of neutrons one has $\Omega_n = 0$, and for an odd number Ω_n is equal to the Ω_i of the last neutron; similarly for protons. Thus for an even-even nucleus $\Omega = 0$, and for an odd-A nucleus $\Omega = \Omega_n$ (for N odd) or $\Omega = \Omega_p$ (if Z is odd). Thus with the Nilsson diagrams one may predict the spin of the ground state, $I = \Omega$, as well as the wave function for any deformed nucleus.

One mode of nuclear excitation involves raising one of the nucleons to a new intrinsic level with a corresponding change in Ω and I.

4. Nuclear Excitations Associated with Collective Motions

The vibrational portion ϕ of the total wave function (10), gives rise to vibrational excited states. In order for this expression for the total wave function to be valid, the vibrations must be related to small distortions of the nuclear surface. For small vibrations, these

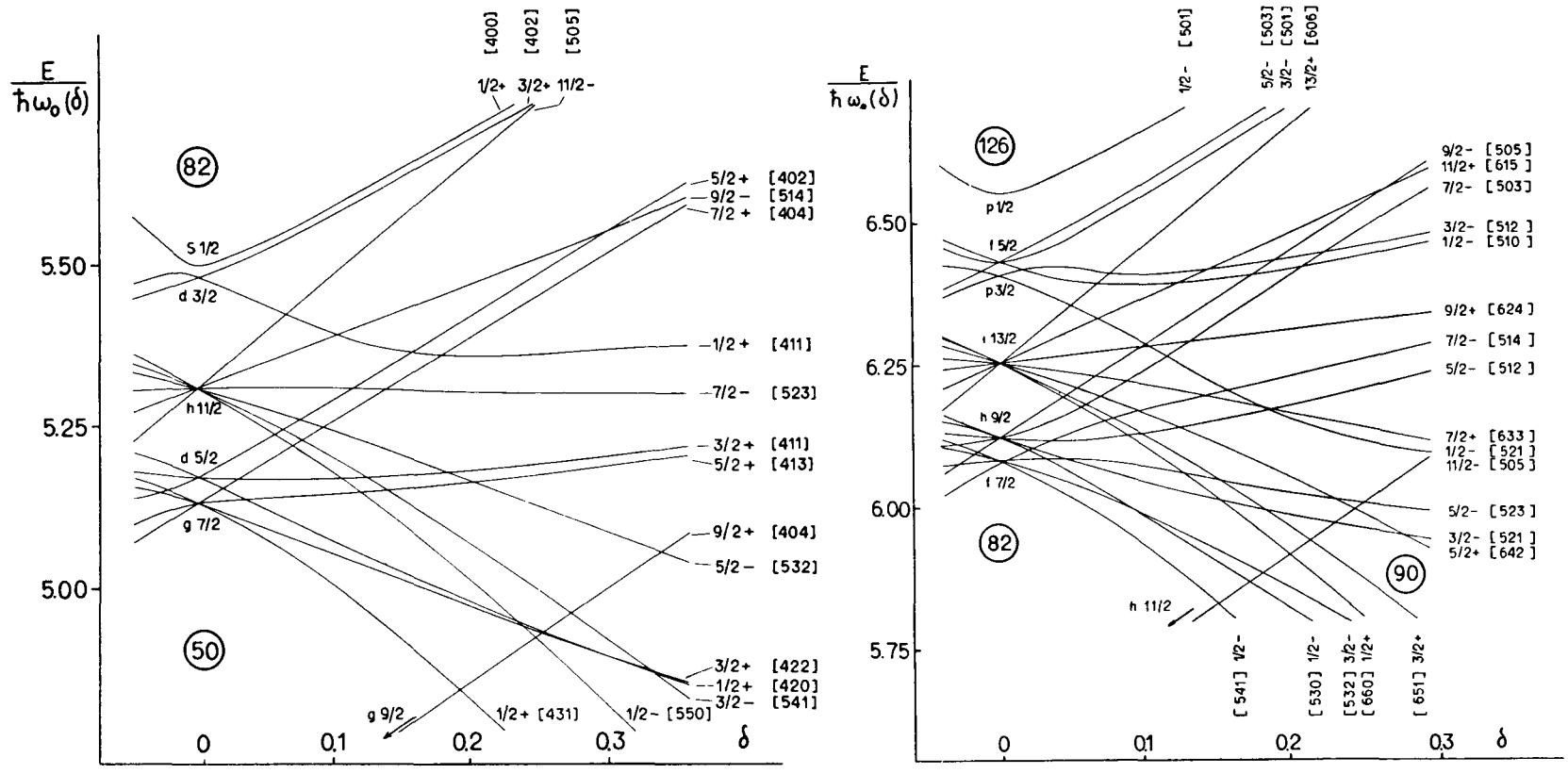

Fig. 3. Energy levels for (a) protons in the region $50 < Z < 82$ and (b) neutrons in the region $82 < N < 126$. The levels are labeled by the quantum numbers $\Omega^{\pi}[Nn_z\Lambda]$. The figures are taken from reference 17.

motions are expected to be nearly harmonic. Then the energy levels for any one type of vibrational motion will be of the form

$$E_n = n\hbar\omega \quad \text{for } n = 0, 1, 2, 3, \cdots \tag{12}$$

In the actual case in which several types of excitations exist in the same nucleus, these motions may interact, thereby altering the harmonic structure of the energy levels.

Vibrational motions are classifed by the quantum numbers ν and λ, where λ is the multipole order of the motion and is related to the change in parity of the nucleus by the expression $\Delta\pi = (-1)^{\lambda}$, and ν is equal to the change in the z component of the total angular momentum (i.e., $\Delta K = \nu$). The value $\lambda = 1$ corresponds to a translation of the whole nucleus and is of no interest. The quadrupole vibrations have $\lambda = 2$ and $\nu = 0, \pm 1, \pm 2$. The cases $\nu = \pm 1$ are related to the rotational motions which will be discussed below. The $\nu = 0$ case corresponds to an oscillation of β around the equilibrium value β_o (β-vibration), while the nuclear surface maintains its axial symmetry at all times [i.e., $\gamma = 0$ in Eq. (9)]. For $\nu = \pm 2$ the value of β is constant and γ oscillates between γ_1 and $-\gamma_1$. Although this nuclear surface is not instantaneously axially symmetric, the average value of γ is zero.

The surface motions which correspond to $\lambda > 2$ can not be expressed in the form (9). They will be discussed in Sec. 7.

Finally one may have rotational excited states based on any intrinsic or vibrational level. The nuclear surface rotates around an axis perpendicular to the symmetry axis and gives rise to a spectrum of the same type as that of a rotating rigid body. (However, the motions do not correspond to an actual rotational flow of the nuclear fluid.) If the rotational states are built on a level which has angular momentum $I_0 = K$, the energy levels are

$$E(I) = \frac{\hbar^2}{2\mathcal{J}}\left[I(I+1) + a(-1)^{I+\frac{1}{2}}(I+\tfrac{1}{2})\,\delta_{K\frac{1}{2}}\right] \quad \text{with } I = I_o,\ I_o+1,\ I_o+2,\ \cdots \tag{13}$$

For $I_o = K = \Omega = 0$ in even-even nuclei, the wave function (10) reduces to $\psi \approx \phi \mathfrak{D}^{I}_{M0}\left[\chi_0 + (-1)^{I}\chi_{-0}\right]$ which vanishes if I is odd. Thus the energy levels are given by

$$E(I) = \frac{\hbar^2}{2\mathcal{J}}\left[I(I+1)\right] \qquad \text{with } I = 0,\ 2,\ 4,\ 6,\ \cdots \tag{14}$$

In summary, the three types of excited states are characterized by changes in different quantum numbers. A particle excitation generally involves a change in Ω and π with the corresponding changes in K and I. A quadrupole vibrational excitation is characterized by a change in the value of K (by zero or two units) with no change in Ω or π. Lastly a rotational excitation is related to a change of I (by one or two units) with no change in K, Ω, or π.

5. Transition Probabilities

For the unified model, Nilsson[16] has derived expressions for the gamma-ray and beta-ray transition probabilities. Of particular interest is the special case of transitions of multipole order L from a given initial state to two members of a single rotational band. If one takes the ratio of the reduced transition probabilities, the integrals of the nuclear wave functions cancel and one obtains the simple formula

$$\frac{B(L,\ I_i \rightarrow I_f)}{B(L,\ I_i \rightarrow I_{f'})} = \left|\frac{\langle I_i\ L\ K_i\ K_f - K_i \mid I_i\ L\ I_f\ K_f\rangle}{\langle I_i\ L\ K_i\ K_f - K_i \mid I_i\ L\ I_{f'}\ K_f\rangle}\right|^2, \tag{15}$$

where $\langle I_i\ L\ K_i\ K_f - K_i \mid I_i\ L\ I_f\ K_f \rangle$ are Clebsch-Gordan coefficients.[18] (In the unusual case, in which $L \geq K_i + K_f$ with $K_f > 0$, this expression is not valid.) This rule holds both for gamma-ray transitions and for pure Gamow-Teller beta-ray transitions.

The existence of the angular momentum quantum number K implies the selection rule $L \geq \Delta K$.[19] Experimentally observed transitions which violate this rule are generally slower than the single-particle model transition rates by a factor of the order of 100 for each degree of forbiddenness. The degree of forbiddenness is equal to $\Delta K - L$. The finite probabilities of these forbidden transitions imply that one of the states involved does not have a pure K value.

Alaga[20] has pointed out that in the limit of large deformations, there are additional selection rules for both gamma-ray and beta-ray emission in odd-A nuclei. These rules, which are related to the asymptotic quantum numbers N, n_z, and Λ, are given in references 17 and 20. Transitions which violate these selection rules are called "hindered" and are expected to be slower than the corresponding "unhindered" transitions.

6. Interactions of Rotational, Vibrational, and Particle Motions

So far in this discussion it has been assumed that the rotational, vibrational, and particle motions are completely independent. In general there will be some interaction. In even-even nuclei, any particle excitation involves the splitting of a pair of nucleons. Since this

process itself necessitates an energy of about 1 Mev, the lowest excited intrinsic states are expected to lie somewhat above 1 Mev. This means that they should have very little effect on the low-lying rotational states. However, the vibrational motions are expected to have some effect on the rotational energies. The first term in such an interaction will be negative and proportional to the square of the rotational energy. Thus the energy levels of the ground-state band are expected to be given more nearly by

$$E(I) = \frac{\hbar^2}{2\mathcal{J}} \{ [I(I+1)] - b [I(I+1)]^2 \} \quad \text{for } K \neq \tfrac{1}{2} . \qquad (16)$$

In most ground-state rotational bands of even-even nuclei, this type of deviation from the $I(I+1)$ interval rule is observed.

In odd-A nuclei the situation is quite different. The odd nucleon can now be excited to new intrinsic states without breaking a pair of particles. Thus one has low-lying intrinsic levels which can interact with the rotational motions. The problem of this interaction has been discussed in detail.[21]

7. Octupole Vibrations in Even-Even Nuclei

All the states arising from rotations and quadrupole vibrations in even-even nuclei have positive parity. Several cases of odd-parity levels have been observed experimentally. The properties of these states indicate that they may be associated with octupole vibrations ($\lambda = 3$, $\Delta\pi = -1$) of the nuclear surface.[22] The only case of

this type of motion which is of interest in this study is for $\nu = 0$. Thus the vibrational level has K = 0 and negative parity. It has been pointed out[22] that the wave function vanishes for even values of I. Therefore, the rotational band based on this state has the spin sequence 1, 3, 5, etc. For an octupole vibration the shape of the nuclear surface can no longer be given by Eq. (8); terms of the form Y_μ^3 must be added.

8. Odd-Odd Nuclei

Until very recently, the only theoretical predictions explicitly dealing with odd-odd nuclei, were those concerning the ground-state spins.[23] Gallagher[24] has now discussed the beta-ray and gamma-ray transition probabilities for these nuclei.

The spin of the ground state is expected to result from the coupling of the odd neutron and odd proton. In the strong-coupling limit, which we have been considering, one expects the two particles to be coupled to the symmetry axis. This means that $\Omega = |\Omega_n \pm \Omega_p|$. Gallagher and Moskowski[23] have derived coupling rules (similar to the Nordheim rules[11] for spherical odd-odd nuclei) which imply that the z components of the intrinsic spins, Σ_n and Σ_p, tend to line up in the same direction. Thus, the ground state should have

$$\Omega = \Omega_n + \Omega_p \qquad \text{if } \Omega_n = \Lambda_n \pm \Sigma_n \quad \text{and } \Omega_p = \Lambda_p \pm \Sigma_p , \tag{17a}$$

and

$$\Omega = |\Omega_n - \Omega_p| \quad \text{if } \Omega_n = \Lambda_n \pm \Sigma_n \quad \text{and } \Omega_p = \Lambda_p \mp \Sigma_p . \tag{17b}$$

While this prediction is correct in most cases, there are also many exceptions.

In the ground state of the odd-odd nucleus it is not possible to determine directly what intrinsic states are occupied by particles. However, it is reasonable to assume that the odd proton is in the same state as the unpaired proton in a neighboring odd-A

nucleus with the same number of protons. The same assumption is made for the odd neutron. In this way it is possible to obtain the asymptotic quantum numbers and corresponding Nilsson levels of the unpaired nucleons.

Let these states be denoted by S_n and S_p.

Now consider the particles in an even-even nucleus which decays by beta emission to this odd-odd nucleus. Before a beta transition takes place, the even-even nucleus has its last pair of neutrons in the Nilsson level denoted by S_n and no protons in the level S_p. Since the beta-decay process involves only one nucleon, one of the neutrons can be assumed to be unaltered by the beta-decay process. The other neutron is then transferred from the state S_n to the state S_p with the corresponding change in quantum numbers. This transition is then identical to the corresponding transition in an odd-A nucleus and, therefore, the asymptotic selection rules given by Alaga[20] should be valid. The results of Gallagher's[24] detailed treatment of this problem agree with this conclusion for almost all cases.

In the simplest picture of odd-odd nuclei, one would expect rotational bands of the same structure as discussed previously. That is, for $K > 0$

$$E = \frac{\hbar^2}{2\mathcal{J}}[\, I(I+1) - I_0(I_0+1)\,] \qquad \text{with } I = I_0,\ I_0+1,\ I_0+2,\ \cdots,$$

and for $K = 0$

$$E = \frac{\hbar^2}{2\mathcal{J}}[\, I(I+1)\,] \qquad \text{with } I = 0,\ 2,\ 4,\ 6,\ \cdots \quad (18)$$

However, the two observed cases of $K = 0$ rotational bands with negative parity suggest that Eq. (18) is not valid. These are the decays of Dy^{166} reported here and of Am^{242} reported by Asaro et al.[25] It appears that the odd-spin states do occur for $K = 0$ bands with negative parity in odd-odd nuclei (i.e., the corres-

ponding wave function does not vanish as in even-even nuclei). Also the levels do not follow the $I(I+1)$ interval rule. A theoretical interpretation of this fact has been proposed by Gallagher[24] and by Kurath.[26] This problem will be discussed in conjunction with the decay scheme of Dy^{166}.

9. Rotational States of Even-Even Nuclei Not Possessing Axial Symmetry

In the Bohr-Mottelson model of the nucleus, discussed above, it is assumed that the nucleus has axial symmetry. As noted previously, the lengths of principal axes of the nucleus can be written in the form

$$R_\lambda = R_0 \left[1 + \sqrt{\frac{5}{4\pi}}\,\beta \cos\left(\gamma - \frac{2\pi\lambda}{3}\right)\right] \quad \text{with } \lambda = 1,\ 2,\ \text{and } 3. \quad (9)$$

Although the nucleus may instantaneously have finite values of γ (γ vibrations), the average value of γ is assumed to be zero.

Within the last two years, calculations of rotational states in even-even nuclei have been made in which this assumption has been dropped. Davydov and Fillipov[27] and DeMille et al.[28] have calculated the energies of these states on the assumption of no rotational-particle or rotational-vibrational interactions. Davydov and co-workers have also considered the electromagnetic transition probabilities between the predicted rotational states[29] as well as the equilibrium nuclear shapes to be expected.[30] A detailed comparison of the theoretical transition probabilities with the available experimental data has been made by Van Patter.[31] Mallman and Kerman[32] have extended the model to include perturbation of the rotational spectrum by β-vibrational motions.

For values of γ less than about 15°, the predictions of the Davydov model are very similar to those for axially symmetric nuclei. For even-even nuclei in the strongly deformed region, the

experimental data as interpreted by the nonaxial model indicate $\gamma \approx 12^{o}$. Hence, for the experimental studies reported here, there is no essential difference between these models.

CHAPTER IV. Experimental Methods and Source Preparation

A. INSTRUMENTATION AND ANALYSIS OF DATA

1. Introduction

The instruments employed in this investigation are all of conventional design and have been described in various publications. However, a brief description of each will be included here. The three instruments used were a set of 180° magnetic spectrographs for internal-conversion-electron studies, a 180° magnetic spectrometer with a variable field for measurements of continuous beta-ray spectra, and a 256-channel coincidence scintillation spectrometer.

2. Internal-Conversion-Electron Spectrographs

Internal-conversion electrons are measured in 180° magnetic spectrographs with fixed, uniform fields. In a uniform magnetic field, charged particles describe helical trajectories about the field lines. It has been shown[33] that a diverging pencil of monoenergetic electrons is radially focused after traversing an angle of 180°. Since the paths are helical, there is no focusing in the direction of the field.

The particular instruments used have been described previously.[34] Figure 4 shows a cross section, perpendicular to the magnetic field lines, of the vacuum chamber which is used in these spectrographs. The electrons are detected by a photographic emulsion (Kodak no-screen plates). A line source, parallel to the field, is used (nominal dimensions 0.05 cm × 1.5 cm). The image is then a line with a fairly sharp high-energy edge. The energy of the electrons can be calculated from the position of the line on the plate together with the dimensions of the box and the magnetic field strength. The strengths of the magnetic fields of the three spectrographs used in this investigation are 121, 345, and 850 gauss. The corresponding observable energy ranges are 9-160 kev, 70-830 kev, and 350-2600 kev.

This type of detection has the advantage that a wide

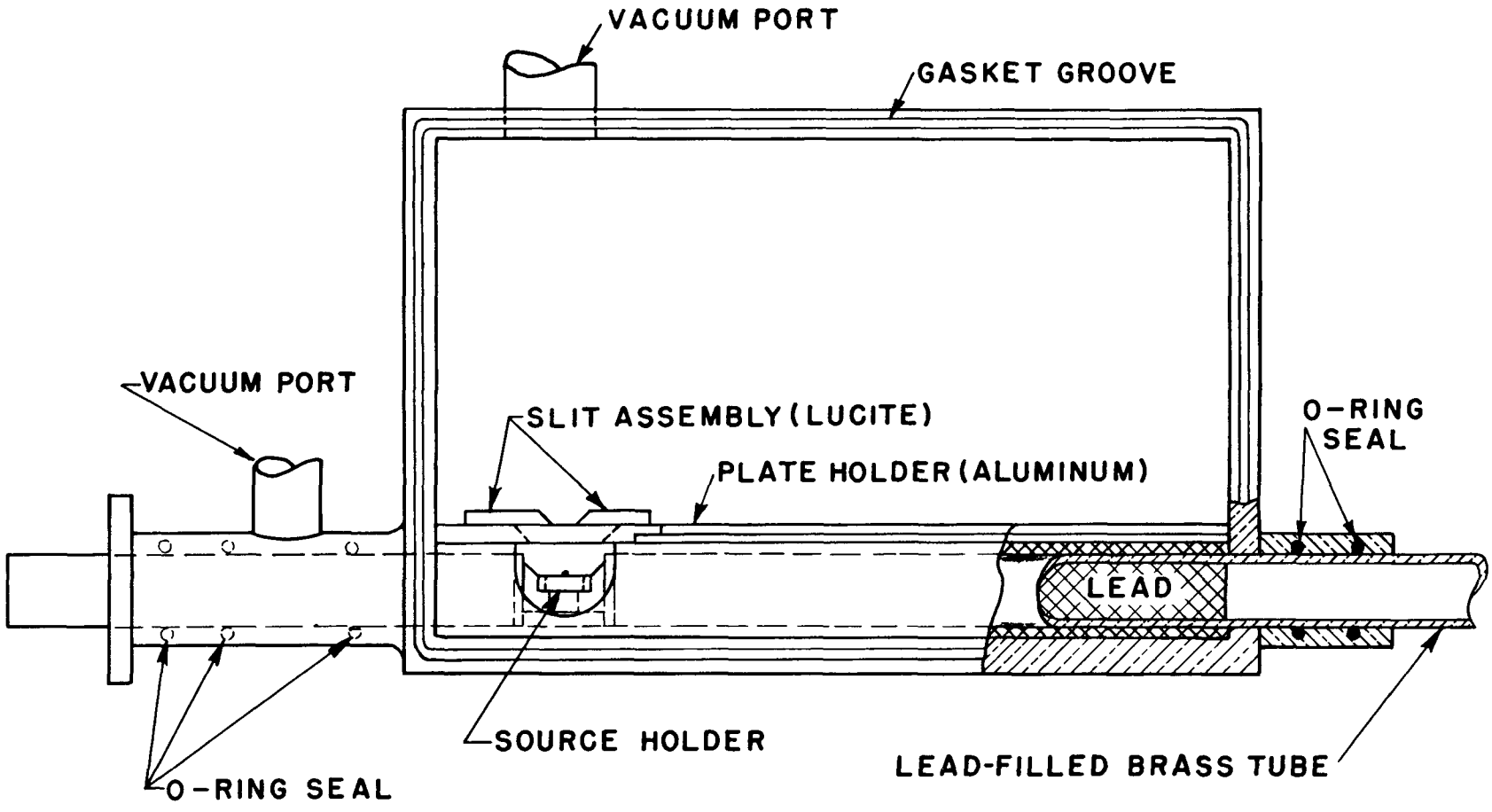

Fig. 4. Vacuum chamber for magnetic internal-conversion-electron spectrographs.

range of energies can be observed simultaneously. This means that all the data on a given plate can be compared without correction for decay of the source. Also, the exposures can be made for a duration of several half-lives over the entire energy range.

The relative intensities of the conversion-electron lines are obtained from measurements of the optical density as a function of the position on the photographic plate. To obtain the intensity the area of the peak, corresponding to a particular line, must be corrected for the sensitivity of the emulsion and the variation of the solid angle with the position. These corrections have been determined empirically and above 40 kev they are expected to be accurate to within about 10%. Below 40 kev the uncertainties become larger. Several errors also arise in the measurements of the areas of the lines. For samples with continuous beta-ray spectra, such as those in this study, there is often an uncertainty in the estimated spectral background under the line. For lines which are closely spaced on a plate, the line profiles may overlap. The decomposition of these lines can involve considerable uncertainty. Another problem is that at low energies the lines are widened noticeably by scattering in the source. This scattering may also introduce an error in the intensity measurements.

As a result of the combination of these errors, it is estimated that the intensity measurements are generally accurate to 20 - 50%.

3. Beta-Ray Spectrometer

Continuous beta-ray spectra associated with the process of beta decay are measured with a 180° magnetic spectrometer with a variable, uniform field. The principle of the focusing of the electrons is the same as in the spectrographs. In contrast to the spectrographs, the spectrometer has the detector at a fixed radius so that a baffle system is used to define the electron trajectories which are accepted.

An anthracene crystal (15 mm X 5 mm X 1.5 mm thick) is used as the electron detector. In order to prevent sublimation of the anthracene into the vacuum chamber, the crystal is covered with a thin aluminum foil (about 200 $\mu g/cm^2$). The light pulses from the detector are transmitted to an RCA-5819 photomultiplier by means of a lucite lightpipe 2 ft long. This is done so that the photomultiplier is well outside the magnetic field. After amplification, all pulses below a certain threshold voltage are eliminated by a discriminator; this removes the noise signals. All pulses above the threshold are counted. Because of the photomultiplier noise, it is not practical to operate this spectrometer below about 100 kev.

The performance of a beta-ray spectrometer is evaluated in terms of the transmission and resolution. For a group of monoenergetic electrons, the transmission is the maximum fraction that can traverse the baffle system and arrive at the detector. The resolution width is defined as the width (in momentum units) of a monoenergetic line at half the peak height divided by the momentum of the line. For a Cs^{137} source of typical size (0.4 cm X 1.5 cm), the measured resolution width of the 624-kev K-conversion line is 1.8%. The theoretical transmission for the baffle system used is about 0.03%. This extremely low transmission is the principal disadvantage of this type of spectrometer.

In any variable-field spectrometer, the accuracy of the measurements depends on the control of the magnetic field as well as the measurement of the field. This particular instrument has an automatic field-control system designed by S. B. Burson et al.[35] In brief, the system works as follows. A rotating coil in the magnetic field produces a sinusoidal voltage signal whose amplitude is proportional to the field strength. Mounted on the same shaft as the coil but outside of the field, is a condenser with a rotor section and two stator sections. Each rotor plate interleaves the stator sections alternately.

The rotor plates are shaped so that when a constant dc voltage is applied across the stator sections, a sinusoidal signal proportional to the applied voltage is produced between the rotor and each stator. If one adjusts the signals from the coil and the condenser so that they are 180° out of phase, the synchronously rectified sum of the two signals can be used as a measure of the difference between the actual field and the desired field (given by the dc voltage applied to the condenser). For automatic field control, this difference signal is used to continuously adjust the current supply of the magnet, thereby maintaining the magnetic field at the desired value.

A stability test was made by checking the reproducibility of the position of the K-conversion line of the 662-kev transition from Cs^{137}. This indicated that the drift was less than one part in 2500 over a period of several days. A linearity check showed no observable deviations from linearity over a range from 0 to 300 gauss (or 0 to 1064 kev).

4. Computer Program for Analysis of Beta-Ray Spectra

A computer program for the analysis of complex beta-ray spectra was developed concurrently with the studies reported here.[36] The program was compiled for use on an IBM-704 computer by the use of Fortran. The complete program consists of four independent but compatible stages. The first three stages perform the mathematical calculations associated with a "conventional" spectral analysis. The fourth stage of the program is designed to make a least-squares fit to several components simultaneously. Usually it is not feasible to carry out such a calculation by hand. Of the three spectra studied, two were analyzed without the use of this program. However, the decomposition of the Tm^{172} spectrum made extensive use of the fourth section, and, in fact, the analysis could not have been carried out by the conventional procedure.

In stage I the experimental counting rate is calculated at each point and corrected for the background and for the decay of the source. The statistical errors are also computed. The chief limitation is that decay corrections can only be made for a single half-life.

In stage II the counting rate can be corrected for the finite resolution of the spectrometer by use of the method of Porter et al.[37] Also the values of η, ϵ, E, f, N, and $\sqrt{N/f}$ are calculated for each experimental point, where

η = electron momentum in units of mc

ϵ = electron energy in units of mc^2

E = electron energy in kev = $510.984(\epsilon - 1)$

f = Fermi function

N = counts per unit time per unit momentum

σ = standard deviation for N

$\sqrt{N/f}$ = ordinate of a Fermi plot

L_0, L_1 = correction parameters for spectral shape for unique first-forbidden spectra

m = slope of linearized Fermi plot

a = fraction of a component which is unique first forbidden (see discussion of stage IV)

r = number of experimental points.

The Fermi functions f are not interpolated from tables, but are calculated by the machine.

Stage III is for use in decomposing the total Fermi plot. One chooses the points which appear to be on the highest energy component, but above the end point of the second component. A weighted or unweighted least-squares fit can then be made to either, or both, of the functions

$$N^1 = m^2 f(\epsilon_0 - \epsilon)^2 \quad , \tag{19a}$$

$$N^2 = m^2 f(\epsilon_0 - \epsilon)^2 [(\epsilon_0 - \epsilon)^2 L_0 + 9L_1] \quad , \tag{19b}$$

where N^1 represents an allowed shape (linear Fermi plot) and N^2 represents an unique first-forbidden shape. After making the least-squares fit to obtain the best values of m and ϵ_0, this component is subtracted from the total spectrum. The process can then be repeated to obtain the complete analysis.

In stage IV, the complete spectrum, or any portion of it, can be fitted to J components with the function

$$\bar{N} = \sum_{j=1}^{J} m_j^2 f(\epsilon_{0j} - \epsilon)^2 \{(1 - a_j) + a_j [(\epsilon_{0j} - \epsilon)^2 L_0 + 9 L_1]\} \tag{20}$$

for all points for which $\epsilon < \epsilon_{0j}$. If $\epsilon > \epsilon_{0j}$, the contribution from the jth component is zero. The parameters are limited to the ranges $0 \leq m_j^2 \leq m_{max}^2$, $1 \leq \epsilon_{0j} \leq \epsilon_{max}$, and $0 \leq a_j \leq 1$. Also any of the parameters may be fixed, and the energy difference between any pair of end points may be fixed. The variable parameters are then varied to obtain the minimum value of the function $\chi^2 = \sum_{i=1}^{r} [(N_i - \bar{N}_i)/\sigma_i]^2$. When the parameters cease to vary, within an arbitrary limit, the program is said to have converged. In principle, all 3J parameters can be varied simultaneously in the least-squares fit. However, in practice if J is "large" such a fit may not converge.

This method has several advantages over stage III. First, a fit can be made to a component whose spectrum is a linear combination of the allowed and unique first-forbidden shapes. The next advantage is that the energy difference between any two or more end points can be fixed in those cases in which it is known from other data. The third advantage is illustrated by the Tm^{172} spectrum reported here. In this case, there are three closely spaced components and there are not sufficient data to make a fit to either of the first two components.

Therefore, it is impossible to subtract them. However, it is possible to make a fit to all three simultaneously.

5. Scintillation Coincidence Spectrometer

The process of beta decay often leaves the nucleus in an excited state. The subsequent de-excitation to the ground state is generally accompanied by the emission of gamma rays. In this investigation three types of measurements are made on the gamma-ray spectra. First, the "singles" spectrum (all gamma radiation emitted by the source—i.e., the spectrum observed without coincidence) is observed in order to determine the number of gamma-ray transitions which are present, together with their energies and relative intensities. Second, in order to determine the energy levels of the daughter nucleus it is necessary to know which transitions occur in succession and which are alternate modes of decay. This is accomplished by gamma-gamma coincidence studies. Lastly, the energy level scheme is verified by observing the energies of the beta-ray transitions which precede a particular gamma ray. These beta-gamma coincidence experiments also determine the total decay energy; that is, the energy difference between the ground states of the parent and daughter nuclides.

The gamma-ray spectra are measured with the scintillation spectrometer shown schematically in Fig. 5a. The photons are detected by a crystal of Tl-activated NaI. This material has the property that the energy absorbed from the photon is emitted as quanta of visible light. When this light falls on the photocathode of the photomultiplier tube, electrons are ejected. This electron pulse is amplified by the photomultiplier and by the linear amplifier. The 256-channel analyzer, whose operation has been described by Schumann and McMahon,[38] then sorts the pulses with peak heights between two voltages V_1 and V_2 into 256 equal voltage ranges or channels. To a very good approximation the voltage of a pulse out of the linear amplifier is proportional to the energy lost in the crystal by the photon. Hence the

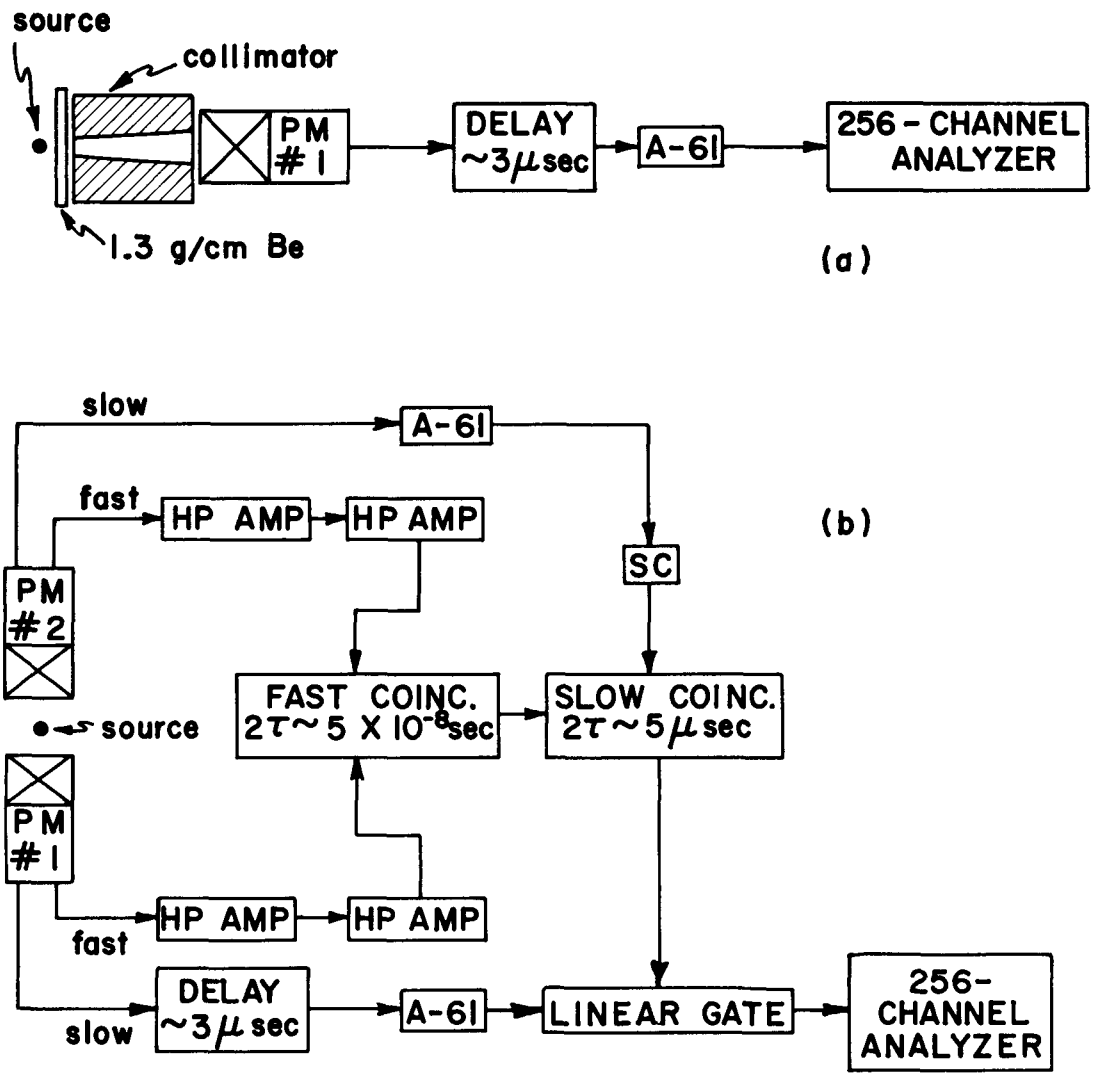

Fig. 5. Scintillation spectrometer: (a) singles system and (b) "fast-slow" coincidence system. Legend: X —$2\frac{1}{4}$ in. cubic NaI(Tl) crystals. PM — Dumont 6292 photomultiplier, HP — Hewlett-Packard 406A wide-band amplifier, A-61 — Argonne linear amplifier, and SC — Argonne D-12 single-channel analyzer.

multichannel analyzer counts the number of events in which the energy loss in the crystal is between E and $E + \Delta E$ for 256 adjacent intervals in the energy range from E_1 to $E_2 = E_1 + 256\ \Delta E$. The values of E_1 and E_2 can be varied over wide ranges of energy.

A photon loses energy in the crystal by the processes of Compton and photoelectric scattering. These processes[39] will not be discussed in detail. It is only necessary to note that either scattering process produces a secondary photon which may escape from the crystal. This means that the output pulses produced in response to a beam of monoenergetic photons will not all be of the same energy. This pulse spectrum is also modified by the statistical variations in the amplification in the photomultiplier. For a typical gamma ray in the energy range of interest, the observed spectrum consists of a photopeak, corresponding to complete absorption of the photon, and at lower energies a continuous distribution of pulses corresponding to various amounts of energy escaping from the crystal. The photopeak has essentially a Gaussian distribution. For a given geometric arrangement, the spectrum for a single gamma ray depends only on the energy of the transition.

The lead collimator which is shown in Fig. 5a is used to restrict the incident radiation to the central portion of the crystal. This reduces the loss of secondary photons resulting from the scattering processes. This simplifies the spectral shapes observed, thereby facilitating to some extent the analysis of complex spectra. The inside conical surface of the collimator is lined with layers of tantalum, tin, and steel. The tantalum layer almost completely absorbs the lead x rays that are produced by the photoelectric absorption of radiation in the lead. The tin and steel layers similarly reduce the tantalum and tin x rays, respectively. The beryllium filter is used to absorb the electrons emitted by the source. For this purpose a low-Z material is desirable, because a high-Z filter would produce a larger number of photons in the process of stopping the electrons.

As noted previously, one wishes to decompose a complex spectrum into its constituents in order to determine their energies and intensities. This analysis is facilitated by the use of spectra that exhibit only one gamma-ray transition. From a set of such spectra one can interpolate to obtain the spectral distribution for any gamma ray in the complex spectrum. An approximate interpolation can be made experimentally by electronically varying the gain of the amplifying system. In this manner the photopeak of a single gamma ray can be moved to the desired position. With the interpolated shapes, the complex spectrum can be synthesized by varying the energies and intensities of the constituents.

The energy of a transition is a linear function of the channel number corresponding to the center of the photopeak. Therefore, the energies of the constituent gamma rays are calculated from a set of photopeaks whose energies are known. The intensities of the individual components are calculated from the areas of the photopeaks. The only corrections are for the absorption in the beryllium and for the net photopeak efficiency of the crystal (i.e., the fraction of the incident radiation which appears in the photopeak). The latter is determined from a semi-empirical correction curve.[40]

Although this technique is very useful, one must always be cognizant of the fact that the poor resolution of a scintillation spectrometer makes it difficult to resolve closely spaced photopeaks. This is especially true for radiations of quite different intensity. Therefore, verifications of the results of such decompositions are always desirable.

To determine which transitions occur in succession (or cascade), the gamma-gamma coincidence circuit shown in Fig. 5b is used. In this case the 256-channel analyzer counts only those pulses which occur during a "gating" signal. This gating signal is produced by the "fast-slow" coincidence circuit together with the single-channel analyzer. As is shown, two simultaneous signals are taken from each photomultiplier. The voltage of the "slow" signal is proportional

to the energy lost in the crystal, and the voltage of the "fast" signal is approximately independent of the energy lost. The slow signal is used for energy analysis while the fast signal is used for time analysis. After amplification and shaping, the fast signals are fed into the fast coincidence circuit ($\tau \approx 2 \times 10^{-8}$ sec). An output pulse is generated whenever the input pulses arrive within the time τ. The slow signal from photomultiplier No. 2 is fed through a linear amplifier, and goes into the single-channel analyzer. The window of this instrument is adjusted to include a particular portion of the spectrum (e.g., the photopeak of a gamma ray). This analyzer produces an output pulse for every input pulse which lies in this portion of the spectrum. The pulses from the single-channel analyzer and the fast coincidence circuit are fed into a slow coincidence circuit ($2\tau \approx 9 \times 10^{-6}$ sec). The output pulses from this slow coincidence circuit gate the 256-channel analyzer. Thus the multichannel analyzer counts only those events for which the radiation followed, or preceded, a pulse accepted by the single-channel analyzer by a time less than about 2×10^{-8} seconds.

In the investigation of one decay scheme (Er^{172}), it was necessary to determine the radiations in simultaneous coincidence with two regions of the spectrum. This was accomplished by adding a third detector and modifying the coincidence circuit as shown in Fig. 6. The slow coincidence circuit generates an output pulse only if there are input pulses from both of the single-channel analyzers. This output pulse is used to gate the multichannel analyzer. This gate is itself the second coincidence circuit.

The last experiments to be discussed are the beta-gamma coincidence measurements. The beta detector is an anthracene crystal which is $\frac{3}{16}$ in. thick by $1\frac{1}{2}$ in. in diameter. The experimental arrangement is identical to that of Fig. 5b, except that the anthracene crystal replaces NaI(Tl) crystal No. 2.

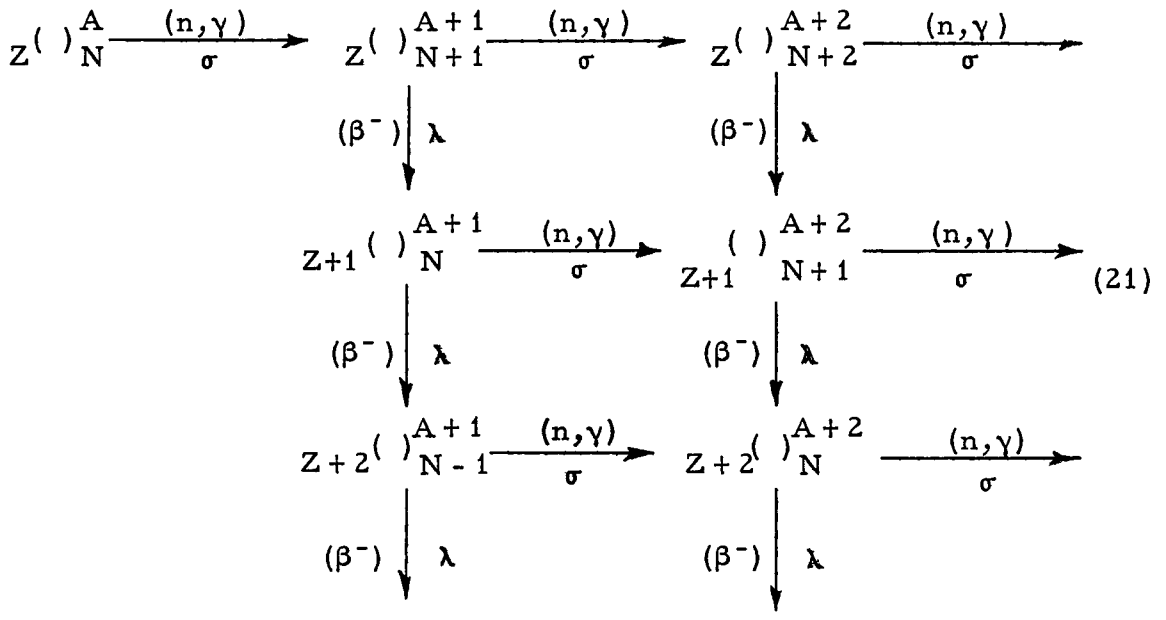

(21)

In this diagram, the σ's are thermal-neutron-capture cross sections, the λ's are decay constants, and (n,γ) and (β^-) represent the capture process and beta decay, respectively. For the purposes of this discussion, one can neglect all triple neutron captures. Also, for the cases in these studies, $_{Z+2}(\ )^{A+2}_{N}$ is stable and either $_{Z+2}(\ )^{A+1}_{N-1}$ or $_{Z+1}(\ )^{A+1}_{N}$ is stable. Hence no further beta decays in these two chains need to be considered.

If N(t) represents the number of atoms of a nuclide present at a time t after the start of the irradiation, scheme (21) can be represented by

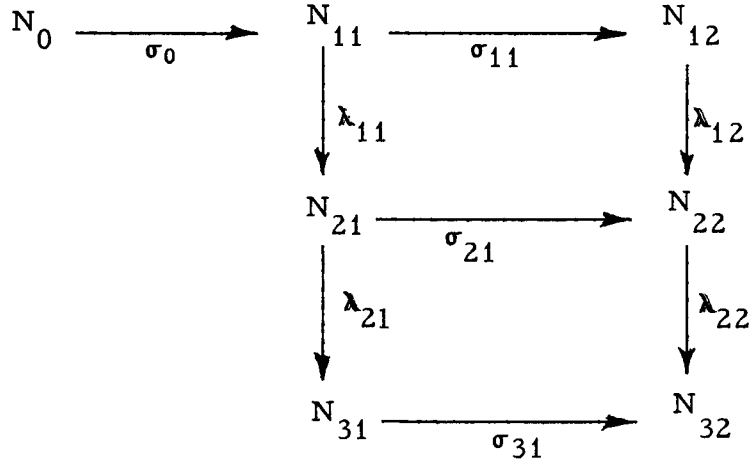

(22)

Here N_{12} and N_{22} represent the abundances of the nuclides of interest and are given by the differential equations

$$\frac{dN_{12}}{dt} = \sigma_{11}fN_{11} - \lambda_{12}N_{12} \qquad \text{with } N_{12}(t=0)=0, \text{ and} \qquad (23a)$$

$$\frac{dN_{22}}{dt} = \sigma_{21}fN_{21} + \lambda_{12}N_{12} - \lambda_{22}N_{22} \qquad \text{with } N_{22}(t=0)=0. \qquad (23b)$$

The abundances N_0, N_{11}, N_{21}, N_{31}, and N_{32} are given by other equations of the same general form. For an irradiation of duration t, the solutions for N_{12} and N_{22} are

$$N_{12}(t) = \frac{n\sigma_0 f\sigma_{11}f}{abc}\left[ae^{-\lambda_{12}t} + be^{-\sigma_0 ft} - ce^{-(\lambda_{11}+\sigma_{11}f)t}\right], \text{ and} \qquad (24a)$$

$$N_{22}(t) = n\sigma_0 f\sigma_{11}f\lambda_{12}\left\{\frac{1}{bcd}\left[e^{-\lambda_{12}t} - e^{-\lambda_{22}t}\right] + \frac{1}{acg}\left[e^{-\sigma_0 ft} - e^{-\lambda_{22}t}\right]\right.$$

$$\left. + \frac{1}{abh}\left[e^{-\lambda_{22}t} - e^{-(\lambda_{11}+\sigma_{11}f)t}\right]\right\} + n\sigma_0 f\sigma_{21}f\lambda_{11}\left\{\frac{1}{jkm}\left[e^{-\sigma_{21}ft} - e^{-\lambda_{22}t}\right]\right.$$

$$\left. + \frac{1}{akg}\left[e^{-\sigma_0 ft} - e^{-\lambda_{22}t}\right] + \frac{1}{ajh}\left[e^{-\lambda_{22}t} - e^{-(\lambda_{11}+\sigma_{11}f)t}\right]\right\}, \qquad (24b)$$

where

$$a = \lambda_{11} + \sigma_{11}f - \sigma_0 f$$
$$b = \lambda_{12} - \lambda_{11} - \sigma_{11}f$$
$$c = \lambda_{22} - \sigma_0 f$$
$$d = \lambda_{22} - \lambda_{12}$$
$$g = \lambda_{22} - \sigma_0 f$$
$$h = \lambda_{22} - \sigma_{11}f - \lambda_{11}$$
$$j = \sigma_{21}f - \sigma_{11}f - \lambda_{11}$$
$$k = \sigma_{21}f - \sigma_0 f$$

$m = \lambda_{22} - \sigma_{21} f$

n = number of nuclei of the isotope $_{Z}(\ )^{A}_{N}$ in the sample before the irradiation.

It is of interest to estimate the specific activities (i.e., N_i/n) obtainable for the nuclides to be investigated.

For the production of Dy^{166} the parameters have been measured to be

$$\sigma_0 = 3.5 \times 10^{-21}\ cm^2 \qquad \lambda_{11} = 8.30 \times 10^{-5}\ sec^{-1}$$
$$\sigma_{11} = 5 \times 10^{-21}\ cm^2 \qquad \lambda_{12} = 2.35 \times 10^{-6}\ sec^{-1}$$

If one lets $f = 2 \times 10^{14}$ neutrons $-cm^{-2}-sec^{-1}$ and t = 80 hr (the half-life of Dy^{166}), the specific activity is

$$\frac{N_{12}}{n} \approx 2 \times 10^{-3} . \tag{25}$$

This is a relatively high specific activity and indicates that it should be feasible to make the thin sources which are needed for measuring beta-ray spectra.

For the production of Er^{172} the parameters are

$$\sigma_0 = 9 \times 10^{-24}\ cm^2 \qquad \lambda_{11} = 2.47 \times 10^{-5}\ sec^{-1}$$
$$\sigma_{11} = 1 \times 10^{-23}\ cm^2 \qquad \lambda_{12} = 1.21 \times 10^{-8}\ sec^{-1}$$

(The value of σ_{11} is chosen arbitrarily since it has not been measured.) If one lets $f = 2 \times 10^{14}$ neutrons $-cm^{-2}-sec^{-1}$ and t = 50 hrs (the half-life of Er^{172}), the specific activity is

$$\frac{N_{12}}{n} \approx 3 \times 10^{-8} . \tag{26}$$

This low specific activity caused several difficulties which will be noted in the discussion of the experimental results.

2. Chemical Separations by Use of an Ion-Exchange Column.

In all of the studies reported here it was necessary to carry out chemical separations of the rare-earth elements. This was due to the presence of other activities which would severely limit the accuracy of the experimental data. Since the elements irradiated have six or seven stable isotopes, materials highly enriched in the heaviest isotope were used. However, other isotopes were still present to the extent of several percent of the total mass. In the study of Dy^{166}, the only interfering activity was that of the daughter nucleus Ho^{166}. The nuclides Er^{172} and its daughter Tm^{172} were produced from Er^{170}. The other activities present in these samples were those of Sc^{46}, Ho^{166}, Er^{169}, Er^{171}, Tm^{170}, Tm^{171}, Yb^{169}, and Yb^{175}. In this case, even after chemical separation there were three active nuclides still present in each fraction to be studied.

The chemical separations were made by means of an ion-exchange column. This method of separating the rare-earth elements is based on the existence of slight differences in their reactivities with the resin. It is observed that these reactivities decrease as the atomic number Z decreases. Therefore, the element with the higher Z is eluted from the column before that with the lower Z.

The basic techniques are similar to those discussed by Ketelle,[42] except that the eluting agent is alpha-hydroxyisobutyric acid.[43] The procedures were continually improved in order to obtain faster and more complete separations. A summary will be given of the procedure that finally evolved.

A schematic diagram of the experimental arrangement is shown in Fig. 7a. The cation-exchange resin is Berolite 220 (8% cross-linked) with a settling rate in water of ≥ 0.5 cm/min. Circulating hot water is used to maintain the temperature of the column at approximately 80°C. Elevation of the temperature reduces the time necessary to make a separation. A column of the dimensions shown

(4 mm X 7 cm) is satisfactory for separating up to about one mg of material. For larger amounts a proportionately larger column is needed unless a broadening of the activity peaks as a result of overloading can be tolerated. The glass wool is placed at the top of the column to prevent splattering of the resin when liquids are added. The flow rate of the liquid through this column is usually adjusted to about 0.1 ml/min, either by the height of the head of liquid or by using nitrogen gas pressure.

Before the separation, the resin is washed with 1 M HCl to remove complexing cations. It is then washed with H_2O, 4 m NH_4Cl, H_2O, the eluting agent to be used, and finally with H_2O. This procedure gets the resin into the "ammoniated form" needed for the separation.

The rare-earth material is irradiated in the oxide form. After the activation it is dissolved in 1 M HCl to produce the chloride. After drying to dispose of the excess HCl, the sample is picked up in a minimum amount of 0.05 M HCl and placed on the column. The glass above the resin is washed successively with 0.05 M HCl, H_2O, and a few drops of the eluting agent in order to remove any active material that is not adsorbed on the resin. The separation is started by adding alpha-hydroxyisobutyric acid.

For the separation of erbium and thulium, the alpha-hydroxyisobutyric acid solution used has approximately an 0.1 M butyrate ion concentration and an 0.2 M total acid concentration. This solution is made by mixing equal volumes of 0.2 M alpha-hydroxyisobutyric acid and 0.2 M ammonium alpha-hydroxyisobutyrate. The neutral salt solution is made by neutralizing a solution of the acid with ammonium hydroxide or ammonia gas to pH 6.4, and adjusting the final volume to give 0.2 M concentration. Since the ionization of the free acid is negligible, and that of the ammonium salt nearly complete, the "butyrate" ion concentration (which determines the elution volume for a given element) is equal to the concentration of the ammonium salt.

The acid concentration is not critical provided the final pH is less than 5. The pH of a 50-50 mixture is about 3.75. With this eluting agent the thulium and erbium nuclides are expected to be eluted from the column in about 10 and 15 free column volumes, respectively. For a similar separation of europium and samarium, for example, the butyrate ion and total butyrate acid concentrations should be about 0.2 M and 0.4 M, respectively.*

An example of a separation made with this procedure is shown in Fig. 7b. The load consisted of 2 mg of erbium. Five drops (about 0.2 ml) were collected in each test tube. The gamma-ray spectrum of each sample was measured on the multichannel analyzer. The counting rate of a selected gamma ray related to a particular radionuclide is plotted as a function of the drop number. The peaks are typically only one-third as wide as these. However, this curve is shown to demonstrate the relative positions of all the elements observed in the erbium samples.

3. Preparation of Sources

In measurements of gamma-ray spectra, the absorption of the gamma rays in the source is completely negligible. Even for beta-gamma coincidence studies, extraordinary precautions are necessary only if the energy of the beta-ray transition is less than a few hundred kev. The techniques of source preparation do become important in those experiments in which it is necessary to measure the original energy of an electron coming from the source. Therefore, only the techniques that were used to prepare sources for the conversion-electron spectrographs and the beta-ray spectrometer will be summarized.

---

* This mixing procedure was suggested by Dr. J. Milsted of the Atomic Energy Research Establishment, Harwell, England, at present with the Chemistry Division of Argonne National Laboratory.

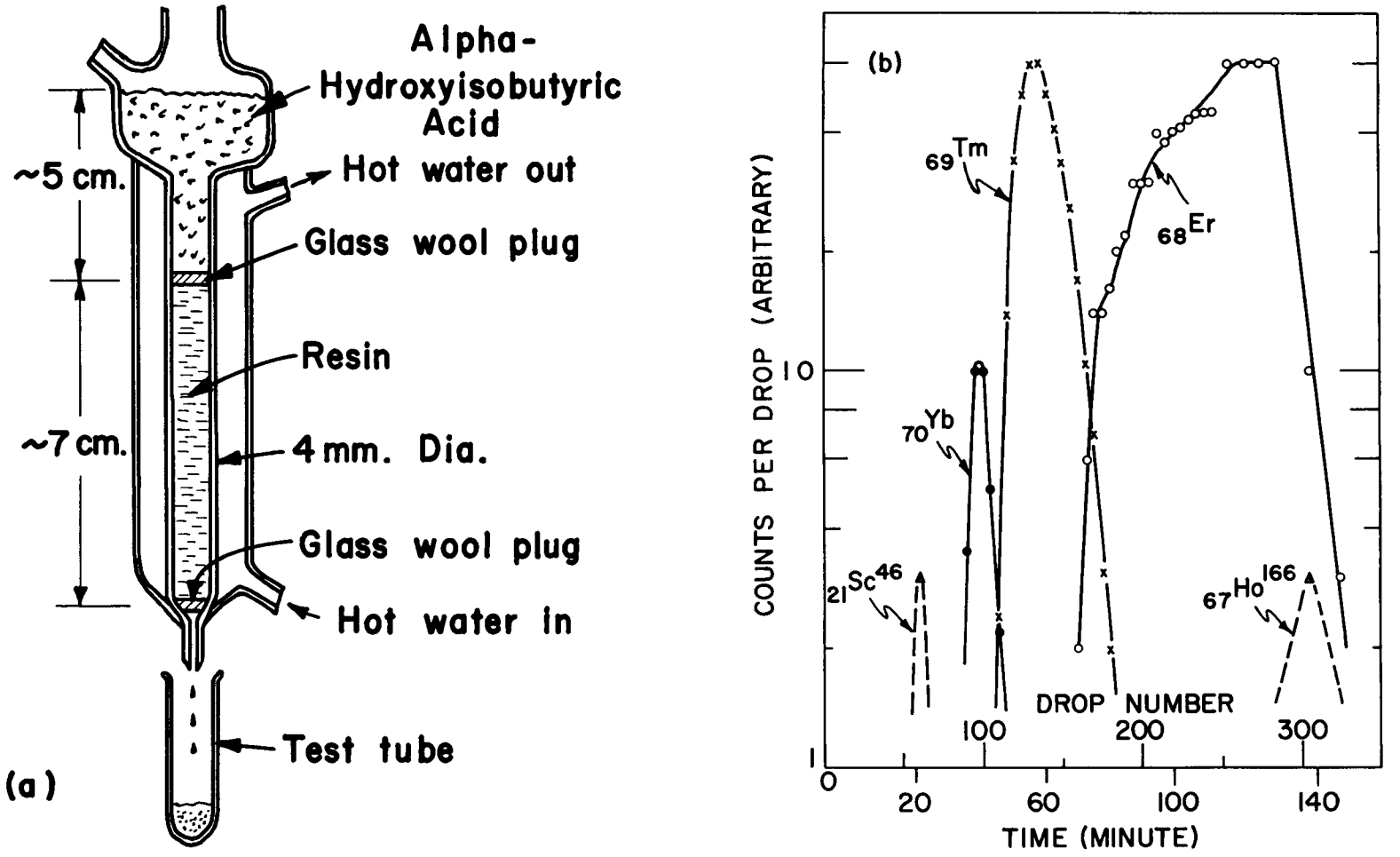

Fig. 7. Ion-exchange column: (a) schematic diagram, and (b) results of a separation.

For the internal-conversion spectrographs, the thickness of the source affects only the "tail" on the low-energy side of the line. Except at very low energies this does not interfere with energy measurements. Since the thickness of the backing is usually not critical, it was found satisfactory to use commercial aluminum foil which has an areal density of 5 mg/cm^2.

In measuring a continuous beta-ray spectrum, the finite thickness of the source and of its backing become of prime importance because of the scattering they produce. In the present study, it was found satisfactory to use backings with an areal density of approximately 1 mg/cm^2. The backing was either pure aluminum or polyester film with aluminum coated on both sides by vacuum evaporation.[44] At energies greater than 200 kev the scattering produced by such a backing seems to be negligible. The thickness of the source is usually a result of a compromise between the desire to minimize the scattering in the source and the need for a usable total counting rate.

Several of the techniques for source preparation are listed below. The first two methods were used for material that had not been chemically separated, while the other three were for chemically separated samples.

(1) The radioactive rare-earth material, in the oxide form, is placed in a few drops of alcohol. A slurry is made and a drop of the alcohol is placed on the backing. This is dried and the process is repeated until a sufficient total activity is present.

(2) The rare-earth oxide material is converted to the chloride form by dissolving it in 1 M HCl. After drying to get rid of the excess HCl, washing with H_2O, and drying again, the chloride is dissolved in alcohol and deposited as in (1).

(3) The chemically separated material comes from the ion-exchange column in the form of a complex of the rare-earth element with the alpha-hydroxyisobutyric acid. The simplest method of source making is to place this solution, a drop at a time, on a backing of aluminum

foil. The drops are dried by heating to approximately 240°C, which is sufficient to volatilize the organic material.

(4) Another method involves a solvent extraction of the active material. The pH of the active fraction of the alpha-hydroxyisobutyric acid is adjusted to about 5 by the addition of NH_4OH. A few drops of a solution of thenoyltrifluoroacetone in benzene are added and the water and benzene phases are mixed thoroughly. By this process the active material is transferred to the benzene solution. The benzene solution is then placed on the backing and dried. A temperature of about 120° C is sufficient to destroy the organic material and yet does not damage polyester film.

(5) The last method, which also serves to remove impurities from the source material, involves the use of another ion-exchange column. The active fraction is made 0.1 N with HCl. This solution is placed on a small column (about 3 cm long and 2 mm in diameter) which is loaded with Dowex-50 resin. As the liquid passes through the column, the active material is adsorbed at the top of the column. After passing 0.1 N, 1 N, and 2 N HCl through the column to remove impurities, the activity is eluted with 6 N HCl. After drying the resulting solution, the rare-earth chloride is picked up in alcohol and placed on the backing.

CHAPTER V. Experimental Results

A. INTRODUCTION

The primary purpose of this investigation was to study the excited states of odd-odd deformed nuclei. As discussed in the previous chapter, these levels are populated by the decay of even-even nuclei. Studies of the radioactive nuclides $_{66}Dy^{166}$ and $_{68}Er^{172}$ are reported as well as the nuclide $_{69}Tm^{172}$ which is associated with Er^{172}. These nuclides are all at approximately the center of the region between the neutron closed shells of 82 and 126, as well as the center of the region between the proton closed shells of 50 and 82. Therefore, the strong-coupling limit of the unified model and the asymptotic quantum numbers are expected to be applicable.

B. LEVELS IN $_{67}Ho^{166}$ FROM THE DECAY OF Dy^{166}

1. Introduction

An 81-hr β^- activity was reported in samples of dysprosium that had been irradiated with neutrons.[45,46] Ketelle, using sources separated in an ion-exchange column, found that this activity was associated with the precursor of a daughter exhibiting a period of 27 hr. For the latter activity, both the half-life and the end-point energy of the beta spectrum (measured by aluminum absorption methods) agreed with those reported for the 27-hr activity of Ho^{166}. The 81-hr activity was therefore assigned to Dy^{166}, which would be produced by double neutron capture. Using a chemically separated sample of Dy^{166}, Ketelle found the end-point of the beta spectrum to be 0.4 Mev. The neutron-capture cross section in Dy^{165} was estimated to be 5000 barns.

Independently, Butement investigated this activity and arrived at the same assignment. Butement also found that the yield of the 81-hr activity was approximately proportional to the square of the neutron flux. In addition, he found that the neutron capture in Dy^{165}

takes place mainly, if not entirely, in the 2.3-hr ground state. Using an unseparated dysprosium source, he found the end-point of the Dy^{166} beta spectrum (by aluminum absorption methods) to be 0.22 Mev. By the usual technique of absorption measurements in aluminum, copper, and lead, some low-energy (less than 50-kev) gamma radiation was found in Dy^{166}.

From the above information, the activities of interest in this study were presumed to be related as follows:

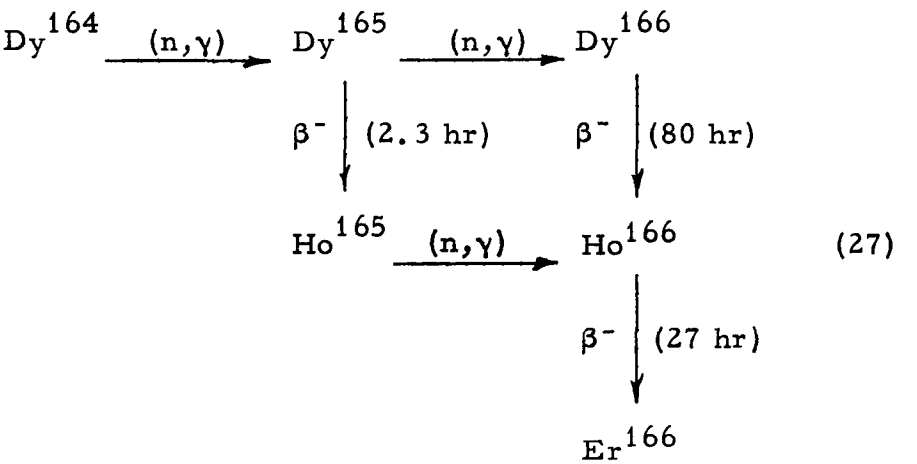

(27)

For simplicity and because of the results of Butement, the 1.2-min isomeric state of Dy^{165} has been omitted from this diagram. In this report references to Ho^{166}, except where otherwise noted, refer to the 27-hr ground state; the long-lived isomer (half-life $\geq$ 30 hr) was not observed. The conclusions of the previous authors concerning the isotopic assignments of the various related activities are confirmed by this study.

The source material used throughout this investigation was dysprosium oxide enriched to 90% in Dy^{164} (supplied by the Stable Isotopes Division, Oak Ridge National Laboratory). The irradiations were made in the Argonne CP-5 reactor in a flux of 3×10^{13} and at the Materials Testing Reactor, Arco, Idaho in a flux of 2×10^{14} neutrons cm^{-2} sec^{-1}. In order to make a separate study of the daughter

activity, Ho^{166}, samples of holmium oxide were also irradiated.

For the studies of the continuous beta-ray spectra, the source backing consisted of polyester film with aluminum vacuum coated on both sides (total density about 1 mg/cm^2). The first of two dysprosium sources (in equilibrium^{47} with the holmium daughter) and the holmium source were made by preparing a slurry of the active powder in alcohol and depositing it on the backing. A second dysprosium source was made from dysprosium that had been separated in an ion-exchange column. The active material was removed from the elutrient by solvent extraction into a solution of thenoyltrifluoroacetone in benzene. This solution was then placed on the backing and dried a drop at a time in an oven at approximately 120° C.

2. Experimental Results

a. Studies of internal-conversion electrons

The internal-conversion-electron lines observed are listed in Table IV along with the interpretations and some relative intensities. Although the decay of the lines was not measured quantitatively, all the lines appeared to decay with the same half-life (within about 30%). The energies of the lines are accurate to about 0.3 kev. In particular, as a criterion of accuracy, we refer to the work of Chupp et al.[48] who report a gamma-ray energy of 80.57 kev for the transition in erbium which we measure to be 80.6 kev.

All of the observed lines are assigned to three of the transitions in Ho^{166} (the ones at 82.5, 54.2, and 28.1 kev) and to the 80.6-kev transition in Er^{166}. For the 82.5-kev transition, the K, L_I, and N lines are observed. Its M line is merged with the N line of the 80.6-kev transition. The K/L ratio of the 82.5-kev transition is found to be 7 ± 3.

The L_{II}, L_{III}, M, and N lines are observed for the

TABLE IV

Data relating to gamma-ray transitions. All energies are in kev.

Transition energy	Internal-conversion lines			Relative intensities		
	Energy	Interpretation	Gamma energy	Conversion electrons[b]	Photons[b]	Transition
			Lines in holmium			
28.1 ± 0.3	18.7	L_I	28.1	~12	-	~12
54.2 ± 0.2	45.3	L_{II}	54.2	6		
	46.2	L_{III}	54.2	6	16	- 16
	52.3	$M_{II,III}$	54.1	4		
	53.8	N	54.2	0.4		
82.5 ± 0.2	26.6	K	82.2	55		
	73.3	L_I	82.6	8	63	14[c] 77
	(80.5)[a]	M	(82.4)	≤ 2		
	82.1	N	82.5	~0.2		
288 ± 4	-			-	0.1 ± 0.05	0.1
344 ± 2	-			-	0.3 ± 0.1	0.3
375 ± 2	-			-	1.1 ± 0.1	1.1
428 ± 2	-			-	1.4 ± 0.1	1.4
			Lines in erbium			
80.6	22.8	K	80.3	22		
	71.4	L_{II}	80.7	25		
	72.3	L_{III}	80.7	23		
	78.9	M	80.7	~ 9		
	(80.5)[a]	N	(80.8)	≤2		

[a] These two lines are not resolved.

[b] The data on photon and conversion-line intensities are normalized by use of the experimental value $\alpha_K^{82} = 4.0$.

[c] All other photon intensities are measured relative to this value.

54.2-kev transition. The multipolarity of this transition is deduced from the relative intensities of the L conversion lines (see Table V). The two lines are observed to be of equal intensity. Of the four possible multipoles (E1, E2, M1, M2), E2 is the only one for which the L_I line is not predominant. The observed intensity ratios can, therefore, be produced only by a transition which has either pure or primarily E2 character. However, the conversion coefficients are such that a substantial admixture of M1 could be present without being observed. As will be seen in the discussion of the decay scheme, the 0^- assignment for the ground state of Ho^{166} requires that the 54.2-kev transition be pure.

TABLE V

Relative intensities of conversion lines of the 28- and 54-kev transitions compared with the theoretical values for various multipole orders.

Transition energy (kev)	Experimental	Ratio $L_I : L_{II} : L_{III}$ Theoretical[a]				Character
		E1	E2	M1	M2	
28.1	1:0:0	1:0.7:1.1	1:110:140	1:0.09:0.02	1:0.07:0.55	M1
54.2	0:1:1	1.9:0.7:1	0.03:0.9:1	67:5.7:1	2.9:0.3:1	E2

[a] See reference 6.

We have interpreted the 18.7-kev internal-conversion line as an L_I for a 28.1-kev transition. This conclusion is supported by several facts. If this were the K conversion line of a 74.3-kev transition, accompanying L lines would have been visible, but none were observed. Considering the line to be the L_I line of a 28.1-kev transition leads to an excellent energy fit to the 82.5-kev transition when combined with the 54.2-kev transition (28.1 + 54.2 = 82.3). The failure to observe

the M and N lines is probably due to the fact that they are masked by the K line for the 82.5-kev transition. Since only the L_I line is observed, the transition must have predominantly M1 character. An L_{III} line with an intensity no greater than one-fourth of that of the L_I line would have been observable. From this fact it is possible to place an upper limit of 1% for the possible E2 content of this transition.

b. Beta-Ray Spectrum

The beta-ray spectrum of the first dysprosium source (Dy^{166} in equilibrium with the holmium daughter, Ho^{166}) is shown in Fig. 8. Normalized to this, is the spectrum of a pure 27-hr Ho^{166} source. These spectra indicate the relative intensities of the two activities in a dysprosium source in equilibrium with holmium. In order to obtain a more accurate Dy^{166} spectrum, another dysprosium spectrum was recorded for a source that had been separated in an ion-exchange column. In the latter source, the relative intensity of the holmium was about 1/7 of that in the original dysprosium source.

The Fermi plot of the Dy^{166} spectrum from the separated sample, after subtraction of the Ho^{166} spectrum, is shown in Fig. 9. For the higher energy component, the straight line represents a least-squares fit to the seven points between 475 and 405 kev. Because of the small number of points for this component, no conclusion about its shape could be reached; therefore, it was assumed to be linear. For the lower energy component, the straight line represents a least-squares fit to the seven points between 400 and 240 kev. The deviation from linearity below 240 kev is probably due to scattering in the source and from the backing.

The decay scheme which is proposed later in this report requires two additional beta-ray branches; these components are both below 120 kev and therefore would not be observed in this spectrum. For completeness these two components are included in Table VI which summarizes these data.

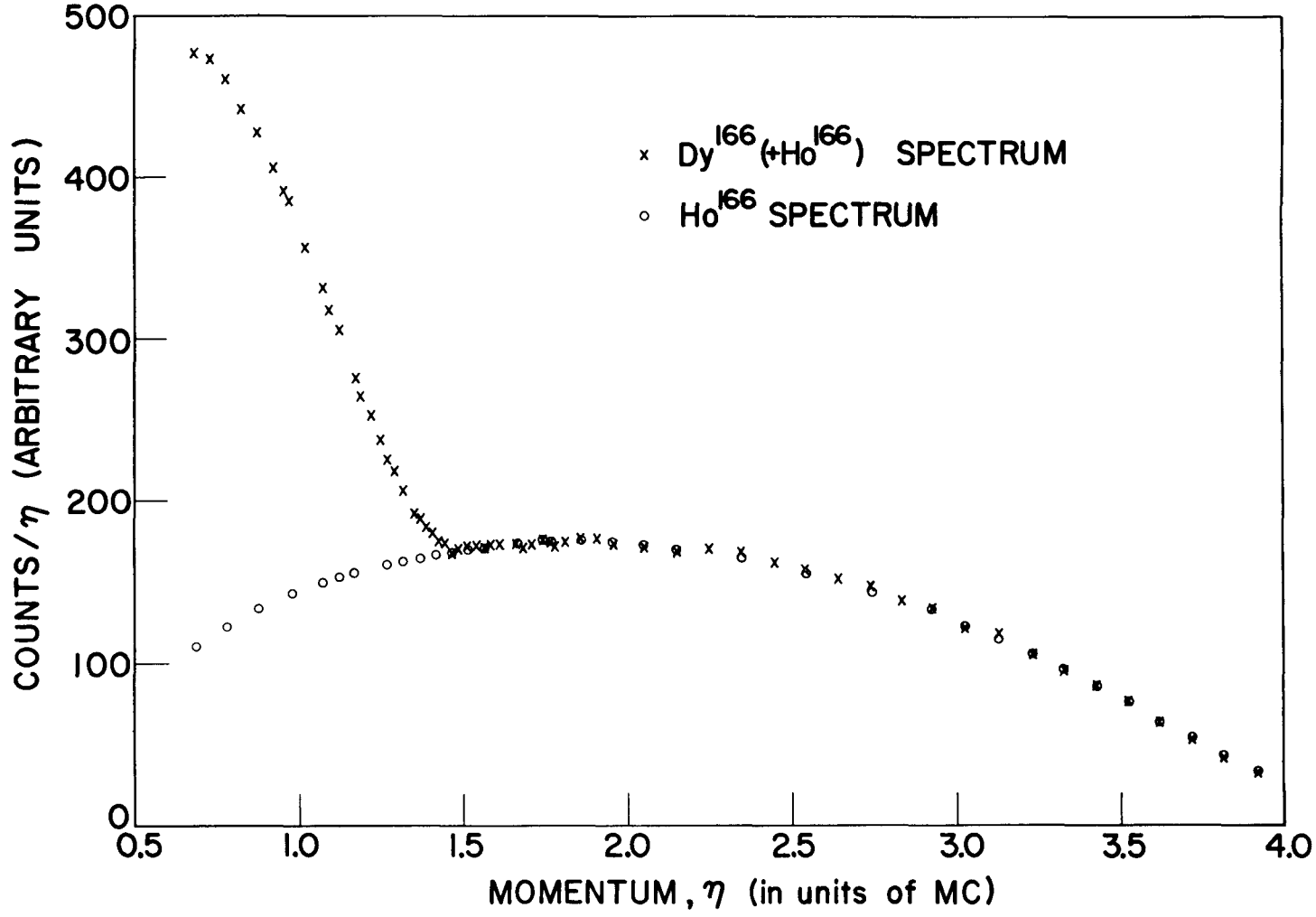

Fig. 8. Beta-ray spectra of Dy^{166} (in equilibrium with the holmium daughter) and Ho^{166}. The statistical uncertainties are less than the dimensions of the experimental points.

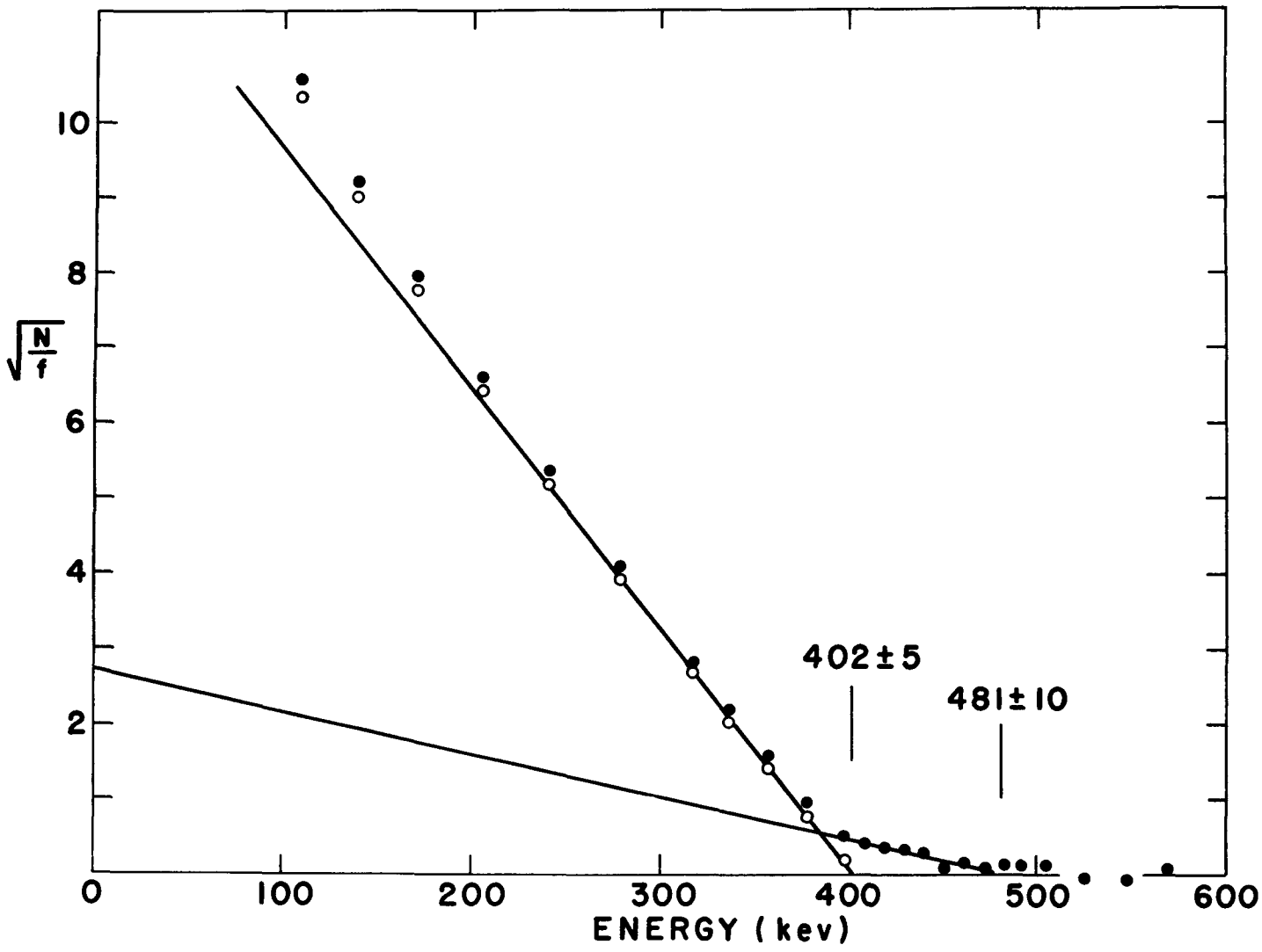

Fig. 9. Fermi plot of the beta-ray spectrum of Dy^{166}. The statistical uncertainties are less than the diameter of the circles indicating the experimental points.

TABLE VI

Summary of beta-ray components.

Energy (kev)	Relative intensity (percent)	Log ft
481 ± 10	5	7.4
402 ± 5	92	6.0
114[a]	≤ 0.1	≥ 7.1
56[a]	2.8	4.8

[a] The data for these two components are calculated from the gamma-ray energies and intensities and the level scheme shown in Fig. 13.

A measurement of the half-life of Dy^{166} was made with the original dysprosium beta-ray source. A set of four points (η = 0.98, 1.47, 2.55, and 2.74 on Fig. 8) was followed for a period of one month. In order to minimize the effect of any drifts in the apparatus, each of these four points was selected where the counting rate is a slowly varying function of the momentum. Initially these data showed a small amount of 27-hr activity that resulted from the production of an excess of Ho^{166} by neutron capture in Ho^{165}. (See Eq. 27.) No indication of impurities of longer half-life was observed at the end of one month. An average of the four determinations gives a value of 80.2 ± 0.5 hr for the half-life of Dy^{166}.

c. Scintillation Studies

The scintillation spectrum for a dysprosium source (in equilibrium with the holmium daughter) is shown in Fig. 10. Normalized to this in the region above 500 kev is the spectrum of a pure holmium source. In Fig. 11 is shown a Dy^{166} spectrum with the holmium subtracted. This spectrum was obtained from a source in which the relative

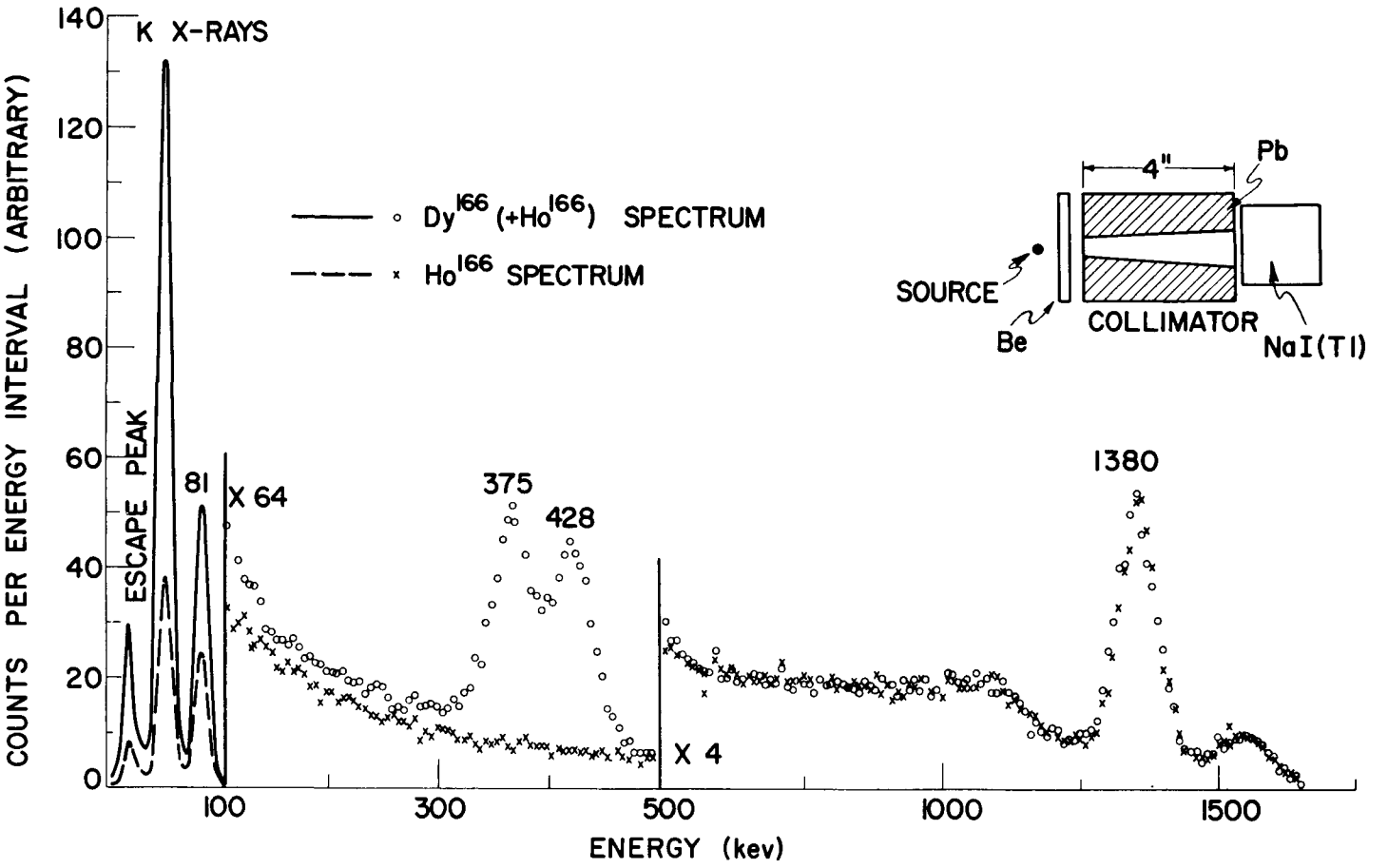

Fig. 10. Gamma-ray spectra of Dy^{166} (in equilibrium with the holmium daughter) and Ho^{166}. The statistical uncertainties are less than the dimensions of the experimental points.

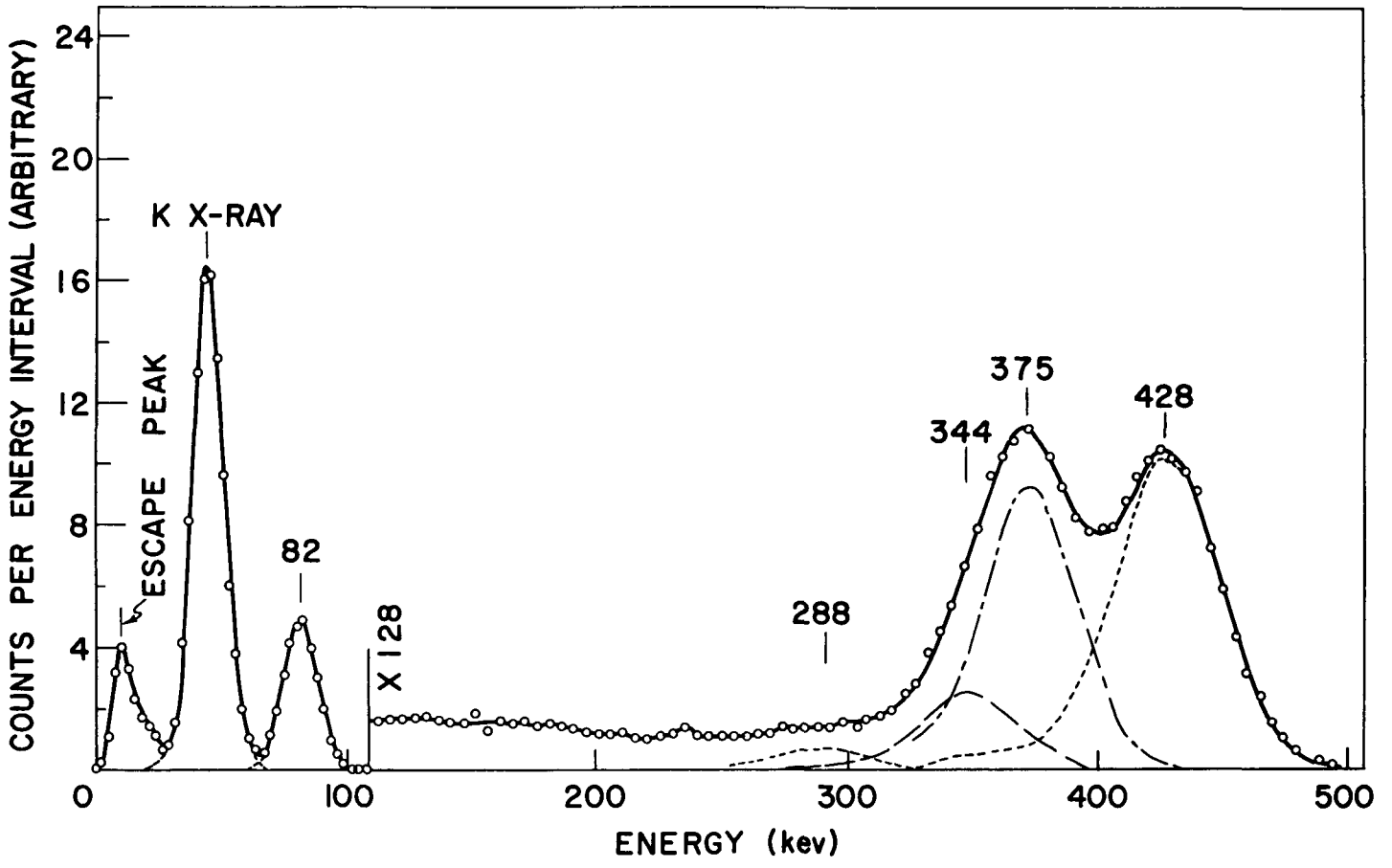

Fig. 11. Gamma-ray spectrum of Dy^{166}. All statistical uncertainties are less than the diameters of the circles indicating the experimental points. The experimental arrangement is the same as in Fig. 10.

holmium activity had been reduced by a factor of six by means of a separation in an ion-exchange column. The dashed lines in the figure show the energies and relative intensities of the individual components that are presumed to be present. Of the energies reported (Table IV, column 1) for the four higher energy transitions, the values for the 428- and 375-kev radiations were obtained from this decomposition of the singles spectrum. The energies for the 344- and 288-kev gamma rays were taken from the coincidence data discussed below. The spectral shapes of single gamma rays were approximated by those of Au^{198} (412 kev), Cr^{51} (323 kev), and Ho^{166} (80-kev gamma ray and 48-kev K x-rays). The solid curve, which is to be compared with the experimental points, represents the sum of the individual components as they are shown. A summary of the relative photon intensities calculated from this scintillation spectrum is presented in column 6 of Table IV.

As can be seen in Fig. 11, the scintillation spectrum for Dy^{166} does not show any evidence of the 54-kev transition whose conversion lines were observed (see Table IV). Hence, since the transition energy of 54 kev is too low to produce K-conversion in holmium, the K x-ray peak must be due almost entirely to K-conversion of the 82-kev transition. (The K x-rays following internal conversion of the four higher energy transitions should be completely negligible in view of the low intensity of these gamma rays.) Thus the K conversion coefficient for the 82-kev transition, α_K^{82}, can be calculated from the spectrum in Fig. 11. After correcting for detector efficiency and fluorescence yield, a value of $\alpha_K^{82} = 4.0 \pm 0.6$ results from these data. Table VII presents a comparison of this value with the theoretical values[6] of α_K for transitions of various multipolarities; the K/L ratio calculated from the data in Table IV is also included in Table VII along with the corresponding theoretical values. These data indicate that the 82-kev transition has primarily M1 character.

TABLE VII

Values of α_K and K/L for the 82- and 80-kev transitions compared with theoretical predictions for various multipole orders.

Transition energy (kev)	α_K Experimental	α_K Theoretical E1	E2	E3	M1	M2
82.5	4.0 ± 0.6	0.44	1.6	4.2	4.0	38
80.6	1.7 ± 0.3	0.46	1.6	3.7	4.6	44

	K/L Experimental	K/L Theoretical E1	E2	E3	M1	M2	Character
82.5	7 ± 3	6.3	0.5	0.04	7.4	3.2	M1
80.6	0.45 ± 0.15	6.0	0.4	0.03	7.3	3.1	E2

In order to check the accuracy of the calculation of α_K^{82} made above, the data in Fig. 10 were used to carry out a similar computation for the 80.6-kev transition in erbium. This transition is from the first excited state to the ground state of an even-even nucleus and is thus presumed to have pure E2 character. The E2 character has been verified by gamma-gamma angular correlation experiments.[49] The calculation for this transition gives a value $\alpha_K^{80} = 1.7 \pm 0.3$; the comparable theoretical value is $\alpha_K^{80}(\text{theor.}) = 1.60$. This agreement indicates that there is probably no large error in these calculations. The value of α_K and the K/L ratio for this transition are included in Table VII.

The results of the most interesting gamma-gamma coincidence measurements are shown in Fig. 12. These spectra were obtained with a separated dysprosium sample; the holmium content at the time of these runs was only one-fourth of the equilibrium amount. Figure 12a shows a coincidence run with the single-channel analyzer set

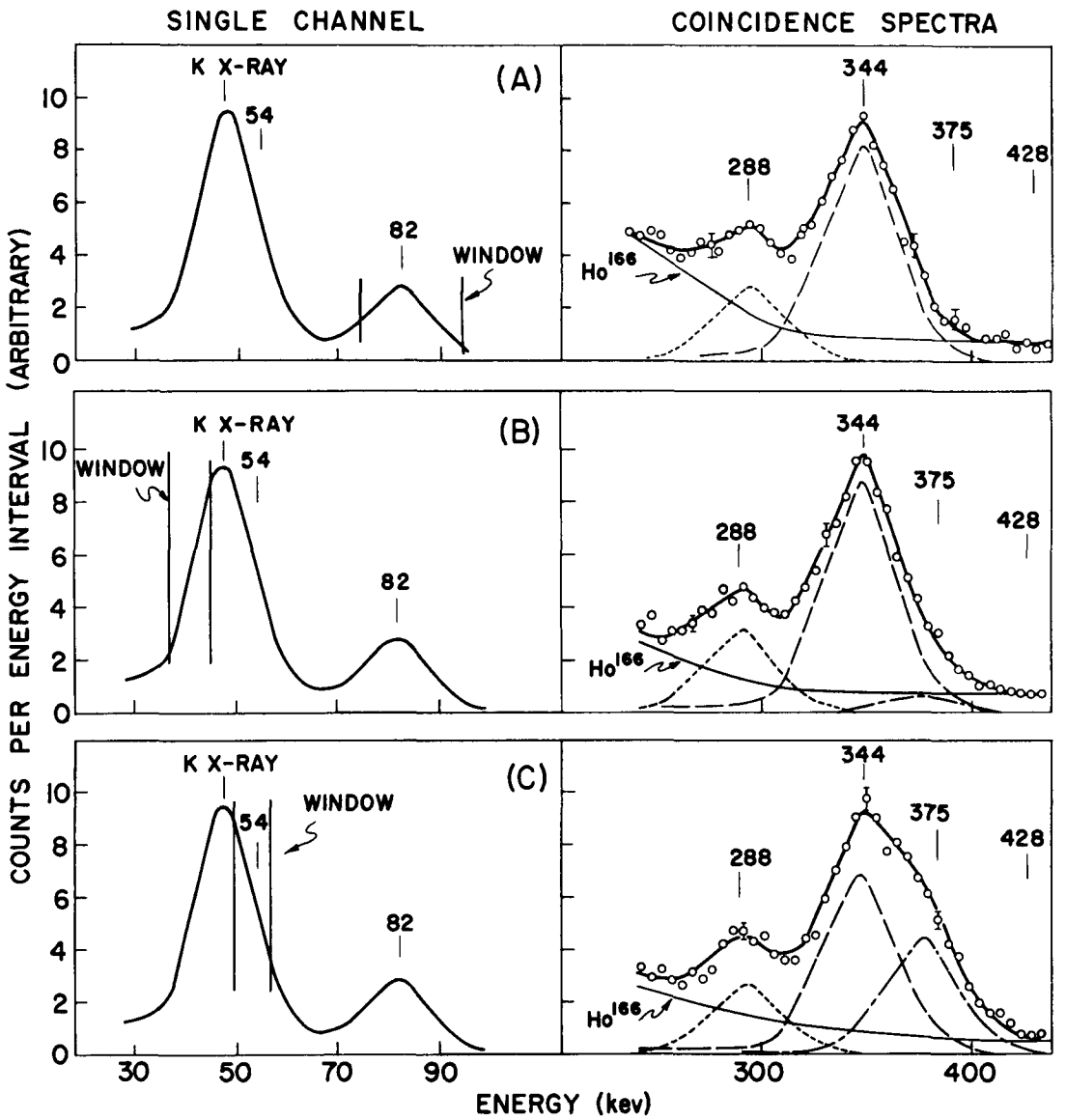

Fig. 12. Gamma-gamma coincidence spectra.

to accept pulses from the 82-kev photopeak. Figure 12b represents a coincidence spectrum taken when the single-channel analyzer was moved to the low-energy side of the x-ray peak. This side of the x-ray peak was selected in order to minimize any coincidences due to the 54-kev radiation. In contrast, Fig. 12c shows the spectrum obtained when the single channel was moved to the high-energy side of the x-ray in order to enhance any effects due to the 54-kev transition. It was found that the number of coincidence in the 288- and 344-kev photopeaks per single-channel count was nearly the same for these three experiments. On the other hand, the 375-kev peak, not present in (a) and barely observable in (b), is approximately as intense as the other two when the single channel is set at the energy at which the 54-kev radiation is expected to be found. From these experiments, it can be concluded that the 375-kev gamma ray is in coincidence with the 54-kev radiation (unobserved in the "singles" spectrum), but not with the 82-kev gamma ray. The 288- and 344-kev gamma rays are in coincidence with the 82-kev radiation and the K x-rays which (as mentioned earlier) arise primarily from internal conversion of the 82-kev transition.

In addition to the experiments described above, a thorough survey of the entire spectrum was made with the single-channel analyzer in a search for other coincident relationships, but none were found. (In all cases it was necessary in the analysis to take into consideration the effects of the daughter activity.)

From beta-gamma coincidence measurements, it was possible to determine the total decay energy. Standard aluminum absorption methods were used to measure the end-point energies of the beta-ray components in coincidence with each particular gamma ray. It was found that the 82-kev gamma ray is in coincidence with a beta-ray branch whose maximum energy is 400 ± 20 kev (half-thickness = 10 mg/cm^2); this is assumed to be the 402 ± 5-kev component found with the magnetic spectrometer. None of the higher energy gamma rays were found to be

in coincidence with this beta-ray branch.

With no absorber between the source and anthracene crystal, except about $\frac{1}{8}$ in. of air, there were some beta-gamma coincidences with the 375- and 428-kev gamma rays. No definite conclusions could be inferred from the coincidences with the 375-kev photopeak, since these events could as well be attributed to internal-conversion electrons as to beta rays. However, the coincidences with the 428-kev gamma ray can be ascribed to beta-rays, since as has been seen, this radiation is in coincidence with no other gamma transitions from which conversion electrons might originate. Although the coincidence rate was low, the attenuation in aluminum (half-value thickness = $0.6 \pm 0.3\,mg/cm^2$) corresponds approximately to an end-point energy of 55 kev.

3. Decay Scheme

a. Construction

The proposed decay scheme is shown in Fig. 13. It is consistent with all of the experimental data. The 428-kev transition was not observed in coincidence with any other gamma ray and the 375-54, 288-82, and 344-82 kev cascades were all observed. The energy fits between the cascades and the cross-over transitions agree within experimental uncertainties.

As noted in Table IV, in order to obtain relative transition probabilities, the two sets of relative-intensity data (scintillation and spectrographic) are normalized by using the experimentally determined value of $\alpha_K^{82} = 4.0$. These transition probabilities (the numbers in parentheses on the decay scheme) have been reduced to percentages of the total number of decays by incorporating the beta-ray branching data from the magnetic spectrometer measurements (Table VI).

The log ft values of 7.4 and 6.0 for the 481- and 402-kev beta-ray branches indicate that these transitions are first for-

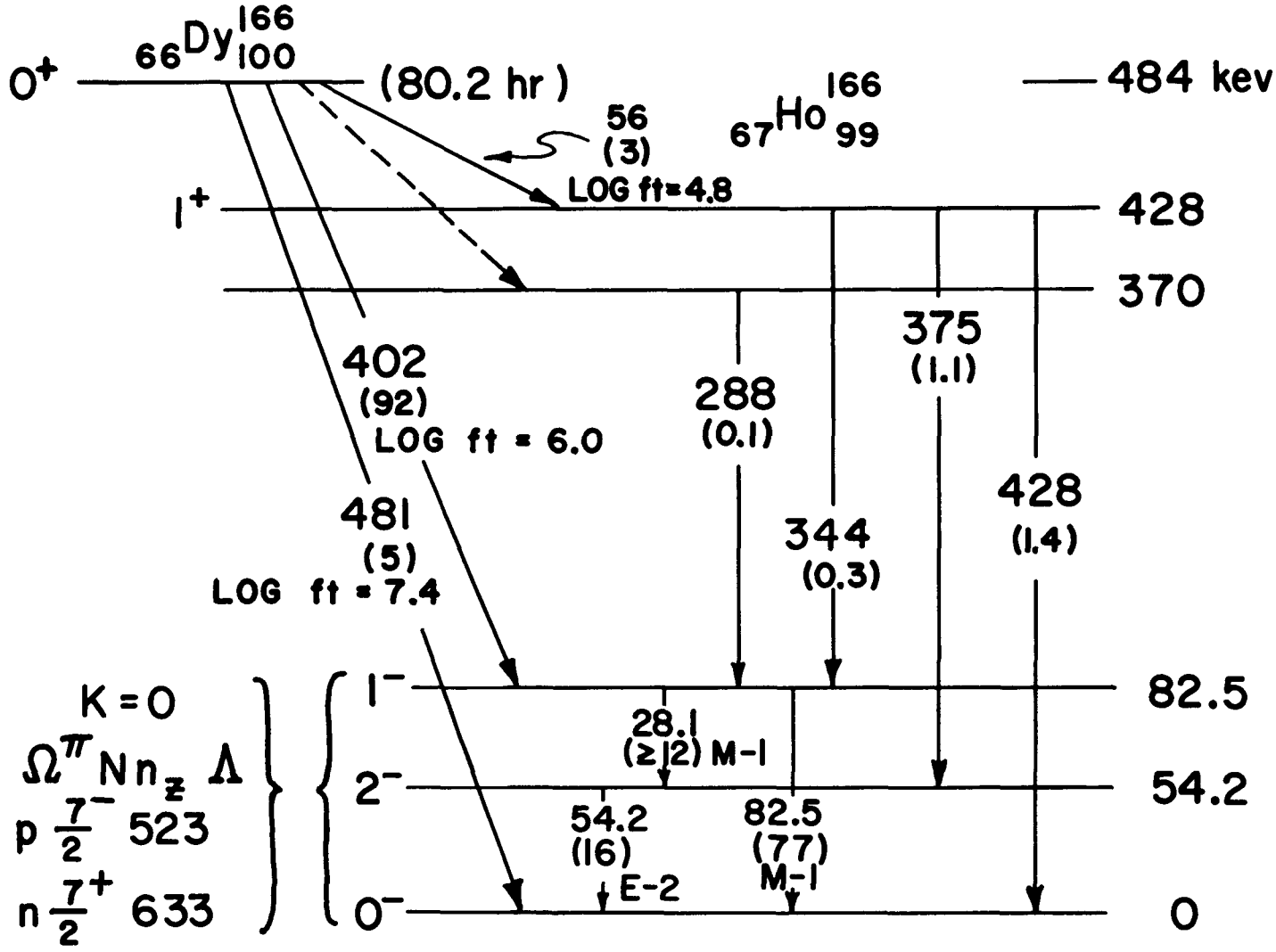

Fig. 13. Proposed decay scheme for $_{66}Dy^{166}$. The relative transition intensities (percent of decays) are shown in parentheses.

bidden. The log ft value of the branch to the 428-kev level is determined[50] by use of a relative intensity of 3% as calculated from the intensities of the gamma transitions. The latter log ft. value of about 4.8 is significant in that it suggests that this branch is allowed.

For any character which might be assigned to the 28-kev transition (except E1), the relative transition intensity is very nearly equal to that of the internal-conversion lines. Although there is considerable uncertainty in this transition intensity, the value calculated (considered together with that of the 54-kev transition), is consistent with this cascade.

There are three other gamma-ray transitions which might occur between the levels indicated: 58, 316, and 370 kev. If the 58-kev transition, between the 428- and 370-kev levels, were present and highly converted, it could be sufficiently intense to obviate the beta-ray branch to the 370-kev level and still be unobservable. If a 316-kev transition occurs between the 370- and 54-kev levels, it must have an intensity less than about 25% of that of the 288-kev transition. The possible 370-kev transition to the ground state would be indistinguishable from the 375-kev gamma ray in the "singles" spectrum. However, interpretation of the coincidence experiments indicates that this ground-state transition, if present must be weak compared to the 375-kev gamma ray.

Since $_{66}Dy^{166}$ is an even-even nucleus, its ground-state spin and parity are assumed to be 0^+. On the basis of the analysis of the beta spectrum and beta-gamma angular-correlation measurements of Graham et al.,[51] the spin and parity of the 27-hr ground state of $_{67}Ho^{166}$ is assumed to be 0^-. This spin assignment is supported by the results of recent atomic-beam measurements.[52] It follows from the latter spin assignment that the gamma-ray transitions to the Ho^{166} ground state must be pure transitions (i.e., they can not be mixtures of different multipole order). Thus, the predominantly

E2 character of the 54-kev transition indicates that the first excited state has spin and parity 2^-. Similarly, the M1 character of the 82-kev transition indicates that the 82-kev level is a 1^- state. The only possible assignments which are consistent with the character of the beta decay to the 428-kev state (log ft $\approx$ 4.8) are 0^+ and 1^+. The fact that this level does decay to the ground state by gamma-ray emission eliminates the 0^+ possibility (since monopole photons do not exist).

b. Interpretation of Energy Levels in Ho^{166}

The spin 0^- for the holmium ground state is consistent with the spins measured for neighboring odd-A nuclei, Ho^{165} with 67 protons and Er^{167} with 99 neutrons. The spin of $_{67}Ho^{165}$ has been measured as $\frac{7}{2}$;[53] Mottelson and Nilsson have interpreted this as the Nilsson level $\frac{7-}{2}$ [523].[17] The spin of Er^{167}, which has 99 neutrons, has been measured as $\frac{7}{2}$;[54] this has been interpreted as the $\frac{7+}{2}$ [633] level.[17] Apparently, in Ho^{166} these two odd particles couple to produce a state of zero spin and odd parity. A long-lived ($\geq$ 30 yr) isomer of Ho^{166} also exists. The high spin necessary for this metastability presumably results from a different coupling of these same two particles to produce a state of spin 7. The existence of this pair of states is in agreement with the theory that predicts the spin of the ground state of an odd-odd nucleus to be one of the two states given by $I = K = \Omega = \left| \Omega_p \pm \Omega_n \right|$, where p and n refer to the odd proton and neutron, respectively.

It is reasonable to assume that the 99th and 100th neutrons in the parent nucleus Dy^{166} are in the same level as the 99th neutron in Dy^{165}, that is, the $\frac{7+}{2}$[633] level. Then the beta decay to the ground state should be characterized by the following changes in quantum numbers: $\Delta I = 0$, $\Delta K = 0$, $\Delta N = -1$, $\Delta n_z = -1$, $\Delta \Lambda = 0$. According to the asymptotic selection rules tabulated in reference 17, this beta transition would be unhindered ordinary first forbidden. This is

consistent with the observed log ft value of 7.4.

The 54-kev level, which has spin 2, is presumed to be an excited state of a rotational band (with K = 0) based on the ground state. The second excited state, which has spin 1, might have either of two values (K = 0 or 1) for the projection of its spin on the symmetry axis. The two radiations which de-excite this level are both essentially pure M1 transitions. By comparing the experimental ratio of the reduced transition probabilities to the theoretical values, we can distinguish between the two possible values of K. (The gamma-ray intensity for the 28-kev transition was computed by use of $\alpha_{L_I}^{28} = 9.6$ from reference 6.) From Eq. (15) the results of such a comparison are

	Theoretical		Experimental
	K = 1	K = 0	
$\frac{B(1:1 \rightarrow 0)}{B(1:1 \rightarrow 2)} = \left\lvert \frac{\langle 11K-K \mid 1100 \rangle}{\langle 11K-K \mid 1120 \rangle} \right\rvert^2 =$	2.0	0.5	0.4 ± 0.2

Thus it is clear that the second excited state also has K = 0 and is probably another member of the rotational band based on the ground state. The fact that the 82-kev state has K = 0 explains why no E2 admixture was observed in the 28-kev transition. The E2 transition probability between these two levels should be proportional to the Clebsch-Gordan coefficient $\langle I_i\ L\ K_i\ K_f - K_i \mid I_i\ L\ I_f\ K_f \rangle = \langle 1200 \mid 1220 \rangle$. This coefficient is zero, so the E2 transition probability vanishes.

If our interpretation of the experimental data is correct and the first two excited states are in fact members of a K = 0 band based on the ground state, then two features of this relationship should be noted. First, both odd-spin and even-spin states are present. Second, the expression which governs the energy spacing of the states must be such as to permit the inversion of the first and second excited states.

The available information concerning the excited state at 370 kev is too meager to attempt any interpretation.

From the character of the beta decay to the 428-kev level, this state has been assigned the spin and parity 1^+. For this spin there is again a choice between the two values K = 0 and K = 1. Although the ground-state transition must be pure dipole radiation, the other transitions might be mixtures of dipole and quadrupole radiation. In Table VIII, the experimental gamma-ray transition intensities are compared with the theoretical transition probabilities.

TABLE VIII

Comparison of experimental transition intensities from the 428-kev level with the theoretical transition probabilities

			Theoretical			
		K = 1				
$\omega^3B(1,1\rightarrow 0)$:	$\omega^3B(1,1\rightarrow 2)$:	$\omega^3B(1,1\rightarrow 1)$	=	3.0	: 1.0:	2.3
$\omega^5B(2,1\rightarrow 0)$:	$\omega^5B(2,1\rightarrow 2)$:	$\omega^5B(2,1\rightarrow 1)$	=	0	: 2.5:	1.0
		K = 0				
$\omega^3B(1,1\rightarrow 0)$:	$\omega^3B(1,1\rightarrow 2)$:	$\omega^3B(1,1\rightarrow 1)$	=	0.75	: 1.0:	0
$\omega^5B(2,1\rightarrow 0)$:	$\omega^5B(2,1\rightarrow 2)$:	$\omega^5B(2,1\rightarrow 1)$	=	0	: 0:	1.0
		Experimental				
$T(1\rightarrow 0)$:	$T(1\rightarrow 2)$:	$T(1\rightarrow 1)$	=	1.3	: 1.0:	0.25

From this comparison, it is clear that the choice K = 1 is incompatible with the experimental data. For the alternative value K = 0, the agreement is only better for a particular range of quadrupole mixing. However, the values are still not within the experimental uncertainties. This may indicate that K is not a good quantum number for this state.

After a report of this work had been submitted for publication,[55] the results of an independent investigation on Dy^{166}

appeared.[56] These data are in substantial accord with the experimental and theoretical conclusions contained in the author's preliminary paper[57] and in this report.

c. Theory of K = 0 Bands in Odd-Odd Nuclei

It has been pointed out[24-26] that in odd-odd nuclei the intrinsic wave function of the nucleus must be written as the product of the intrinsic wave functions of the two unpaired particles. For Ho^{166} one has the special case in which the particles couple to zero spin, i.e., $K = \Omega = \Omega_p - \Omega_n = 0$. In this case the wave function, Eq. (10), becomes

$$\psi = (\text{constant})\,\phi \left[\chi_{\Omega_p} \chi_{-\Omega_n} + (-1)^{I - j_p - j_n} \chi_{-\Omega_p} \chi_{\Omega_n} \right] \mathcal{D}^{I}_{M0} \qquad (28)$$

The two functions $\chi_{\Omega_p} \chi_{-\Omega_n}$ and $\chi_{-\Omega_p} \chi_{\Omega_n}$ are not in general identical and therefore the wave function does not vanish for any value of I. This explains the existence of the odd-spin states in this rotational band. Also the second term in the intrinsic function (in the bracket) changes sign for each successive increase in I. Therefore, there is one intrinsic function for the odd-spin levels and a different intrinsic function for the even-spin levels. If there is a residual interaction between the two unpaired nucleons, these two intrinsic functions will result in different intrinsic energies. In the resulting rotational band the odd-spin and even-spin states will thus be displaced by a constant energy although separately they both obey the I(I + 1) interval rule, i.e.,

$$E(I) = \frac{\hbar^2}{2\mathcal{J}} I(I+1) + \Delta E\, \delta_{I,\text{odd}} \,, \qquad (29)$$

where $\delta_{I,\text{odd}}$ equals zero if I is even and one if I is odd. The sign of ΔE depends on the particular intrinsic states involved.

Asaro et al.[25] have recently proposed a level scheme for Am^{242} in which the ground state has I = 1, K = 0, and negative parity. The spin 1 for the ground state is interpreted as meaning that ΔE is negative and sufficiently large to displace this level below the state with zero spin. However, the other members of the rotational band are not observed so that the values ΔE and $\hbar^2/2\mathcal{I}$ are not known.

For the levels in Ho^{166} reported here, one has $\Delta E = +64$ kev and $3\hbar^2/\mathcal{I} = 54$ kev. The corresponding value of the moment of inertia $\mathcal{I}$ is slightly larger than those of the ground states of the neighboring odd-mass nuclides (e.g., in Ho^{165}, $3\hbar^2/\mathcal{I} = 64$ kev and in Dy^{163}, $3\hbar^2/\mathcal{I} = 64$ kev), and is considerably larger than those of the neighboring even-even nuclei (e.g., in Er^{166}, $3\hbar^2/\mathcal{I} = 81$ kev).

In a theoretical study of Ho^{166}, Kurath[26] has shown that for a delta-function interaction between the proton and the neutron and for the appropriate Nilsson wave functions, the energies of the odd-spin states should be raised in agreement with the experimental data.

C. DECAY OF Tm^{172}

1. Introduction

The radioactive nuclide $_{69}Tm^{172}$, which decays to Yb^{172} by β^- emission, has been reported by Nethaway, Michel, and Nervik.[58] They obtained this isotope from the decay of Er^{172} which was produced by two successive neutron captures in stable Er^{170}. The thulium activity was identified by its generic relationship to the Er^{172} activity. The mass assignment was verified by time-of-flight isotopic separation. The thulium half-life was measured to be 63.6 ± 0.3 hr. Gamma rays of 0.076, 0.18, 0.40, 1.09, 1.44, and 1.79 Mev were reported.

Excited states in Yb^{172} are also populated by electron capture in Lu^{172}. The latter activity has been studied by

several groups.[59-61] Wilson and Pool[59] have proposed a decay scheme with excited states at 0.079, 0.260, 0.530, 1.172, 1.283, 1.375, 1.662, (1.699), and 2.072 Mev. They have assigned spins, K values, and parities to all of these states, except the one at 1.699 Mev.

The source material used throughout this investigation was Er_2O_3 enriched to 87% in Er^{170}. The irradiations were made primarily in the Materials Testing Reactor, Arco, Idaho in a flux of approximately 2×10^{14} neutrons $-cm^{-2} - sec^{-1}$. A few irradiations were made in the Argonne CP-5 reactor in a flux of 3×10^{13}.

The activities of interest in this study are related as follows.

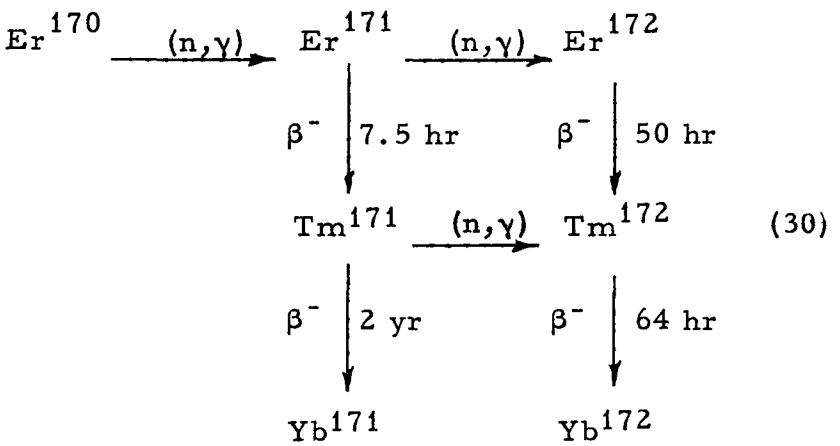

(30)

In addition to the above activities, observable amounts of Tm^{170} (125 day), Er^{169} (9 day), Yb^{169} (35 day), Yb^{175} (4 day), Ho^{166} (1 day), and Sc^{46} (85 day) were present. Because of these contaminants, in addition to the Er^{171} and Er^{172}, chemical separations were used to produce pure thulium. For this purpose the ion-exchange column was used. The 2-yr activity in Tm^{171} is characterized by beta-ray transitions of 30 and 100 kev and a 67-kev gamma-ray transition. Their presence did not interfere with the measurements made in this study. It only remained necessary to make corrections for the 965- and 880-kev beta rays and 84-kev gamma ray

associated with the decay of Tm^{170}.

2. Experimental Results

a. Studies of Internal-Conversion Electrons

Internal-conversion-electron groups were observed which correspond to the K, L_{II}, L_{III}, M, and N lines for a 0.0787-Mev transition and to the K and L lines for a 0.181-Mev transition. All of these lines have been previously reported[60] in the studies of Lu^{172}. In addition, a weak conversion line was observed which corresponds to the K conversion group for a transition of about 0.145 Mev. And as will be seen, the existence of this transition is verified by coincidence measurements.

Visual estimates of the relative intensities of the lines indicate that these results support the previous assignments of E2 character for both the 0.079- and 0.181-Mev transitions.[60]

b. Scintillation Studies

The gamma-ray spectrum is shown in Fig. 14. The light lines show the energies and intensities of the individual components that are presumed to be present. In should be emphasized that this figure does not constitute a decomposition of the total singles spectrum independent of other experimental information. Rather, it represents more nearly a synthesis in which the relative intensities and approximate energies of many of the constituents are taken directly from the coincidence experiments. For example, the relative intensities of the 0.91-, 1.19-, 1.28-, 1.37-, and 1.46-Mev transitions are imposed by the values obtained from the spectrum in coincidence with the 0.181-Mev transition. The heavy line, which is to be compared with the experimental points, represents the sum of the individual gamma rays shown. The spectral shapes of single gamma rays were interpolated from those of V^{52} (1.42 Mev), Na^{22} (1.28 and 0.511 Mev), Zn^{65} (1.12 Mev), Cs^{137} (0.662 Mev) and Ce^{141}

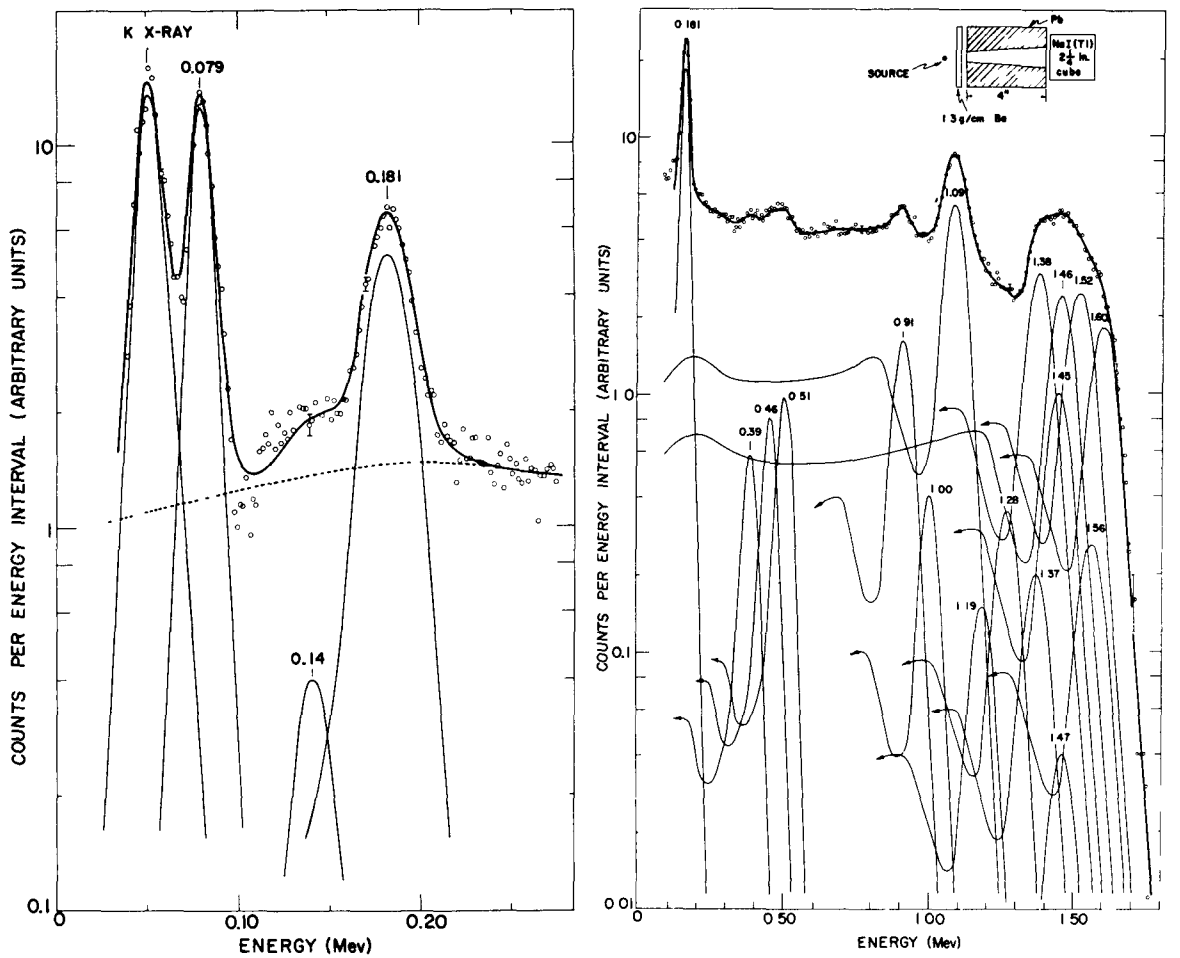

Fig. 14. Gamma-ray spectrum of Tm^{172}. The dashed line represents the sum of the gamma rays whose energies are above 0.2 Mev.

(0.142 Mev). A summary of the relative photon intensities calculated from this spectrum is given in Table IX.*

TABLE IX

Gamma-ray energies and relative intensities calculated from the decomposition of the scintillation spectrum.

Transition energy (Mev)	Relative photon intensities
1.60 ± 0.015	73 ± 15
1.56 ± 0.02	12 ± 8
1.52 ± 0.015	93 ± 15
1.47 ± 0.03	1.0 ± 0.7
1.46 ± 0.015	79 ± 20
1.45 ± 0.02	34 ± 15
1.38 ± 0.015	93 ± 15
1.37 ± 0.025	4.4 ± 1
1.28 ± 0.02	8 ± 1
1.19 ± 0.03	3.5 ± 0.7
1.09 ± 0.01	112
1.00 ± 0.02	6 ± 5
0.91 ± 0.01	24 ± 4
0.51 ± 0.025	6 ± 2
0.46 ± 0.025	4.4 ± 2
0.39 ± 0.03	3 ± 1
0.181 ± 0.004	35 ± 2
0.142 ± 0.008	2.4 ± 1
0.079 ± 0.002	47 ± 12
x-ray	63 ± 16

* During a recent conversation, P. Gregers Hansen of the Chemistry Division, Atomic Energy Commission, Research Establishment Risø, Roskilde, Denmark, showed the author a gamma-ray spectrum measured with a three-crystal pair spectrometer. This spectrum exhibited four well resolved gamma rays that the author interpretes as those corresponding to the four strongest photopeaks in this decomposition above 1.2 Mev (i.e., the 1.38-, 1.46-, 1.52-, and 1.60-Mev transitions). This fact is noted in support of the foregoing analysis.

A large number of coincidence measurements were made in order to determine the energies and intensities of the radiations present, as well as to determine their positions in the decay scheme.

In order to ascertain the coincidence relationships between the radiations with energies above 1 Mev and those below 0.4 Mev, the region between 1.1 and 1.6 Mev was scanned with the single-channel analyzer. A window approximately 35 kev wide was used and 13 coincidence spectra were taken. Figure 15 is an example of this series. This spectrum, taken in coincidence with the pulses in the energy interval between 1.46 and 1.50 Mev, was selected because the photopeak at 0.14 Mev, which was not apparent in the singles spectrum, demonstrates the existence of a gamma ray of this energy. (The observation of K conversion electrons for this transition has been noted previously.) The analysis of the 13 coincidence spectra is presented in Fig. 16. The intensities of the three low-energy transitions (0.079, 0.14, and 0.181 Mev) are plotted as functions of the energy corresponding to the center of the single-channel window. Again the dashed lines indicate the energies and intensities of the individual radiations presumed to be present. The interpretation of these spectra is presented in the succeeding paragraphs.

The relationships suggested by the above data were further studied by setting the single-channel window on each of the three low-energy photopeaks. The results of these runs are presented in Fig. 17. As before, the decompositions into individual components are shown. In the spectrum of radiations in coincidence with the photopeak at 0.181 Mev, Fig. 17a, the peak at 1.09 Mev is interpreted as being due to coincidences with backscattered radiation arising from gamma rays of 0.50 to 0.35 Mev. (It will be shown later that these coincidences exist.) This interpretation is supported by the absence of a corresponding peak at 1.09 Mev in Fig. 16a. With the exception of the 1.09-Mev photopeak, the curves in Figs. 16a and 17a are practically identical. Therefore, it is concluded that the 0.181-Mev transition

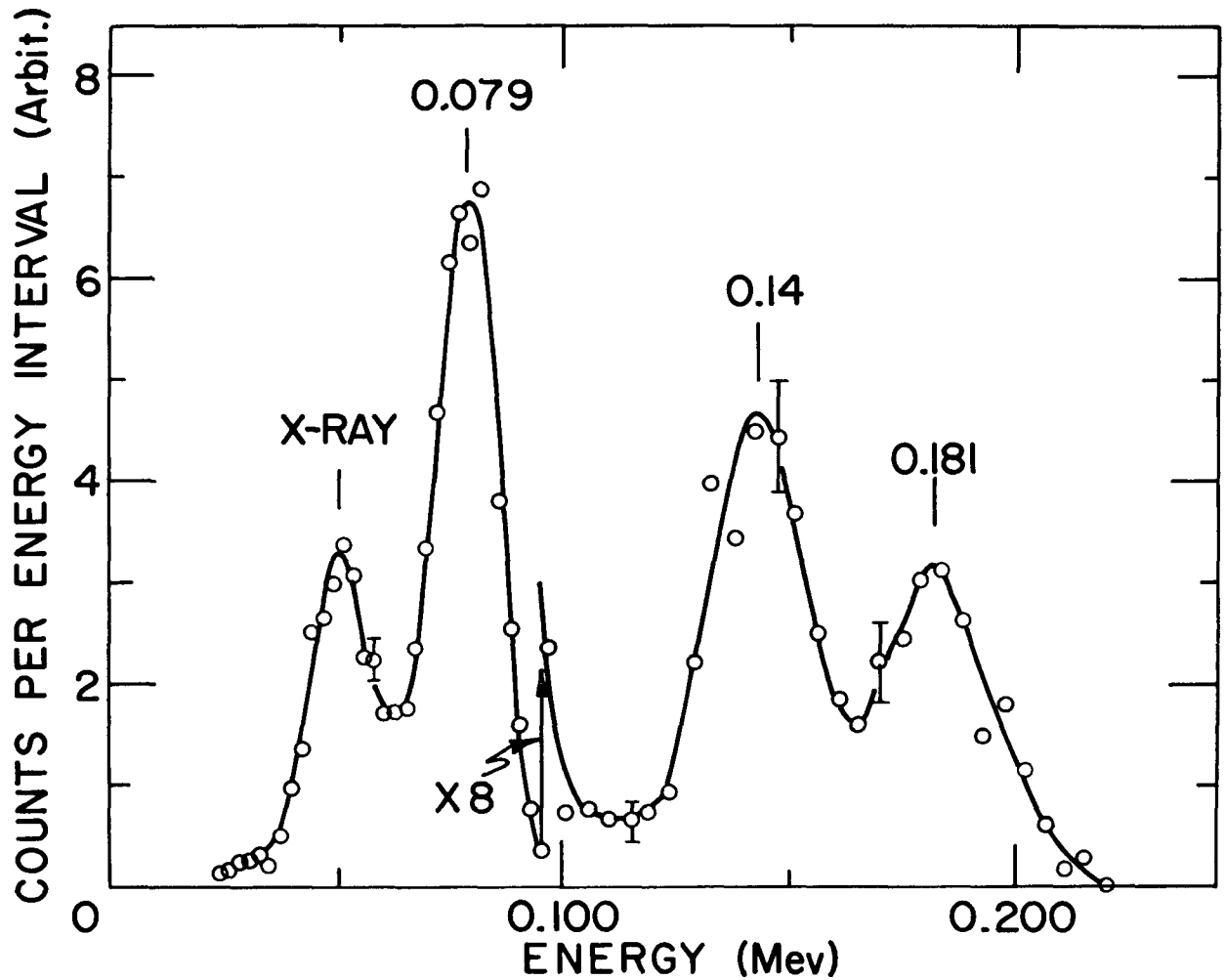

Fig. 15. Gamma-ray spectrum in coincidence with pulses in the range from 1.46 to 1.50 Mev.

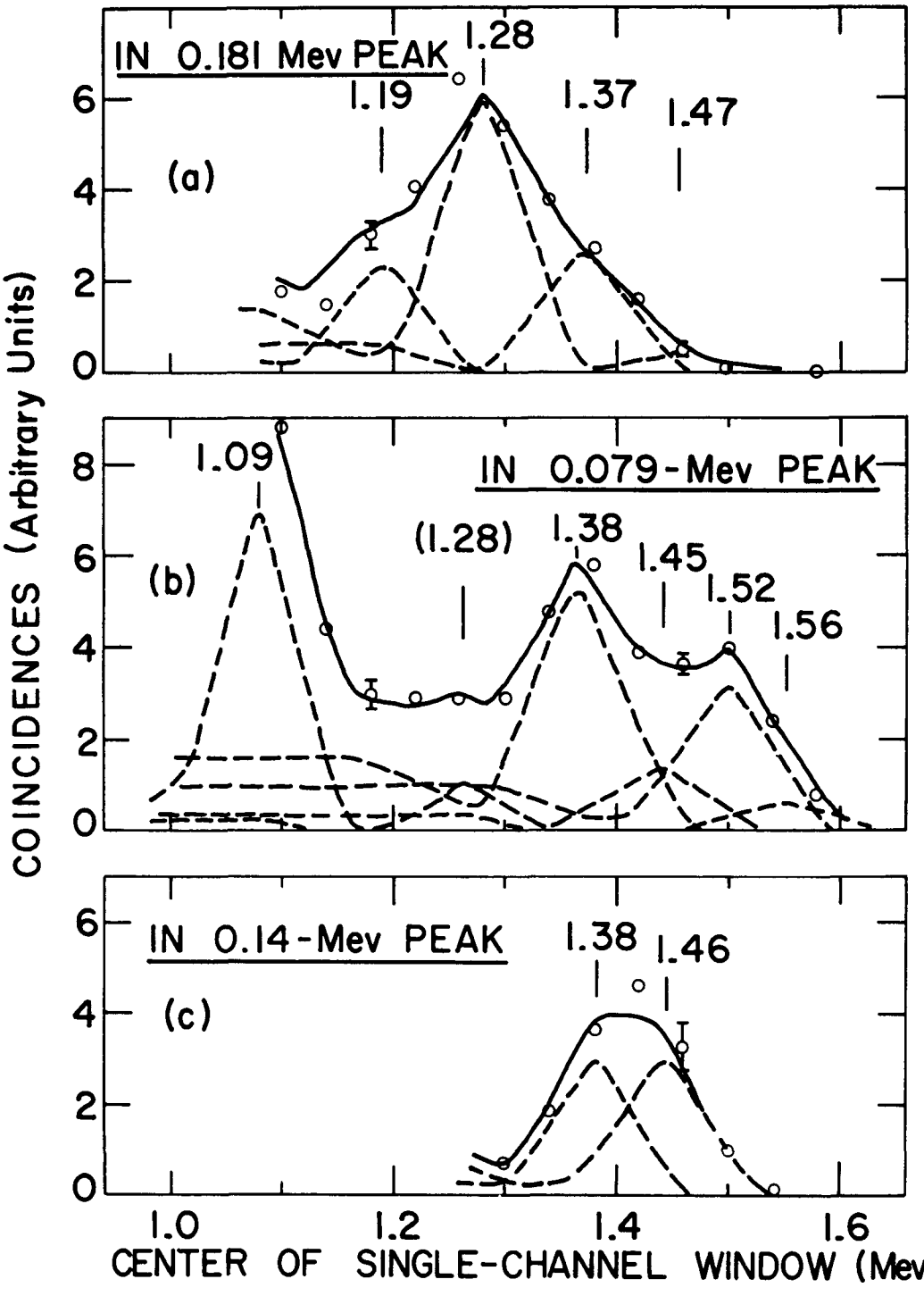

Fig. 16. Summary of coincidence spectra. The areas of the photopeaks at (a) 0.181 Mev, (b) 0.079 Mev, and (c) 0.14 Mev are plotted as a function of the energy corresponding to the center of the single-channel window.

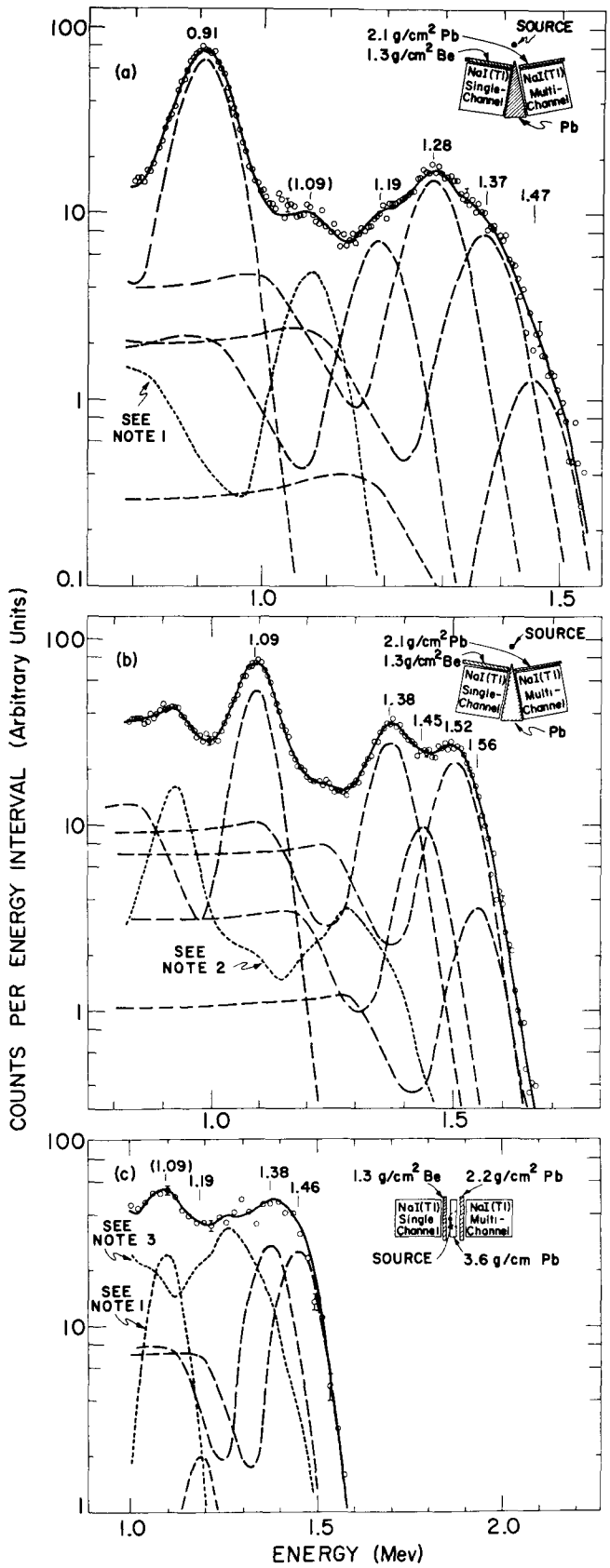

Fig. 17. Coincidence spectra of Tm^{172}. The gamma-ray spectra in coincidence with the (a) 0.181-Mev, (b) 0.079-Mev, and (c) 0.14-Mev transitions. Note I: In curves (a) and (b), the 1.09-Mev photopeak is interpreted as being due to coincidences with backscattered radiation from gamma rays whose energies are from 0.4 to 0.5 Mev. Note II: The dotted curve represents the radiations which are in coincidence with the 0.079-Mev transition via the 0.181-Mev transition. Note III: This curve represents coincidences with the 0.181-Mev gamma ray.

is in coincidence with gamma rays at 1.47, 1.37, 1.28, 1.19, and 0.91 Mev.

The gamma rays of 0.079 and 0.181 Mev are in cascade. (The experiments demonstrating this relationship are not described here.) From their intensities as well as the studies of Lu^{172}, [59] it is apparent that the 0.079-Mev transition goes to the ground state, and the 0.181-Mev transition goes from the second excited state at 0.260 Mev to the 0.079-Mev level. Therefore, the spectrum in coincidence with the 0.079-Mev photopeak, Fig. 17b, also shows the radiations found in coincidence with the 0.181-Mev transition (Fig. 17a). The resulting analysis of Fig. 17b indicates that the 0.079-Mev level is fed directly by transitions of 1.56, 1.52, 1.45, 1.38, and 1.09 Mev. Again the data in Fig. 16b are consistent with this interpretation.

When the single-channel window is set to bracket the region of the weak 0.14-Mev radiation, most of the pulses registered arise from the spectral background. In Fig. 17c the dotted curves correspond to radiations which are interpreted as resulting from coincidences with this spectral background. The peaks at 1.46, 1.38, and 1.19 Mev are interpreted as representing gamma rays which are in coincidence with the 0.14-Mev transition. These conclusions are supported by the spectrum in Fig. 16c.

One observes the spectrum shown in Fig. 18 when the single-channel analyzer is set to bracket the 1.09-Mev photopeak. This indicates the 1.09-Mev transition is in coincidence with gamma rays at about 0.52, 0.48, 0.42, and 0.38 Mev as well as 0.079 Mev. The peaks at 0.181 and 0.14 Mev are due to coincidences with higher energy transitions whose Compton distributions are counted in the single-channel window. The unresolved radiations below 0.35 Mev may be in coincidence with either the 1.09-Mev gamma ray or the underlying Compton distributions. When the single-channel window is moved to the 0.91-Mev photopeak, the observed spectrum is similar

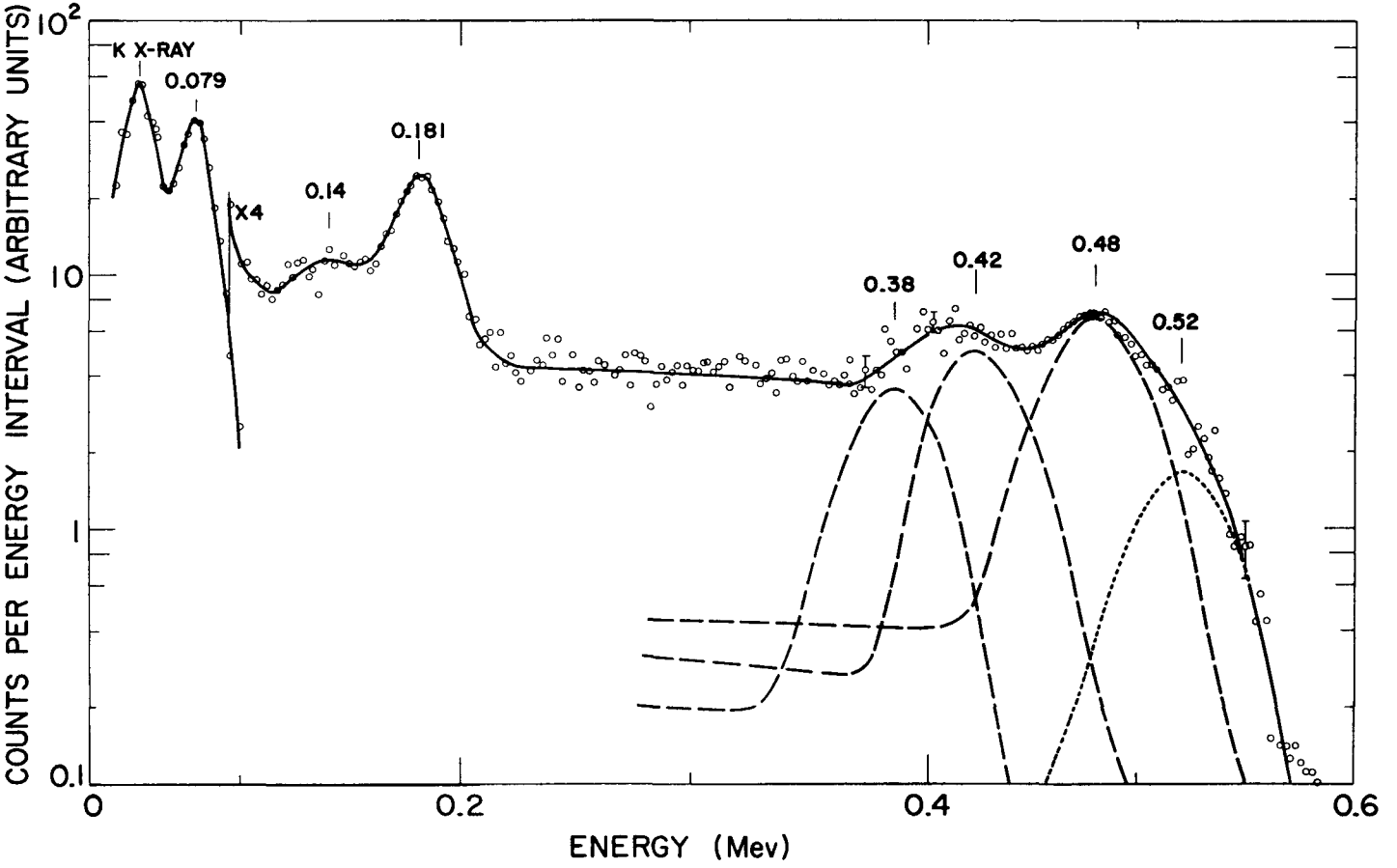

Fig. 18. Gamma-ray spectrum in coincidence with the 1.09-Mev transition.

to this one, except for a strong 0.181-Mev peak. Therefore, it is concluded that the 0.91-Mev transition is also in coincidence with the gamma rays of 0.52, 0.48, 0.42, and 0.38 Mev as well as those of 0.181 and 0.079 Mev.

All of the coincidence data are summarized in Table X. Relative gamma-ray intensities calculated from these coincidence spectra are also given.

TABLE X

Gamma-gamma coincidences observed and relative gamma-ray intensities calculated from these data.

Gamma ray in single-channel window (Mev)	Coincident gamma rays (Mev)	Relative photon intensities
0.181	1.47	4
	1.37	18
	1.28	33
	1.19	14
	0.91	100.0
0.079	1.56	13
	1.52	81
	1.45	31
	1.38	83
	1.09	100.0
0.14	1.46	100.0
	1.38	100
	1.19	6
1.09	~0.51	-
	~0.47	-
	~0.42	-
	~0.38	-

The energies of the beta rays in coincidence with the dominant gamma rays were measured by absorption in aluminum. From these data, end-point energies were determined for the beta rays in coincidence with the gamma rays of 0.079, 0.181, 0.91, 1.09, 1.38,

1.46, 1.52, and 1.60 Mev. The analysis of the data in the energy interval from 1.3 to 1.6 Mev required a decomposition of the coincidence spectra into individual components. The results of these coincidence measurements are summarized in Table XI.

TABLE XI.

Summary of beta-gamma coincidence results.

Gamma-ray energy (Mev)	Coincident beta-ray energies (Mev)
1.60 1.52 }	0.30 ± 0.04
1.46 1.38 }	0.43 ± 0.03
1.09 0.91 }	0.74 ± 0.06
0.181	1.72 ± 0.12 ~0.74 ~0.36
0.079	1.83 ± 0.07

From the relative gamma-ray transition intensities, together with the beta-gamma coincidence data, it follows that the beta-ray branches of (1.72 ± 0.12) and (1.83 ± 0.07) Mev, in coincidence with the 0.181- and 0.079-Mev gamma rays, are in fact two different transitions.

The proposed decay scheme requires the 0.079-Mev gamma ray to be in coincidence with beta-ray branches of about 0.74, 0.45, and 0.32 Mev in addition to the one listed at 1.83 Mev. These were not observed because of the presence of stronger coincidences between the 0.084-Mev gamma ray of Tm^{170} and a 0.88-Mev beta-ray component.

c. Beta-Ray Spectrum

The Fermi plot of the beta-ray spectrum of Tm^{172} is shown in Fig. 19. In the original data, more than 15 000 counts were collected at each point below 1.3 Mev. This spectrum includes the long-lived Tm^{170} which has beta-ray branches of about 0.96 and 0.88 Mev.

As noted in the previous section, it was concluded from the analysis of beta-gamma coincidence data, together with the proposed decay scheme (Fig. 20), that there are two beta-ray transitions differing in energy by 0.1815 Mev; the end-point of the higher energy branch is about 1.80 Mev. These two transitions go to the 0.260- and 0.079-Mev levels. The ground-state beta branch, if present, would then have an energy of about 1.88 Mev. The data in Fig. 19 are not sufficient to allow differentiation of these three components (i.e., the "conventional" analysis, by the use of Stage III of the computer program discussed in Chapter IV, is not possible).

The portion of this spectrum above 1 Mev was analyzed by use of Stage IV of the computer program. The data were fitted with the function

$$\overline{N} = \sum_{j=1}^{J} m_j^2 f(\epsilon_{0j} - \epsilon)^2 \left\{ (1 - \alpha_j) + \alpha_j [(\epsilon_{0j} - \epsilon)^2 L_0 + 9 L_1] \right\} , \qquad (20)$$

where the parameters to be varied are the m_j^2, ϵ_{0j}, and α_j. Fits were made on the assumption of the presence of one, two, three, and four components (J = 1, 2, 3, and 4). The end-point energies were related by $\epsilon_{01} - \epsilon_{02} = 0.1815$ Mev for J = 2, and $\epsilon_{01} - \epsilon_{02} = 0.0787$ Mev and $\epsilon_{01} - \epsilon_{03} = 0.2602$ Mev for J = 3 and J = 4. Thus, except for the case of J = 4, there is only one independent energy parameter. The resulting values of ϵ_{0j}, α_j and the relative intensities are given in fit Nos. 1-4 in Table XII. In column 7 the value of $\chi^2 = \sum_i [(N_i - \overline{N}_i)/\sigma_i]^2$ is given.

TABLE XII

Summary of computer fits to the beta-ray spectrum of Tm^{172}. The decomposition shown in Fig. 19 corresponds to results in fits Nos. 3, 5, and 6.

Fit number	Energy range (Mev)	Number of components	Parameters from fit			χ^2	p
			Energy (Mev)	a	Intensity (arbitrary)		
1	1.00 - 1.87	1	1.847 ± 0.003	0.30	4.6 ± 0.7	60.9	≈ 0.99995
2	1.00 - 1.87	2	1.852 ± 0.003	1.0	4.2 ± 0.1	44.8	0.995
			1.671 ± 0.003	1.0	0.7 ± 0.1		
3	1.00 - 1.87	3	1.880 ± 0.011	1.0	2.1 ± 0.7	22.6	0.57
			1.802 ± 0.011	0.63	2.6 ± 0.5		
			1.620 ± 0.011	1.0	0.07 ± 0.2		
4	1.00 - 1.87	4	1.880 ± 0.011	1.0*	2.1 ± 0.7	22.6	0.57
			1.802 ± 0.011	0.63*	2.6 ± 0.5		
			1.620 ± 0.011	1.0*	0.07 ± 0.2		
			0.0	0.0	0.0		
5	0.38 - 0.98	6	1.880*	1.0*	2.1*	16.3	0.36
			1.802*	0.63	2.6*		
			1.620*	1.0*	0.07*		
			0.962 ± 0.004	0.23	11.0 ± 2.0		
			0.878 ± 0.004	0.0	3.2 ± 1.0		
			0.710*	0.0*	1.1 ± 0.6		
6	0.18 - 0.46	10	1.880*	1.0*	2.1*	9.0	0.47
			1.802*	0.63*	2.6*		
			1.620*	1.0*	0.07*		
			0.962*	0.23*	11.0*		
			0.878*	0.0*	3.2*		
			0.710*	0.0*	1.1*		
			0.420*	0.0*	1.3 ± 0.6		
			0.340*	0.0*	0.0		
			0.280*	0.0*	1.2 ± 1.0		
			0.240*	0.0*	1.9 ± 2.0†		
7	0.46 - 0.98	6	1.880*	1.0*	2.1*	15.6	0.26
			1.802*	0.63*	2.6*		
			1.620*	1.0	0.07*		
			0.963 ± 0.004	0.0*	13.8 ± 1.2		
			0.878 ± 0.004	0.0*	0.3 ± 1.2		
			0.710*	0.0*	0.44 ± 0.4		
8	0.18 - 0.46	8	1.880*	1.0*	2.1*	10.1	0.48
			1.802*	0.63*	2.6*		
			1.620*	1.0*	0.07*		
			0.963*	0.0*	13.8*		
			0.878*	0.0*	0.3*		
			0.710*	0.0*	0.66 ± 0.4		
			0.420*	0.0*	1.8 ± 0.4		
			0.280*	0.0*	2.0 ± 1.0†		

* These parameters were not allowed to vary.

† These intensities are expected to be too large because of the presence of electron scattering in the source at low energies.

From χ^2 and the number of degrees of freedom (i.e., the number of experimental points minus the number of independent parameters), one can compute the probability p of obtaining a better fit. That is, on the assumption that the true spectrum is given by a function of the form (20) with the parameters listed, p is the probability that any one set of experimental data from a large group of such sets would give a better fit (i.e., lower χ^2). These probabilities are given in column 8. A value of p near 1.0 may indicate that the particular form of Eq. (20) used is not correct (e.g., the number of components assumed to be present may be incorrect).

The program is designed to compute the standard deviation associated with the best value of each of the variable parameters, except those for which the final value is at one extreme of the allowable interval of variation (e.g., $m_j^2 = 0$, $a_j = 0$, or $a_j = 1$). In Table XII the uncertainties in the energies are those computed by the program, and include no systematic errors. The uncertainties in the relative intensities are calculated from the errors in the corresponding m_j^2 only and neglect the effect of the errors in ϵ_{0j} and a_j.

It is concluded from the data in Table XII that a ground-state beta transition exists. This conclusion is based on the decrease in p in going from the fit with two components to that with three. As shown, the addition of a fourth component in this region does not further decrease the value of p. And, in fact, the best fit is with zero intensity for a fourth component.

For the best fit, that with three components, the value $a_2 = 0.63$ indicates that the second beta branch consists of a combination of an allowed shape and unique first-forbidden shape. The intensity of the allowed portion is $(6 \pm 6)\%$ of the total intensity. (This error is an estimate.) Therefore, this branch has predominently unique first-forbidden character. It should similarly be noted that the values $a_1 = a_3 = 1.0$ mean that these components have unique first-forbidden

character.

Below 1 Mev the analysis of the Tm^{172} spectrum is hampered by the presence of the Tm^{170} spectrum consisting of two components of about 0.96 and 0.88 Mev. The energy difference $\epsilon_{04} - \epsilon_{05}$, as determined from the reported gamma-ray energy, is 0.0842 Mev. The spectrum of Tm^{170} has been studied by several groups.[62-64] Two of the more recent results[62,63] agree that the 0.88-Mev component constitutes about 24% of the total intensity and that its Fermi plot is linear. However, these reports[62,63] do not agree as to the shape of the Fermi plot of the 0.96-Mev transition. Pohm et al.[62] report that this component is linear ($a_4 = 0$). The shape reported by Graham et al.[63] can not be expressed exactly in the form of Eq. (20); that is, it is not a linear combination of allowed and unique first-forbidden shapes.

Because of this uncertainty in the shape of the Fermi plot of the 0.96-Mev transition, it is not possible to analyze the remainder of the spectrum unambiguously. Two attempts were made to fit the spectrum between 0.71 and 0.96 Mev. In the first case, the values of a_4 and a_5 were allowed to vary (e.g., see fit No. 5 in Table XII). The resulting parameters agree with the previous data[62,63] in that the 0.88-Mev component is linear ($a_5 = 0$) and has an intensity of (23 ± 10)%. On the other hand, the shape of the 0.96-Mev branch is nonlinear ($a_4 = 0.23$), which is not in agreement with the results of Pohm et al.,[62] but is in accord with the nonlinearity observed by Graham et al.[63] The second fit to the data in this region (see No. 7, Table XII) was made on the assumption that both components are linear ($a_4 = a_5 = 0$). The quality of the fits, as given by the values of p, gives no basis for a choice between these two cases, except that in the former case the relative intensities are in better agreement with the experimental results. However, this is not sufficient to discard the second fit for the following reason. The total Fermi plot published by Graham et al.[63] appears to be almost linear. Thus, a combination of two linear components might very well

result in a good over-all fit to the experimental data, but still contain a large error in the relative intensities. Therefore, the analysis of the spectrum below 0.7 Mev was carried out for both of these cases.

The beta-ray intensities, as derived from the gamma-ray intensities, suggest that all the components below 0.8 Mev (see Fig. 20) have allowed or ordinary first-forbidden character. Therefore, the corresponding a_j were all set equal to zero. Also, the end-point energies of all the branches were fixed at those values determined from the gamma-ray energies together with the proposed decay scheme. The resulting relative intensities are given in fits Nos. 5, 6, 7 and 8 in Table XII. The two sets of relative intensities for the components below 0.8 Mev, corresponding to $a_4 = 0$ and $a_4 = 0.23$, agree within one standard deviation. However, the intensity of the 0.71-Mev component calculated with $a_4 = 0.23$ is in much closer agreement with the value calculated from the gamma-ray intensities. Therefore, the values from this decomposition (Nos. 3, 5, and 6) are shown in Table XIII and Fig. 19.

The end-point energies, relative intensities, and log ft values are shown in Table XIII. It should be noted that the relative intensities from the analysis of the beta-ray spectrum are in excellent agreement with those computed from the gamma-ray intensities.

The statistical evaluation of the fit to the complete spectrum is compatible with the data. For 68 experimental points, the value of χ^2 is 47.9. For 17 variable parameters this corresponds to $p = 0.36$; that is, the probability of obtaining a better fit is only 36%.

The log ft values of the three highest energy transitions indicate that they all have unique first-forbidden character ($\Delta I = 2$, yes). This conclusion is supported by the spectral shape, at least for the two higher energy components. The log ft values of the lower energy transitions all lie in the range from 6 to 8, which normally corresponds to ordinary first-forbidden transitions ($\Delta I = 0$ or 1, yes).

TABLE XIII

Summary of beta-ray components.

Energy (Mev)	Relative intensity		Log ft
	From gamma intensities (per cent)	From beta spectrum (per cent)	
1.88 ± 0.02	(20)	24 ± 8	8.9
1.80	25	29 ± 6	8.0
1.62	1 ± 1	1 ± 3	10.0
0.71	14 ± 2	12 ± 6	7.6
0.42	$\leqslant$17	15 ± 7	6.7
0.34	4 ± 3	-	7.0
0.28	$\geqslant$17	13 ± 10	6.2
0.24	2 ± 1	-	6.8
0.15	0.1 ± 0.3	-	7.6

3. Decay Scheme

a. Construction of Level Scheme

The proposed decay scheme is shown in Fig. 20. The existence of levels at 0.079 and 0.260 Mev is in agreement with a diverse group of experimental data. Coulomb excitation experiments[65] suggest the presence of an excited state at 0.079 Mev in Yb^{172}. As previously noted, the internal-conversion-electron data indicate that the 0.079-Mev gamma ray has E2 character. Using this fact together with the relative gamma-ray intensity in the thulium activity, one finds that this transition is more intense than the sum of all the other transitions. Hence, it must go directly to the ground state. Also the beta-gamma coincidence measurements reported herein require that both the 0.079- and 0.181-Mev gamma transitions must go to levels near the ground state. Finally, these two levels in Yb^{172} are also populated in the decay of Lu^{172}. The gamma-gamma coincidences to be expected from the 0.079-0.181 Mev cascade were observed. (These spectra are not shown.)

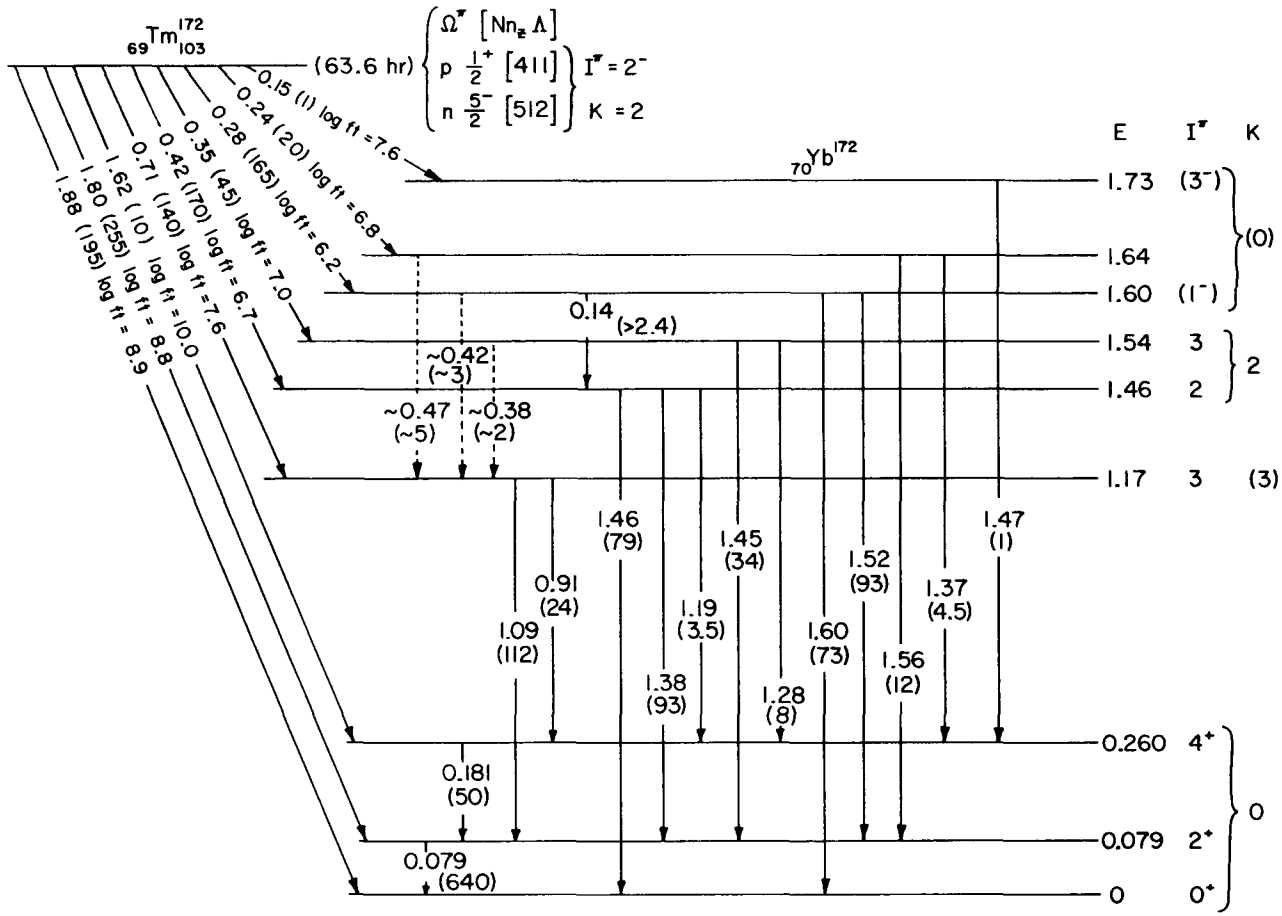

Fig. 20. Proposed decay scheme for Tm^{172}. The relative transition intensities (1000 total decays) are shown in parentheses. All energies are in Mev.

The levels at 1.73, 1.64, 1.54, 1.46, and 1.17 Mev are indicated by the spectrum in coincidence with the 0.181-Mev gamma ray. It is seen that this gamma ray is in coincidence with gamma rays of 1.47, 1.37, 1.28, 1.19, and 0.91 Mev. The absence of coincidences between any two of the latter transitions and the fact that the sum of any pair exceeds the total decay energy of about 1.9 Mev, both support this interpretation.

Of the five radiations in coincidence with the 0.079-Mev gamma ray and not in coincidence with the 0.181-Mev gamma ray (Fig. 17b), four (1.56, 1.45, 1.38, and 1.09 Mev) are associated with transitions to the first excited state from levels deduced in the previous paragraph. The 1.46-Mev gamma ray observed in the singles spectrum (Fig. 14) is interpreted as the transition from the level at 1.46 Mev to the ground state. The fifth radiation, 1.52 Mev, is placed between a level at 1.60 Mev and the first excited state. The existence of this level is further supported by observation of the 1.60-Mev cross-over transition in the singles spectrum.

The experiments involving the 0.14-Mev gamma ray support a number of features of the decay scheme. This transition is placed between the levels at 1.46 and 1.60 Mev. Observation of coincidences between the 0.14-Mev gamma ray and radiations of 1.46, 1.38, and 1.19 Mev tends to confirm this conclusion.

The radiations of approximately 0.47, 0.42, and 0.38 Mev, which are in coincidence with the 1.09-Mev gamma ray (Fig. 18), are interpreted as transitions to the 1.17-Mev level from the states at 1.64, 1.60, and 1.54 Mev.

There are a few weak transitions which have not been discussed. In the analysis of the singles spectrum, there are gamma rays of about 1.00 and 0.51 Mev. There is also evidence that a transition of about 0.52 Mev and several possible radiations below 0.35 Mev are in coincidence with the 1.09-Mev gamma ray. Since there is no

definite evidence for the positions of these radiations in the decay scheme, there are omitted from it.

The results of the beta-gamma coincidence measurements (Table XI) substantiate the existence of the proposed levels at 1.17, 1.46, and 1.60 Mev as well as the placement of the transitions depopulating these levels.

Estimates of the relative intensities of the gamma-ray and beta-ray transitions (total number of transitions = 1000) are given in parentheses. For the transitions above 0.4 Mev, internal conversion is assumed to be negligible. As noted, conversion-electron measurements[60] indicate that the 0.079- and 0.181-Mev transitions have E2 character. Hence the corresponding conversion coefficients were used in calculating these intensities. For the 0.14-Mev transition, the available conversion data are not sufficient to determine the multipolarity. Therefore, only a lower limit is quoted for the intensity.

b. Spins and Interpretations of Levels

Ground-State Rotational Band in Yb^{172}. Since Yb^{172} is an even-even nucleus, the spin and parity of its ground state are assumed to be 0^+. Both the Coulomb excitation data[65] and the fact that the 0.079-Mev transition is E2 require that the first excited state at 0.079 Mev have 2^+ character. The E2 character of the 0.181-Mev transition requires that the spin of the state at 0.260 Mev lie between 0 and 4 and that it have positive parity. The ratio of energies of the levels agrees quite well with that predicted by the $I(I + 1)$ interval rule for rotational levels with $I = 2$ and 4. This fact, together with the systematics of even-even nuclei, suggests that these three levels form a rotational band with $K = 0$, positive parity, and $I = 0$, 2, and 4.

Thulium Ground State. The ground-state spin of the odd-odd nucleus $_{69}Tm^{172}$ is expected to result from the coupling of the 69th proton and the 103rd neutron. The spin of the odd-A nucleus $_{69}Tm^{169}$ has been measured as $\frac{1}{2}$;[66] Mottelson and Nilsson[17] have

interpreted this as the Nilsson level $\frac{1}{2}^+[411]$. The spin[67] of Er^{171} and that[68] of Yb^{173}, which have 103 neutrons, have both been measured as $\frac{5}{2}$; these have been interpreted[17] as the $\frac{5}{2}^-[512]$ level. In general, the resulting spin of Tm^{172} would be given by $I = K = \Omega = |\Omega_p \pm \Omega_n|$, where p and n refer to the odd proton and neutron, respectively. If one assumes that the odd particles in Tm^{172} are in the same states as in the neighboring odd-A nuclei, this relationship gives $I^\pi = 2^-$ or 3^-. Gallagher and Mozkowski[23] have derived coupling rules which predict that the ground state will be the one in which the projections of the intrinsic spins lie in the same direction. For Tm^{172}, this rule predicts that the $I^\pi = 2^-$ state should be the ground state. However, several exceptions to these coupling rules are known.

The spin of the ground state of thulium is determined from the properties of the beta decay to the K = 0 rotational band. The choice I = K = 3 can be excluded, since the decay to the ground state of ytterbium would be third forbidden ($\Delta I = 3$, yes) and should have a log ft value of approximately 15. If K is a good quantum number, the transitions to the first and second excited states would likewise be third forbidden because of the change in the quantum number K ($\Delta K = 3$). However, the measured log ft values are about 9 for all three branches. On the other hand, for the choice I = K = 2 the calculated log ft values agree with those observed experimentally. The unique first-forbidden shape for the transition to the 2^+ level is explained by the change of the quantum number K. It should be pointed out that the assignment I = K = 2 could be deduced without recourse to the arguments concerning the Nilsson levels and the spins of the individual particles.

This assignment is further supported by the agreement between the experimental and theoretical beta-ray branching ratios to the members of the ground-state rotational band. For the case of L = 2 transitions, the theoretical ratios are

$$B(2, 2 \rightarrow 4) : B(2, 2 \rightarrow 2) : B(2,2 \rightarrow 0) = 0.5 : 10 : 7$$

where $B(2,2 \rightarrow I) = (\text{constant}) \left| \langle 222 - 2 \,|\, 2210 \rangle \right|^2$. The corresponding experimental ratios $(0.35 \pm 0.30) : 10 : (6 \pm 4)$, where B = (constant)/ft, agree well within the experimental errors.

A restriction can now be placed on the choice of spins which may be assigned to all the higher levels in Yb^{172}. The beta-ray branches which populate these states are all ordinary first-forbidden (or "slow" allowed) transitions, so that the spins of these levels must be 1, 2, and 3. Also, if one assumes that K is a good quantum number, the value of K for any of these states would similarly be limited to the values 1, 2, and 3.

State in Yb at 1.17 Mev. The state at 1.17 Mev is depopulated by transitions to the 2^+ and 4^+ levels. The intensity of the transition to the 0^+ state is less than 3% of that of the 1.09-Mev gamma ray. If only the changes in I are considered, a spin of either 3 or 4 for the 1.17-Mev level would be consistent with these observations.

This state can then have K = 0, 1, 2, 3, or 4 since $K \leq I$. The value K = 4 is excluded since it would require 2^4-pole radiations for the transitions to the K = 0 band. The lifetimes of such transitions would be too long to allow observation of the measured coincidences. A choice between the remaining possibilities is made on the basis of the relative reduced transition probabilities to the various members of the ground-state band. The theoretical probabilities, which are listed in Table XIV, are considered to be proportional to the squares of the Clebsch-Gordan coefficients $\langle I_i \, L K_i \, K_f - K_i \,|\, I_i \, L I_f K_f \rangle$. Without calculation of the magnetic and electric moments, the relative intensities for the two cases I = 4, K = 1 and I = K = 1 are indeterminate. Hence, these possibilities are ignored in the following discussion.

TABLE XIV

Theoretical relative reduced transition probabilities to the I = 4, 2, and 0 members of a rotational band with K = 0 from states with various values of I and K. The ratios are given in the form $B(L, I \to 4) : B(L, I \to 2) : B(L, I \to 0)$ where $B(L, I_i \to I_f) = (\text{constant}) |\langle I_i\ L\ K_i\ K_f - K_i \mid I_i\ L\ I_f\ K_f \rangle|^2$. (The ratios are read vertically). Where the values are not shown for L = 1 or L = 2, the three corresponding probabilities all vanish.

	I = 4					I = 3				
	K = 3	K = 2	K = 1		K = 0	K = 3	K = 2	K = 1		K = 0
	L = 3	L = 2	L = 2	L = 1	L = 2	L = 3	L = 2	L = 2	L = 1	L = 1
B(L,I→4)	10	3	9	1	10	54	2	5	3	4
B(L,I→2) =	11	1	110	0	11	275	5	2	4	3
B(L,I→0)	0	0	0	0	0	132	0	0	0	0

	I = 2				I = 1				I = 0
	K = 2	K = 1		K = 0	K = 1		K = 0		K = 0
	L = 2	L = 2	L = 1	L = 2	L = 2	L = 1	L = 1		L = 2
B(L,I→4)	1	96	0	18	0	0	0		0
B(L,I→2)	20	15	1	10	1	1	2		1
B(L,I→0)	14	56	0	7	0	2	1		0

For the 1.17-Mev state the corresponding experimental values are

$$B(L,I\to4) : B(L,I\to2) : B(L,I\to0) = \begin{cases} (1.8 \pm 0.4) : 5 : <0.1 & \text{for } L=1 \\ (2.6 \pm 0.6) : 5 : <0.1 & \text{for } L=2 \\ (3.8 \pm 0.8) : 5 : <0.1 & \text{for } L=3 \end{cases}.$$

The only theoretical prediction that is within the experimental limits is the one for I = 3, K = 2. From this it follows that the transitions have quadrupole character. However, this assignment for the K value would imply that this state would be the first excited state of a rotational band based on an intrinsic or vibrational level with I = K = 2. This hypothetical I = 2 state, which should lie about 0.08 Mev below the

1.17-Mev level, is not observed, in spite of the fact that theoretically the beta branch to it would be more intense than that to the 1.17-Mev level.

It is therefore suggested that the 1.17-Mev state has I = K = 3. This means that quadrupole transitions to the K = 0 band are K forbidden by one degree of forbiddenness (i.e., $\Delta K - L = 1$). As discussed on page 30, such transitions usually are slower than the single-particle estimates by a factor of the order of 100 for each degree of forbiddenness. If the 1.17-Mev state has positive parity, the competition is between E2 and M3 transitions. In spite of a hindrance factor of 100 for the E2 probabilities, the transitions would still be expected to be predominantly electric quadrupole. (The finite probabilities for quadrupole radiations indicates that the K value of one of the states involved, probably the 1.17-Mev level, is not pure.)

The assignment of I = 3 to the 1.17-Mev level is supported by the intensity of the beta branch to this level. As noted previously, the fact that log ft = 7.6 implies that this level does not have spin 4.

One would favor the assignment of positive parity to the 1.17-Mev level, as well as to all the higher excited states, on the basis of the log ft values for the beta decay. However, some of these branches might be allowed transitions which are hindered by violations of selection rules for the asymptotic quantum numbers or K.

States at 1.46, 1.54, and 1.64 Mev. It is concluded that the 1.46-Mev state has spin 2 because it decays to all three members of the ground-state band. The value I = 2 requires that K = 0, 1, or 2. A definite choice between these possibilities is made on the basis of the relative reduced transition probabilities to the ground-state band. For quadrupole transitions, the experimental ratios are

$$B(2,I \rightarrow 4) : B(2,I \rightarrow 2) : B(2,I \rightarrow 0) = (6.5 \pm 2) : 10 : (0.8 \pm 0.3).$$

This result is clearly inconsistent with an assignment of K = 0 or 1, but is in good agreement with the choice K = 2 (see Table XIV).

An interpretation of the 1.54-Mev state as a member of a rotational band based on the 1.46-Mev level is consistent with all of the experimental data. The energies of the levels of such a band are given by $E(I) = (\hbar^2/2\mathcal{J})[I(I+1) - K(K+1)]$, with K = 2, $3\hbar^2/\mathcal{J} \approx 0.08$ Mev, and I = 3, 4, etc. For I = 3, the calculated energy of the first excited state of the band is E ≈ 1.54 Mev which agrees with the measured value, well within experimental uncertainty. If the transitions to the K = 0 band are assumed to have quadrupole character, the experimental ratios of the reduced transition probabilities are (2.2 ± 0.4) : 5 : ≈ 0. This is in good agreement with the theoretical ratios of 2 : 5 : 0.

The next rotational state in the K = 2 band based on the 1.46-Mev level would be at approximately 1.64 Mev and have I = 4. Since a state with this energy is, in fact, found in the decay scheme, the transition probabilities are again compared with the theoretical ratios of 3 : 1 : 0. The corresponding experimental ratios are (0.7 ± 0.5) : 1 : 0. From this disagreement, it is concluded that this state is probably not the spin-4 member of the K = 2 rotational band. The accuracy of the data is not sufficient to warrant the consideration of any other interpretation, so no conclusion is reached as to the nature of this state.

States at 1.60 and 1.73 Mev. The state at 1.60 Mev is observed to decay to the 0^+ and 2^+ members of the ground-state band. An upper limit of the intensity of the unobserved 1.34-Mev transition to the 4^+ level is placed at 10% of that of the 1.60-Mev transition. A spin of either 1 or 2 would be acceptable for the 1.60-Mev state. The experimental reduced transition probabilities are

$$B(L, I \rightarrow 4) : B(L, I \rightarrow 2) : B(L, I \rightarrow 0) = \begin{cases} (<0.2) : (1.4 \pm 0.4) : 1 & \text{for } L = 1 \\ (<0.3) : (1.5 \pm 0.4) : 1 & \text{for } L = 2 \end{cases}.$$

From the theoretical predictions in Table XIV, the values for both $I = K = 2$ and $I = 1$, $K = 0$ lie within the experimental errors. If this level has $I = K = 2$, the first excited state of a rotational band based on this level should occur at about 1.68 Mev. The failure to observe transitions to or from such a level suggests that the level at 1.60 Mev does not have $I = K = 2$.

As noted on page 30, several examples of states with $I = 1$, $K = 0$, and negative parity have been reported in even-even deformed nuclei. These are interpreted as states produced by octupole vibrations of the nuclear surface. In a rotational band accompanying this state, one finds the spin sequence 1, 3, 5, etc. If the moment of inertia of the ground-state band is used, the $I = 3$ state should lie approximately 0.13 Mev above the $I = 1$ state. This prediction agrees with the experimental energy for the 1.73-Mev level. For the 1.73-Mev state, only the transition to the 4^+ level has been observed. From an estimate of the upper limit for the intensity of the transition to the 2^+ ($K = 0$) state, the limit on the ratio of the reduced transition probabilities is calculated to be

		experimental	theoretical ($I = 3$, $K = 0$)
$\frac{B(1, I \rightarrow 4)}{B(1, I \rightarrow 2)}$	=	$\frac{4}{\leq 3.3}$	$\frac{4}{3}$

Although this argument is not conclusive, the result is not inconsistent with this interpretation.

The interpretation of these states as the result of an octupole vibration, requires that they have negative parity. If the K selection rules are neglected, the beta-ray transitions have allowed character ($\Delta I = 1$, no). The fact that $\Delta K = 2$ suggests that these

transitions may be expected to be hindered by a factor of the order of 100. The log ft values to be expected would then be increased from the normal range of 4 to 6 to the range of 6 to 8. The experimental log ft values of about 6.2 and 7.6 do lie within the latter range. On the basis of this interpretation, a qualitative explanation can be given for the difference between these two log ft values. The breakdown of the K selection rule is interpreted as meaning that the wave functions of the states at 1.60 and 1.73 Mev contain some terms with K = 1. Then allowed beta transitions take place to the K = 1 portion of the state. The ratio of the reduced probabilities for this allowed beta decay is

$$\frac{B(1,\ 2 \rightarrow 3)}{B(1,\ 2 \rightarrow 1)} = \frac{|\langle 212-1\ |2131\rangle|^2}{|\langle 212-1\ |2111\rangle|^2} = \frac{1}{9} .$$

Thus the branch to the 1.73-Mev level should have a log ft value about one unit higher than that of the branch to the 1.60-Mev level. This is in qualitative agreement with the experimental difference of about 1.4 units.

It is of interest that in $_{68}Er^{166}$ there is a level at 1.66 Mev which has been interpreted as an octupole vibrational state with I = 1, K = 0, and negative parity. Since the energy of this vibrational state is not expected to vary rapidly with neutron and proton number, this information adds support to the proposed interpretation of the 1.60-Mev level in Yb^{172}.

c. Discussion

From the experimental results of this study, it has been concluded that the ground-state spin of Tm^{172} is I = 2. The measured spins of neighboring nuclei and the Nilsson level diagrams combine to indicate that this state results from the coupling of a $\frac{1}{2}^+$ [411] proton and a $\frac{5}{2}^-$ [512] neutron with a result of K = 2 and

negative parity.

The experimental data agree with the previous suggestion of a K = 0 rotational band based on the ground state of Yb^{172}. The observed levels of this band are 0.00, 0.079, and 0.260 Mev with spins and parities 0^+, 2^+, and 4^+, respectively.

It is concluded that a state with I = K = 2 exists at 1.46 Mev. This level might be either a gamma vibrational state or an intrinsic state produced by excitation of a nucleon. This level is the basis of another rotational band with an excited state at 1.53 Mev (I = 3). The second excited state of this band would be at about 1.64 Mev. A state of this energy is, in fact, observed but the probabilities of the transitions to and from this state are not in agreement with such an interpretation.

It has also been noted that the properties of the state at 1.60 Mev are consistent with an assignment I = 1, K = 0. Such an assignment is in agreement with an interpretation of this as an octupole vibrational state. The state at 1.73 Mev can then be interpreted as a rotational state with I = 3, K = 0. The observed probabilities of the beta transitions to these states necessitate a breakdown of the K selection rule. In other words, this interpretation would require these states to include mixtures of a higher K value in their wave functions.

The experimental data for the 1.17-Mev level suggest the assignment I = K = 3. A state with this spin could arise from a particle excitation.

Since there is some evidence for possible intrinsic states of spin 2 at 1.46 Mev and of spin 3 at 1.17 Mev, it is of interest to see if any such states are suggested by theory. The Nilsson level diagrams indicate that at least three particle configurations having these spins can be formed by the excitation of a single nucleon. When only the pertinent levels are considered, the nucleon configurations in the

ground state of thulium and ytterbium are assumed to be

$$\left.\begin{array}{l}\{\frac{1}{2}^{+}[411]\}^{1}\\ \{\frac{1}{2}^{-}[521]\}^{2}\{\frac{5}{2}^{-}[512]^{1}\end{array}\right\} I = K = 2^{-} \text{ for Tm,}$$

$$\left.\begin{array}{l}\{\frac{1}{2}^{+}[411]\}^{2}\\ \{\frac{1}{2}^{-}[521]\}^{2}\end{array}\right\} I = K = 0^{+} \text{ for Yb.}$$

The first excited intrinsic state is formed by decay of a $\frac{1}{2}^{-}[521]$ neutron into the $\frac{1}{2}^{+}[411]$ proton level; the second is obtained when a neutron in the $\frac{5}{2}^{-}[512]$ level decays to a proton in the $\frac{5}{2}^{-}[402]$ level; and the third is produced when the same neutron decays into the $\frac{7}{2}^{+}[404]$ proton level. The particle configurations in these cases are

$$\left.\begin{array}{l}\{\frac{1}{2}^{+}[411]\}^{2}\\ \{\frac{1}{2}^{-}[521]\}^{1}\{\frac{5}{2}^{-}[512]\}^{1}\end{array}\right\} \text{for } I = K = 2^{+} \text{ or } 3^{+} ,$$

$$\left.\begin{array}{l}\{\frac{1}{2}^{+}[411]\}^{1}\{\frac{5}{2}^{+}[402]\}^{1}\\ \{\frac{1}{2}^{-}[521]\}^{2}\end{array}\right\} \text{for } I = K = 2^{+} \text{ or } 3^{+} ,$$

$$\left.\begin{array}{l}\{\frac{1}{2}^{+}[411]\}^{1}\{\frac{7}{2}^{+}[404]\}^{1}\\ \{\frac{1}{2}^{-}[521]\}^{2}\end{array}\right\} \text{for } I = K = 3^{+} .$$

For the beta decay that would populate the first two states, the changes in quantum numbers are identical; they are $\Delta I = \Delta K = \Delta\Omega = 0$ or 1, $\Delta N = \Delta n_z = -1$, $\Delta\Lambda = 0$ with a change in parity. This corresponds to an unhindered first-forbidden transition, which is

compatible with the observed log ft values for the transitions to both the 1.17- and 1.46-Mev levels. In the third case $\Delta N = -1$, $\Delta n = -1$, $\Delta \Lambda = 2$, which corresponds to a hindered first-forbidden transition. The log ft value of 7.6 for the transition to the 1.17-Mev level is also in the range of values observed for other decays of this type.

D. ENERGY LEVELS IN $_{69}Tm^{172}$ FROM THE DECAY OF $_{68}Er^{172}$

1. Introduction

The radioactive nuclide Er^{172}, which decays by beta emission to Tm^{172}, has been reported by Nethaway et al.[58] They report a half-life of 49.8 ± 1.0 hr for the erbium activity. No measurements of the radiations associated with this activity have been reported.

The production of the nuclide Er^{172} has been desribed in the discussion of the daughter nuclide Tm^{172} (page 82). After activation, the Er^{170} samples were separated with an ion-exchange column. These samples contained the radionuclides Er^{169} (9 day), Er^{172}, and some Tm^{172} which had grown back in during and after the separation. The only gamma ray associated with Er^{169} is an 8-kev transition that did not interfer with these studies.

2. Studies of the Internal-Conversion Electrons and the Beta-Ray Spectrum

Several attempts were made to observe the internal-conversion electrons associated with the erbium activity. Chemically separated erbium samples were used as well as sources in which the Tm^{172} daughter had not been removed. The only conversion line which was consistently observed, and which was not associated with some other activity, was interpreted as the K line of a transition of approximately 408 kev. As will be shown, such a transition exists in the erbium activity.

Observation of lower energy conversion lines was prevented by the presence of an intense beta-ray spectrum (end point about 330 kev) resulting from the decay of Er^{169}. This nuclide is

produced by neutron capture in Er^{168} which constituted about 9% of the original source material. At the end of a 50-hr irradiation the calculated specific activity of the Er^{169} is about 6×10^{-6}, compared to the value of 2×10^{-8} for the Er^{172} [Eq. (26)]. After correcting for decay which took place prior to preparation of the sources, these computations indicate that the rate of decay of the Er^{169} was about 1000 times as great as that of the Er^{172}.

The beta-ray spectrum of a chemically separated source was measured in the magnetic spectrometer. Because of the low specific activity [Eq. (26)], this source had to be made very thick in order to have a usable counting rate. Because of the growth of the Tm^{172}, the counting rate at each experimental point on the spectrum was followed for a period of one month as the source decayed. Above about 880 kev, the data at each value of the magnetic field follow (within experimental error) the theoretical curve for the growth and the decay of Tm^{172}. Below 330 kev only the intense beta-ray spectrum of Er^{169} is observable. In the region between about 330 and 880 kev, the experimental data indicate the presence of both Er^{172} and Tm^{172}. In order to separate the erbium spectrum it was necessary to determine what fraction of the original counting rate was due to the daughter Tm^{172}. This was done by graphically fitting the decay curve at each magnetic field setting with an empirical curve. This curve was derived by adjusting the portions of two theoretical decay curves which represent the decay of the two activities considered separately.

The Fermi plot resulting from this analysis is shown in Fig. 21. The errors shown are estimates. This plot suggests the presence of beta branches of about 900 and 400 kev with relative intensities of $(10 \pm 8)\%$ and $(90 \pm 8)\%$, respectively. Because of the complexity of the analysis, the indicated uncertainties are only estimated.

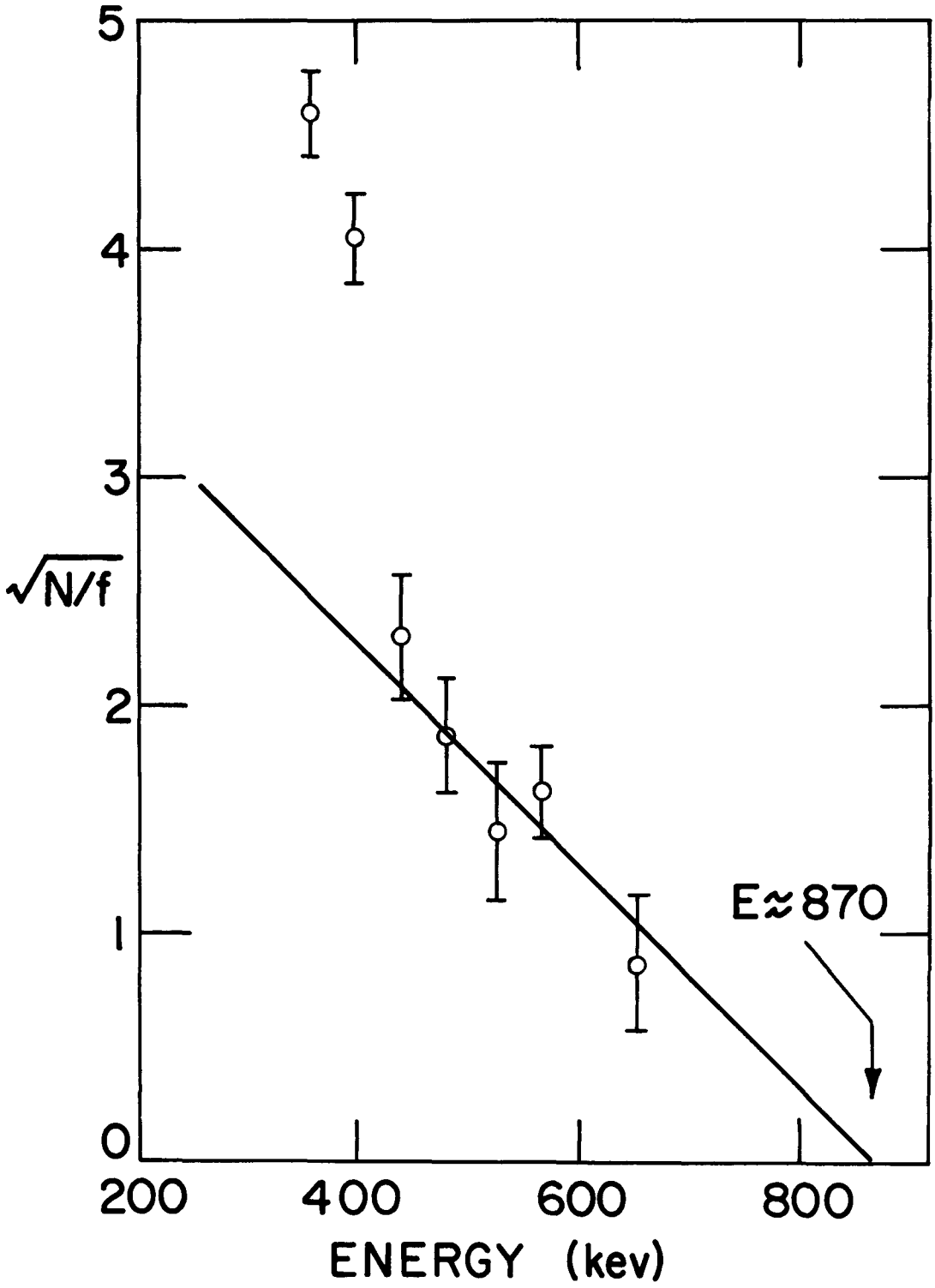

Fig. 21. Fermi plot of the beta-ray spectrum of Er^{172}.

3. Scintillation Studies

a. Singles

The scintillation spectrum of a chemically separated sample is shown in Fig. 22. The decomposition of the spectrum into individual components is shown. The amount of Tm^{172} present is indicated by the intensities of the 181- and 79-kev photopeaks and the Yb K x-ray which are associated with the thulium. The spectral shapes for single gamma rays are interpolated from those of Cs^{137} (662 kev), Au^{198} (412 kev), Ce^{141} (142 kev), and Eu^{152} (122 kev). The shape of the thulium K x-ray peak was derived from the ytterbium K x-ray from a source of Tm^{171} + Tm^{170}. The gamma-ray energies and relative intensities calculated from this spectrum are listed in Table XV.

TABLE XV

Gamma-ray energies and relative intensities calculated from the scintillation spectrum.

Gamma-ray energy (kev)	Relative Intensity
610 ± 8	42
450 ± 10	2.7 ± 1.5
408 ± 4	44 ± 5
200 ± 6	0.8 ± 0.4
160 ± 4	1.0 ± 0.5
125 ± 3	3.1 ± 1.0
K x ray	69 ± 15

b. Sum Spectra

The singles spectrum in Fig. 22 was measured in the geometric arrangement shown in Fig. 5(a), in which the collimator defines a solid angle of approximately 0.3% of 4π. This small solid angle, together with the absorbers used, reduces the summing of any coincident radiations to a negligible amount. In order to investigate any strong coincidence relationships, singles spectra were taken with solid angles of nominally 2π (with one crystal) and 4π

(with two crystals) as depicted in the insert of Fig. 23. (When two crystals are used, the gains of the photomultipliers are matched and the output pulses are added electronically before being amplified.)

The observed spectra are shown in Fig. 23. There is no detectable summing with the 610-kev gamma ray; therefore the two curves have been normalized on this photopeak. In curve (a), for 2π solid angle, a sum peak appears at about 460 kev and is interpreted as the sum of a 50-kev radiation and the 408-kev gamma ray. This conclusion is supported by a corresponding decrease in the intensity of the 408-kev photopeak. In curve (b), (the case of 4π solid angle), there is a peak at 510 kev, in addition to the peak at 460 kev. The 510-kev peak is interpreted as a "double-sum" peak which is produced by the summing of a 408-kev gamma ray with two 50-kev radiations. The possibility that these sum peaks result from accidental summing of noncoincident radiations is ruled out by two independent facts. First, any radiation intense enough to cause accidental sums with the 408-kev gamma ray, would likewise cause sums with the 610-kev gamma ray. Since no sums of any type were observed with the 610-kev transitions, all of the observed sums must be real. Second, to further verify this conclusion these spectra were also measured with a source that was one-fourth as strong. The spectral shapes were identical, within experimental errors, with those in Fig. 23. (The intensity of an accidental sum peak varies as the square of the source strength, while that of a real sum peak varies as the source strength.) Therefore, it is concluded that there must be two radiations of approximately 50 kev. These radiations are in coincidence with each other and with the 408-kev transition. Each of the 50-kev radiations could result from a transition of approximately 50 kev, or from K conversion of a transition whose energy is higher than the K-electron binding energy of 59.4 kev. A 100-kev sum peak, corresponding to the summing of two 50-kev radiations, was also observed in many spectra taken with a large solid angle.

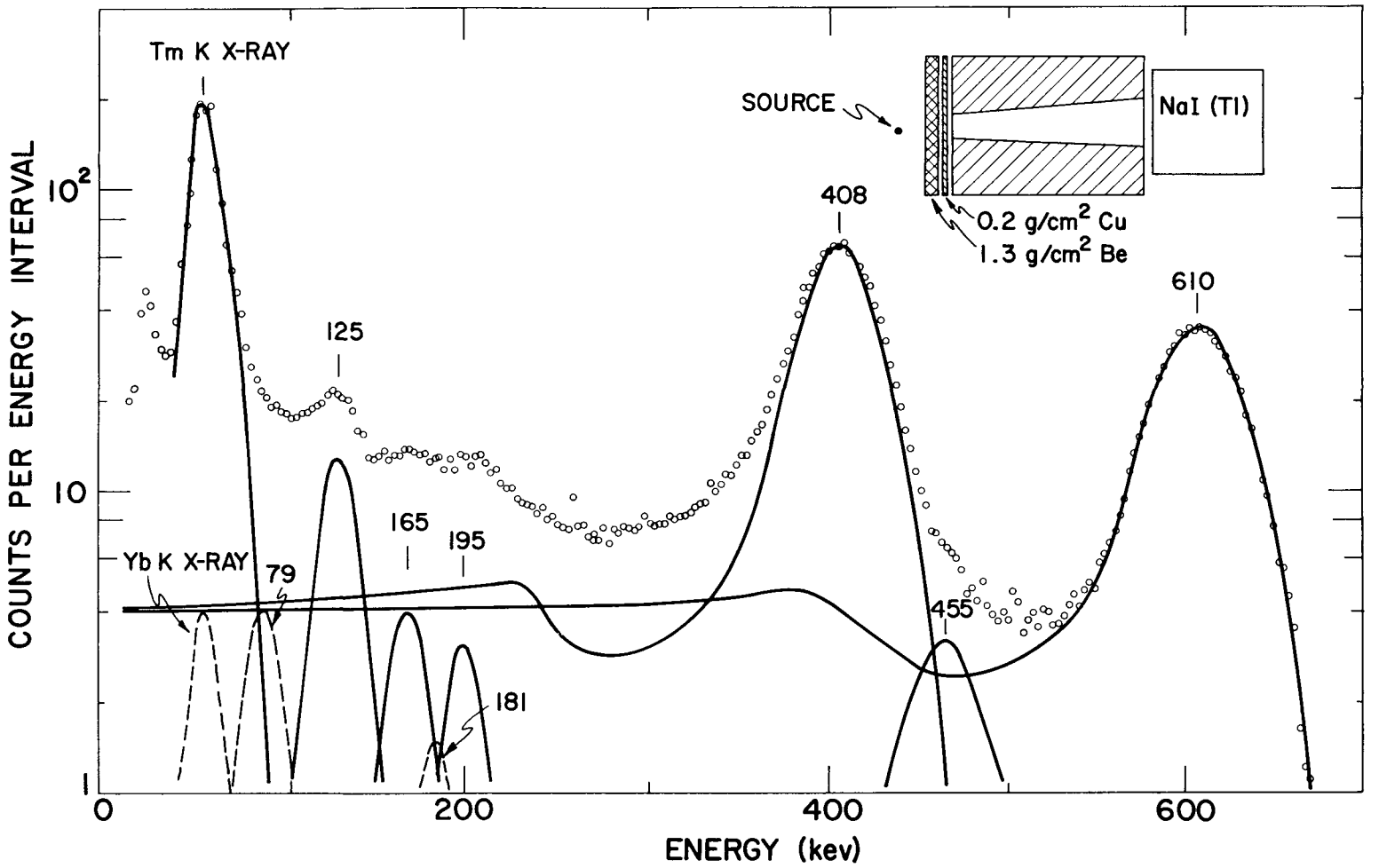

Fig. 22. Gamma-ray spectrum of Er^{172}. The dashed lines represent the contribution of the thulium daughter.

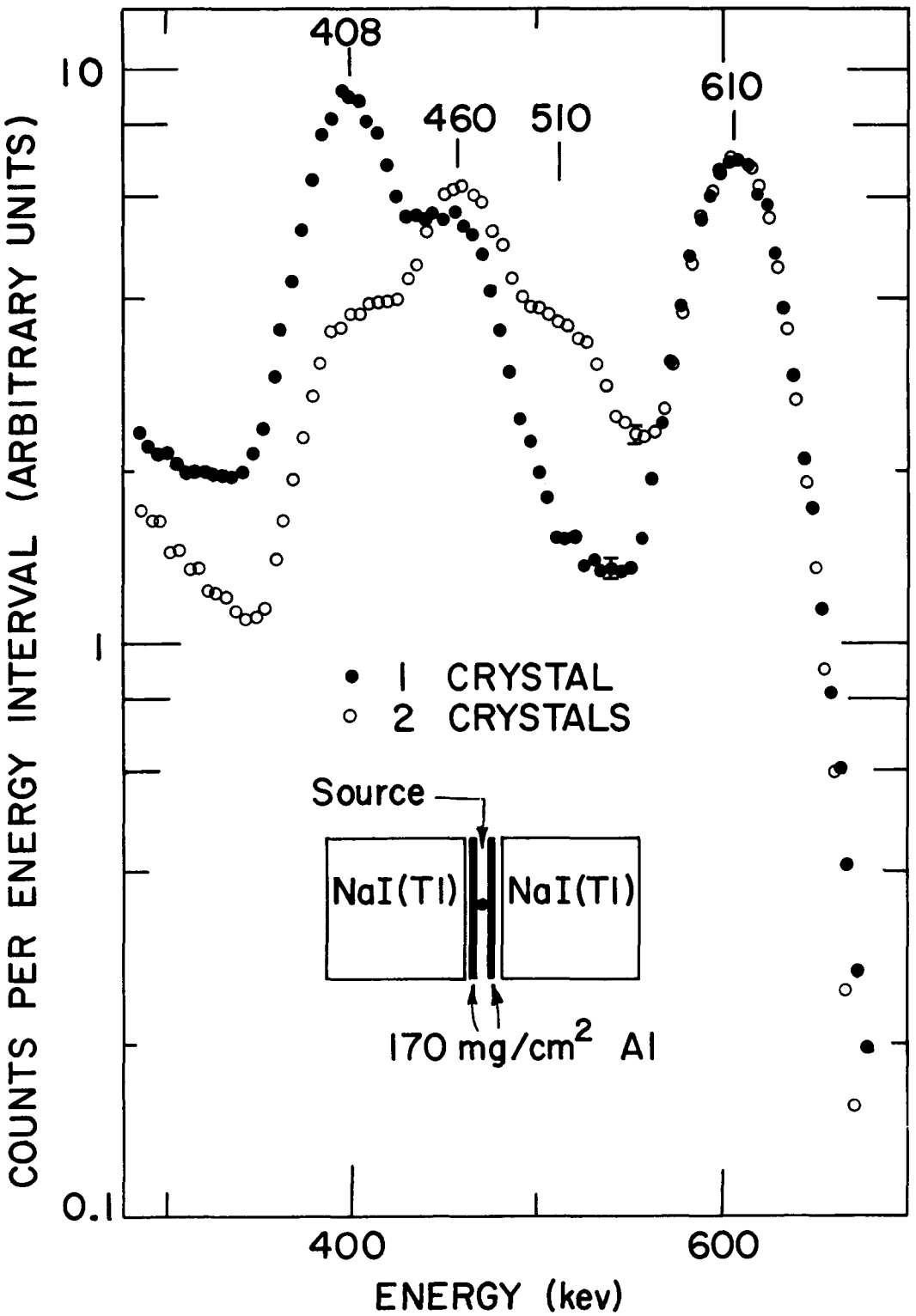

Fig. 23. Sum spectra of Er^{172}.

c. Beta-Gamma Coincidence Measurements

The end-point energies of the beta-ray components in coincidence with the dominant gamma-ray transitions were measured by the standard aluminum absorption method. These data indicate that the 610- and 408-kev gamma rays are in coincidence with beta branches of (310 ± 30) and (370 ± 30) kev, respectively. The difference in the energies of these two beta-ray components is estimated to be 60 ± 20 kev.

It was not possible to determine the energies of the beta rays in coincidence with the other radiations. However, there was no indication of the existence of any beta branches other than these two.

d. Gamma-Gamma Coincidence Measurements

No gamma rays were found to be in coincidence with the 610-kev transition.

A series of coincidence spectra were measured in order to determine the radiations in cascade with the 408- and 450-kev transitions. This set of runs was taken with a single-channel analyzer window about 20 kev wide. Five successive spectra were measured with the analyzer set to accept adjacent portions of the spectrum between about 380 and 480 kev. The geometric arrangement shown in the insert of Fig. 24 was chosen to prevent scattering from one crystal to the other. The Cu absorbers are used to reduce the 100- and 460-kev sum peaks in the multichannel and single-channel spectra, respectively. Two of the resulting spectra are shown in Fig. 24. These two spectra are normalized to the same counting interval and source strength for the erbium activity. (The radiations resulting from the decay of Tm^{172} are not normalized.) Analysis of these spectra indicates that the 408-kev transition is in coincidence with radiations of 200 ± 6, 160 ± 15, and 125 ± 4 kev, in addition to the K x ray. The 450-kev gamma ray is in coincidence only with a 160 ± 4 kev transition and the K x ray. This analysis also indicates that the numbers of 160-kev transitions in coincidence with the 408- and 450-kev gamma rays are about equal. The photopeaks at 79 and 181 kev, as well as a portion of the K x-ray peaks,

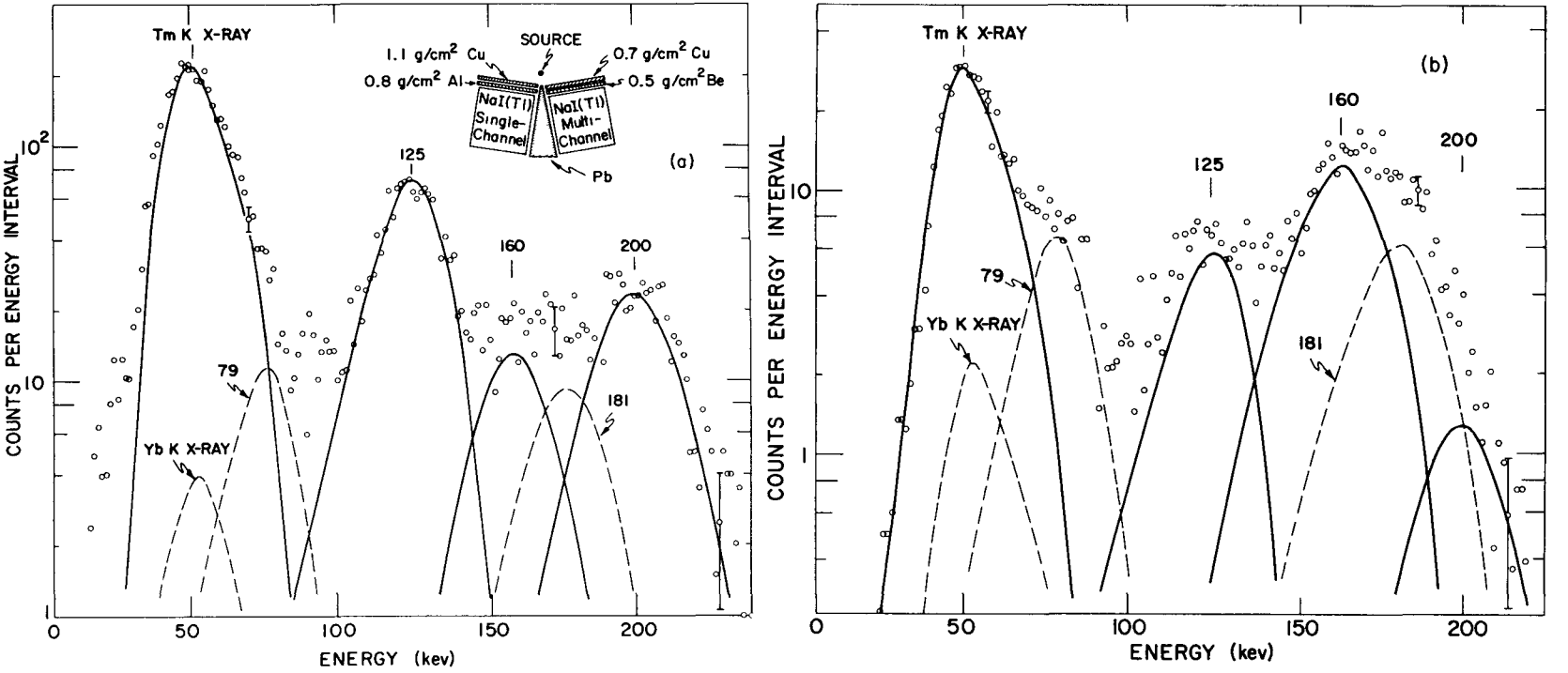

Fig. 24. Gamma-gamma coincidence spectra for Er^{172}. Spectra in coincidence with the (a) 410-kev and (b) 450-kev regions.

result from coincidences following the decay of the daughter Tm^{172}. These transitions are in coincidence with several radiations between 400 and 1600 kev.

A series of spectra was taken with the single-channel analyzer window accepting portions of the spectrum below 250 kev. The results of the analysis of these data are consistent with the above interpretation.

In addition to the experiments described above, a thorough search was made for any coincidences between the 125-, 160-, and 200-kev gamma rays. None were found.

In order to investigate further the nature of the 50-kev radiations which sum with the 408-kev peak, the triple-coincidence circuit (Fig. 6) was used. Two triple coincidence spectra were measured. In the first, the two single-channel analyzers were set to bracket the 408- and 50-kev peaks. The resulting coincidence spectrum displayed only a peak corresponding to the K x ray. In the second experiment, both single-channel windows were set to bracket the K x-ray peak. The resulting spectrum, which is shown in Fig. 25, exhibits peaks at 408 kev and at the K x-ray energy. This result suggests two possibilities. Either there are three low-energy transitions producing 50-kev radiations, all of which are in coincidence with each other; or the x rays in Fig. 25 result from internal conversion of the 410-kev transition. A combination of both effects may be present.

If one assumes that the 408-kev transition is in cascade with only two 50-kev radiations, an estimate of its K conversion coefficient can be made from these data. For any other decay scheme this calculation yields an upper limit for α_K^{408}. It is assumed that the detection efficiencies of crystals 1 and 2 (Fig. 6) are identical in the energy range of interest and that the efficiency of crystal 3 is the same for all three 50-kev radiations. It then can be shown that

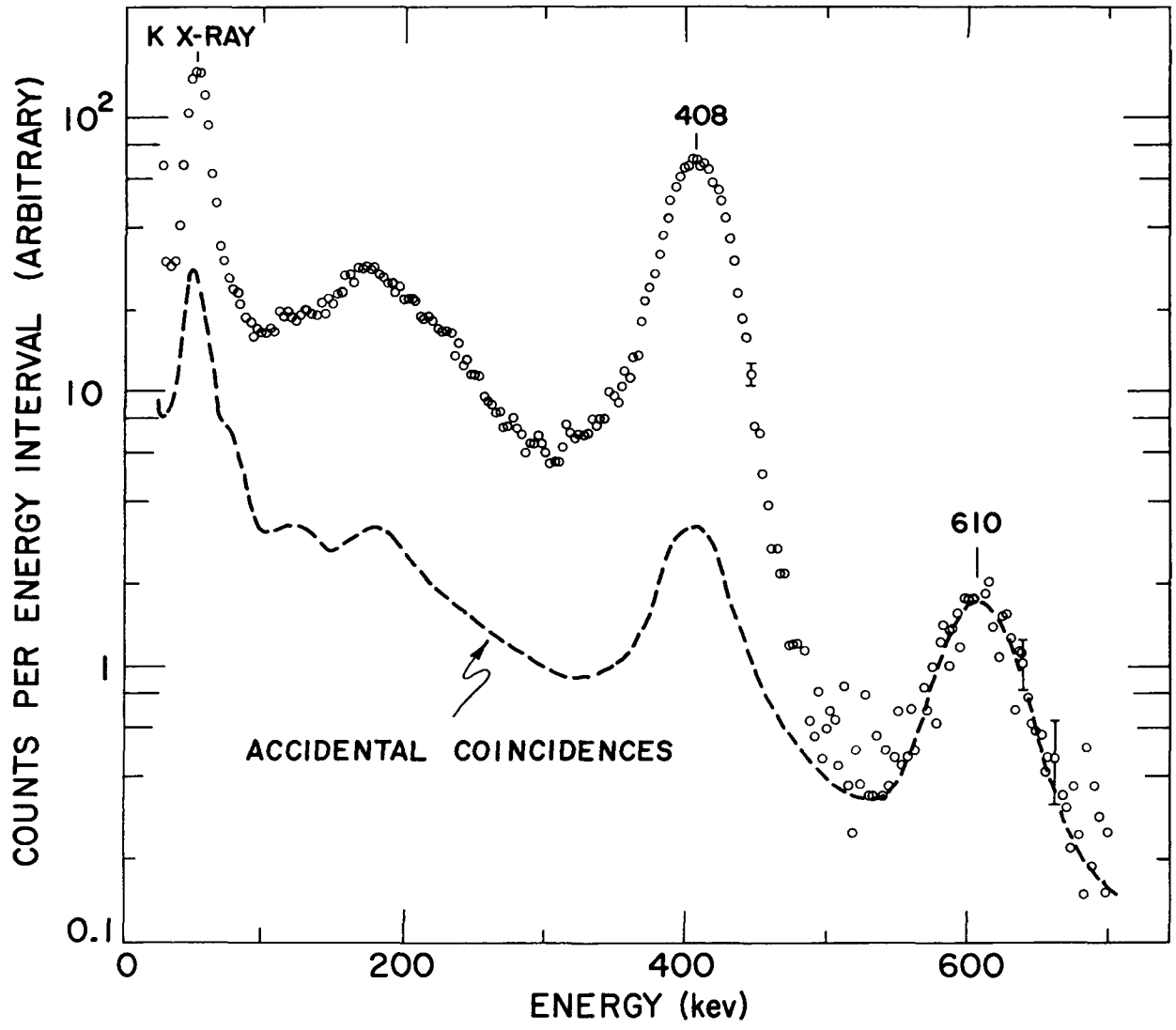

Fig. 25. Gamma-ray spectrum in coincidence with two 50-kev radiations.

$$\alpha_K^{408} = \frac{N^x \quad \epsilon^{408}}{N^{408} \quad 3\epsilon^x \quad \omega},$$

where N^x and N^{408} are the number of counts in the x ray and 408-kev peaks, ϵ^{408} and ϵ^x are the detection efficiencies for 408-gamma rays in crystal 1 and for K x rays in crystal 3, respectively, and ω is the fluorescence yield. Experimentally $N^x/N^{408} = 0.74 \pm 0.15$ and $\epsilon^{408}/\epsilon^x = 0.46 \pm 0.1$; these values yield $\alpha_K^{408} = 0.12 \pm 0.05$. The corresponding theoretical values[7] of α_K^{408} are

E1	0.0077	E2	0.023	E3	0.063
M1	0.055	M2	0.18	M3	0.50.

The observation of coincidences with the 408-kev transition limits the lifetime of this transition to a value less than about 10^{-7} sec. This restricts the multipole order to dipole or quadrupole. The value $\alpha_K^{408} \approx 0.12$ is then consistent with a transtion which is either predominantly M1 or M2. However, if there are three 50-kev radiations, in addition to those from the 408-kev transition, in coincidence with each other, this result could be consistent with an E1 or E2 transition.

4. Decay Scheme

a. Construction

The proposed decay scheme is shown in Fig. 26. The relative transition intensities are shown in parentheses.

The absence of any gamma rays in coincidence with the 610-kev transition indicates that this transition goes to the ground state and that there is an excited state at 610 kev. From the coincidence of this gamma ray with a beta-ray branch of approximately 310 kev, it follows that the total decay energy is about 900 kev.

The observation of 408-200 kev gamma-ray coincidences suggests that this cascade is parallel to the 610-kev transition. The intermediate level is placed at 408 kev for several reasons. First, the 408-kev gamma ray is much more intense than the 200-kev transition, even when possible conversion is considered. Second, the 408-kev transition is in coincidence with betas of about 370 kev, and

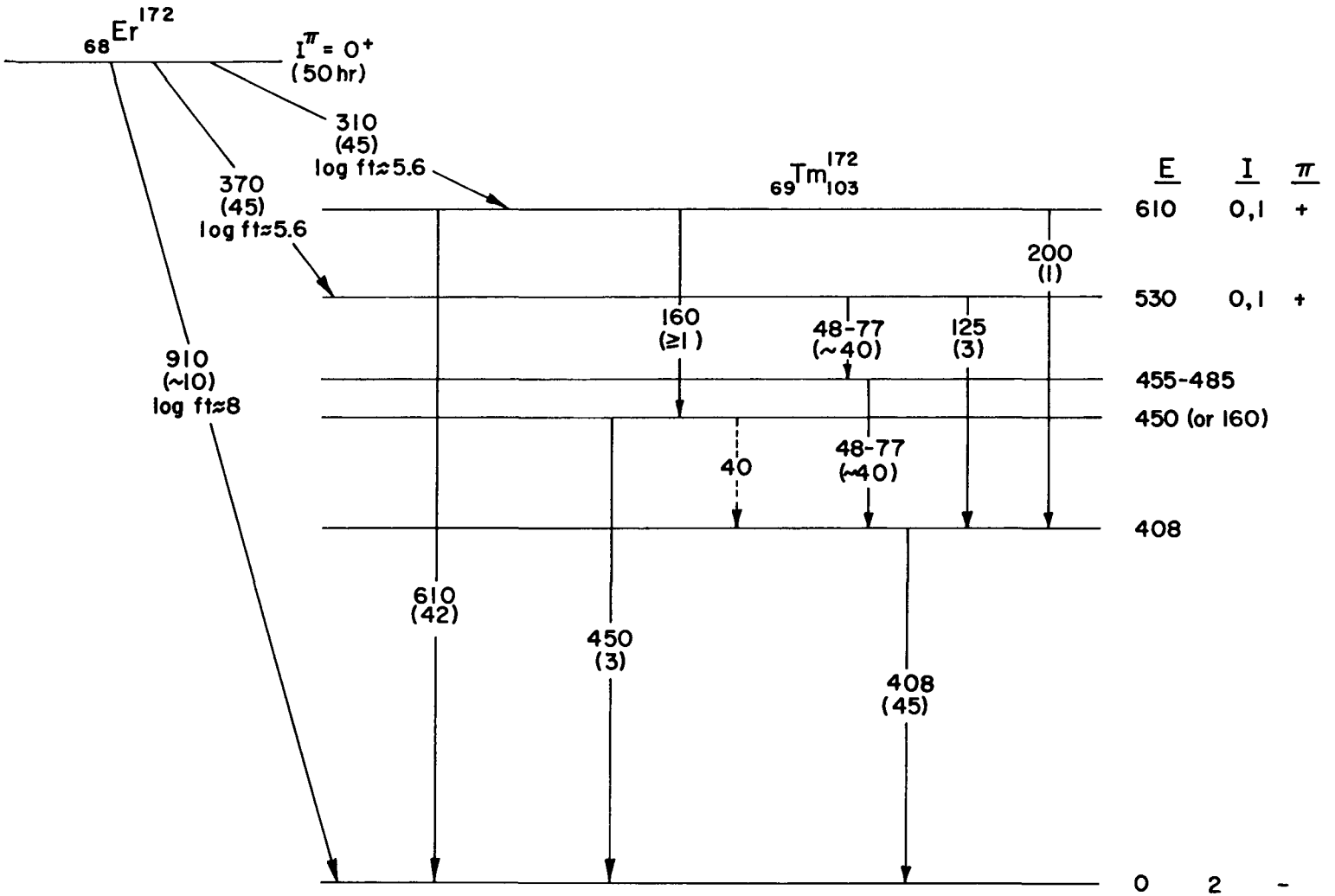

Fig. 26. Proposed decay scheme of Er^{172}. The relative transition intensities (in percent of decays) are shown in parentheses. All energies are in kev.

therefore can not depopulate the 610-kev level. These beta-gamma coincidence data require that the 408-kev level is populated via a level of about 900 - 370 = 530 kev. The transitions between this 530-kev state and the 408-kev level are concluded to be the two transitions which produce the intense 50-kev radiations in parallel with the 125-kev gamma ray. The energy of each of the two transitions producing 50-kev radiations must be above about 48 kev. If it is accepted that the sum of the two transitions is 125 kev, an upper limit of about 77 kev may be placed on these energies. Thus the level between these transitions is placed at 470 ± 15 kev.

The coincident gamma rays of 450 and 160 kev also sum to 610 kev. The sequence of the transitions is not unambiguous. However, placement of the intermediate level at 450 kev is preferred. If the intermediate state were placed at 160 kev, one would have to postulate a transition of about 150 kev between the 610- and 470-kev levels in order to explain the observed 408-160 kev coincidences. Also in this case one might expect to observe transitions from the high-energy states to the 160-kev level. With the intermediate state at 450 kev, as is shown in Fig. 26, one must still postulate an additional transition to explain the 408-160 kev coincidences. This gamma ray could be either a 150 ± 20 kev transition between the 610- and 470-kev levels, or a 40-kev transition between the levels at 450 and 408 kev. The latter possibility is shown in the decay scheme.

For the beta-ray branches to the 530- and 610-kev levels, the log ft values indicate the transitions have allowed character. There is no experimental evidence for beta-ray transitions to the 408-, 450-, and 470-kev levels. The log ft value of the branch to the ground state suggests that this transition probably has unique first-forbidden character.

b. Spin Assignments

Since Er^{172} is an even-even nucleus, the spin and parity of its ground state are assumed to be 0^+.

From the study of the decay of Tm^{172}, the spin and parity of the ground state of Tm^{172} were concluded to be 2^-. These two spin assignments are consistent with the unique first-forbidden character of the beta transition to the ground state.

Since the beta transitions to the 610- and 530-kev levels are allowed, the spin of each of these levels is either 0 or 1 with positive parity. There is no experimental information on which to base a choice between these values. (It is only of interest to note that these states could be members of a rotational band if the 530-kev level has spin 0. The 610-kev level would then have $I = 1$ and $K = 0$.)

From the apparent absence of the beta decay to the levels at 410, 450, and 470 kev, it is concluded that these states have $I \geq 2$.

CHAPTER VI. Summary

The decay schemes of three radioactive nuclides Dy^{166}, Tm^{172}, and Er^{172} have been studied. Prior to this investigation, no decay schemes had been proposed for any of these. Each nuclide was produced by the successive capture of two neutrons in a single stable nucleus. In order to obtain chemically pure sources, separations were carried out in an ion-exchange column.

Continuous beta-ray spectra were measured in a magnetic beta-ray spectrometer. Gamma-ray transitions were studied with internal-conversion-electron spectrographs and with a multichannel scintillation spectrometer. Gamma-gamma and beta-gamma coincidence measurements were performed in order to determine the decay schemes. When possible, spin, parity, and other appropriate quantum numbers were assigned. These assignments are based on the unified model description of axially symmetric nuclei.

The results of this study are summarized below. Also included is a brief list of the type of additional measurements which the author feels would be helpful in verifying or completing the proposed decay schemes.

Dy^{166}. Six gamma-ray transitions were found, along with evidence for four beta-ray branches. Excited states in the odd-odd nucleus $_{67}Ho^{166}$ were established at 54.2, 82.5, 370, and 428 kev. The total decay energy was found to be approximately 483 kev. It has been proposed that the levels at 0, 54, and 82 kev form a rotational band with K = 0 and negative parity. They have the spin sequence 0, 2, 1. The deviation of the level energies from the I(I + 1) interval rule is apparently due to an interaction between the unpaired neutron and proton. The theoretical explanation of the deviation (discussed in Chapter V) predicts energy levels of $E(I) = (\hbar^2/2\mathcal{J})\,I\,(I+1) + \Delta E\ \delta_{I,\mathrm{odd}}$ for K = 0 bands in odd-odd nuclei.

The report of Geiger et al.[56] confirms a major portion of the proposed decay scheme. It would be of interest to verify the 1^+ spin assignment of the 428-kev level by directional correlation measurements between successive gamma rays or between a gamma ray and a conversion-electron line.

Tm^{172}. Analysis of the gamma-ray spectra indicated the existence of at least 17 gamma-ray transitions. From the gamma-gamma and beta-gamma coincidence data, a level scheme was constructed for the even-even nucleus $_{70}Yb^{172}$. The levels, along with the spin and parity assignments, are 0 (0^+), 0.079 (2^+), 0.260 (4^+), 1.17 (3), 1.46 (2), 1.54 (3), 1.60 (1), 1.64, and 1.73 (3) Mev. The total decay energy was found to be approximately 1.88 Mev. The first three states (0, 0.079, and 0.260 Mev) form a rotational band with K = 0 and positive parity. The states at 1.46 and 1.54 Mev are interpreted as members of a rotational band with K = 2. Tentatively, the states at 1.60 and 1.73 Mev are interpreted as members of a rotational band with K = 0 and negative parity. Such a band with I = 1, 3, 5, . . . has been observed in several nuclei. The state at 1.17 Mev is tentatively assigned K = 3. Such a state could be associated with the excitation of a particle. The beta-ray spectrum was analyzed by the use of a computer program that performs a least-squares fit simultaneously to several components. From this analysis it was concluded that the spin of the thulium ground state is I = K = 2 with negative parity.

Above 1 Mev the gamma-ray spectra of Tm^{172} are very complex. The analyses of these spectra are to some extent speculative because of the low resolution inherent in scintillation spectrometry. Therefore, a verification of the existence of the gamma-ray transitions reported by techniques which are able to clearly resolve the many transitions would be desirable (e.g. by observation of the conversion lines). If feasible, the spin assignments should be verified by gamma-gamma directional correlation measurements. Also a

measurement of the ground-state spin of Tm^{172} would be useful.

Er^{172}. Eight gamma-ray transitions were found along with three beta-ray transitions. Gamma-gamma, beta-gamma, and gamma-gamma-gamma coincidence measurements were carried out in order to deduce the decay scheme. The proposed scheme has excited states in the odd-odd nucleus $_{69}Tm^{172}$ at 408, 450 (or 160), 475 ± 15, 530 and 610 kev. The total decay energy was found to be 900 kev. The three observed beta-ray transitions populate the levels at 0, 530 and 610 kev. From the beta-ray intensities it was concluded that the states at 530 and 610 kev have I = 0 or 1 and positive parity, and the states at 408, 450 (or 160), and 475 kev have $I \geq 2$. These data are consistent with the assignment of $I^{\pi} = 2^{-}$ for the ground state of thulium.

The chief problem in this study was the presence of the Er^{169} with its intense 330 kev beta spectrum. This difficulty would be obviated only by the use of samples that have a much lower abundance of Er^{168}. With this problem solved, internal-conversion-electron studies would be useful in determining the energies of the transitions. Directional correlations between gamma rays and conversion electrons might then be feasible for determining the spins of some of the excited states.

BIBLIOGRAPHY

1. E. Fermi, Z. Physik 88, 161 (1934).
2. T. D. Lee and C. N. Yang, Phys. Rev. 104, 254 (1956).
3. C. S. Wu, E. Ambler, R. W. Hayward, D. D. Hoppes, and R. P. Hudson, Phys. Rev. 105, 1413 (1957).
4. J. S. Allen, R. L. Burman, W. B. Herrmannsfeldt, P. Stahelin, and T. H. Braid, Phys. Rev. 116, 134 (1959), and references therein.
5. M. E. Rose, C. L. Perry, and N. M. Dismuke, Tables for the Analysis of Allowed and Forbidden Beta Transitions, ORNL-1459 (1953) (unpublished). See also Beta- and Gamma-Ray Spectroscopy, edited by K. Siegbahn (Interscience Publishers Inc., New York, 1955), Appendix III.
6. M. E. Rose, Internal Conversion Coefficients (Interscience Publishers, Inc., New York, 1958).
7. L. A. Sliv and I. M. Band, Coefficients of Internal Conversion of Gamma Radiation: K- and L-Shell, (Academy of Sciences of the U.S.S.R., Leningrad, 1956), issued in U.S.A. as Reports 57 ICC K1 and 58 ICC L1, P. Axel, Physics Department, University of Illinois.
8. M. G. Mayer and J.H.D. Jensen, Elementary Theory of Nuclear Shell Structure (John Wiley and Sons, Inc., N.Y., 1955).
9. M. G. Mayer, Phys. Rev. 75, 1969 (1949); O.Haxel, J. H.D. Jensen, and H. E. Suess, Phys. Rev. 75, 1766 (1949).
10. B. H. Flowers, Phil. Mag. 25, 329 (1954).
11. L. W. Nordheim, Revs. Modern Phys. 23, 322 (1951).
12. S. A. Moszkowski, Beta- and Gamma-Ray Spectroscopy, edited by K. Siegbahn (Interscience Publishers Inc., New York, 1955), Chapter XIII.
13. C. H. Townes, H. M. Foley, and W. Low, Phys. Rev. 76, 1415 (1949); M. Goldhaber and A. W. Sunyar, Phys. Rev. 83, 906 (1951).

14. A. Bohr and B. R. Mottelson, Kgl. Danske Videnskab. Selskab, Mat.-fys. Medd. 27, No. 16 (1953).

15. J. Rainwater, Phys. Rev. 79, 432 (1950).

16. S. G. Nilsson, Klg. Danske Videnskab. Selskab, Mat.-fys. Medd. 29, No. 16 (1955).

17. B. R. Mottelson and S. G. Nilsson, Kgl. Danske Videnskab. Selskab, Mat.-fys. Skrifter 1, No. 8 (1959).

18. E. U. Condon and G. H. Shortley, Theory of Atomic Spectra (Cambridge University Press, London, 1935).

19. G. Alaga, K. Alder, A. Bohr, and B. R. Mottelson, Kgl. Danske Videnskab. Selskab, Mat.-fys. Medd. 29, No. 9 (1955).

20. G. Alaga, Phys. Rev. 100, 432 (1955); Nuclear Phys. 4, 625 (1957).

21. A. Bohr, Kgl. Danske Videnskab. Selskab, Mat.-fys. Medd. 26, No. 14 (1952); A. K. Kerman, Kgl. Danske Videnskab. Selskab, Mat.-fys. Medd. 30, No. 15 (1956); T. V. Marshall, University of California Radiation Laboratory Report, UCRL - 8740 (1950) (unpublished).

22. R. K. Sheline, Revs. Modern Phys. 32, 1 (1960).

23. C. J. Gallagher, Jr. and S. A. Moszkowski, Phys. Rev. 111, 1282 (1958).

24. C. J. Gallagher, Nuclear Phys. 16, 215 (1960).

25. F. Asaro, I. Perlman, J. O. Rasmussen, and S. G. Thompson, Phys. Rev. 120, 934, (1960).

26. D. Kurath, Argonne National Laboratory Report ANL-6130 and ANL-6214 (1960) (unpublished).

27. A. S. Davydov and G. F. Filippov, Nuclear Phys. 8, 237 (1958); also Acta Phys. Acad. Sci. Hung. 9, 169 (1958).

28. G. R. DeMille, T. M. Kavanagh, R. B. Moore, R. S. Weaver, and W. White, Can. J. Phys. 37, 1036 (1959).

29. A. S. Davydov and U. S. Rostovski, Nuclear Phys. 12, 58 (1959).

30. A. Davydov and G. Filippov, Nuclear Phys. 10, 654 (1959).

31. D. M. Van Patter, Nuclear Phys. 14, 42 (1959-60). See also references therein.

32. C. A. Mallman and A. K. Kerman, Nuclear Phys. 16, 105 (1960).

33. J. Danysz, Le Radium 9, 1 (1912), and 10, 4 (1913).

34. W. C. Rutledge, J. M. Cork, and S. B. Burson, Phys. Rev. 86, 775 (1952); J. Cork, Phys. Rev. 72, 581 (1947).

35. S. B. Burson, D. W. Martin, and L. C. Schmid, Rev. Sci. Instr. 30, 513 (1959).

36. This program was compiled by W. J. Cody and J. A. Gregory of the Applied Mathematics Division of Argonne National Laboratory in cooperation with S. B. Burson and R. G. Helmer.

37. F. T. Porter, M. S. Freedman, T. B. Novey, and F. Wagner, Jr., Argonne National Laboratory Report ANL-5525 (1956) (unpublished).

38. R. W. Schuman and J. P. McMahon, Rev. Sci. Instr. 27, 675 (1956).

39. See for example C. M. Davisson, Beta- and Gamma-Ray Spectroscopy, edited by K Siegbahn (Interscience Publishers Inc., New York, 1955), Chapter II.

40. D. W. Martin, Dissertation, University of Michigan (1956) (unpublished).

41. Radiochemical Studies: The Fission Products, edited by C. D. Coryell and N. Sugarman (McGraw-Hill Book Company, Inc., 1951), Book 1, p. 18.

42. B. H. Ketelle and G. E. Boyd, J. Am. Chem. Soc. 69, 2800 (1947).

43. G. R. Choppin and R. J. Silva, J. Inorg. and Nuclear Chem. 3, 153 (1956); H. L. Smith and D. C. Hoffman, J. Inorg. and Nuclear Chem. 3, 243 (1956).

44. Obtained from Alexander Vacuum Research, Inc., 258 Madison Avenue, New York, New York.

45. B. H. Ketelle, Phys. Rev. 76, 1256 (1949).

46. F. D. S. Butement, Proc. Phys. Soc. (London) A63, 532 (1950).

47. "Equilibrium" is here used in reference to a source which has aged for a sufficiently long time so that the holmium daughter no longer exhibits its own characteristic 27-hr period, but rather decays with the 80-hr period of the Dy^{166} parent.

48. E. L. Chupp, J. W. M. DuMond, F. J. Gordon, R. C. Jopson, and H. Mark, Phys. Rev. 112, 518 (1958).

49. J. S. Fraser and J. C. D. Milton, Phys. Rev. 98, 1173A (1955).

50. E. Feenberg and G. Trigg, Revs. Modern Phys. 22, 399 (1950).

51. R. L. Graham, J. L. Wolfson, and M. A. Clark, Phys. Rev. 98, 1173A (1955); see also J. M. Cork, M. K. Brice, R. G. Helmer, and R. M. Woods, Jr., Phys. Rev. 110, 526 (1958).

52. L. S. Goodman, W. J. Childs, Richard Marrus, Ingvar P. K. Lindgren, and Amado Y. Cabezas, Bull. Am. Phys. Soc. 5, 344 (1960).

53. J. E. Mack, Revs. Modern Phys. 22, 64 (1950); J. M. Baker and B. Bleaney, Proc. Phys. Soc. (London) A68, 1090 (1955).

54. B. Bleaney and H. E. D. Scovil, Proc. Phys. Soc. (London) A68, 204 (1951).

55. R. G. Helmer and S. B. Burson, Phys. Rev. 119, 788 (1960).

56. J. S. Geiger, R. L. Graham, and G. T. Ewan, Bull. Am. Phys. Soc. 5, 255 (1960).

57. R. G. Helmer and S. B. Burson, Bull. Am. Phys. Soc. 4, 427 (1959).

58. D. R. Nethaway, M. C. Michel, and W. E. Nervik, Phys. Rev. 103, 147 (1956).

59. R. G. Wilson and M. L. Pool, Phys. Rev. 118, 1067 (1960).

60. J. W. Mihelich, B. Harmatz, and T. H. Handley, Phys. Rev. 108, 989 (1957).

61. Iu. G. Bobrov, K. Ia. Gromov, B. S. Dzhelepov, and B. K. Preobrazhenskii, Izvest. Akad. Nauk S.S.S.R. Ser. Fiz. 21, 940 (1947), [translation: Bull. Acad. Sciences U.S.S.R. 21, 942 (1957)];

V. M. Kel'man, R. Ia. Metskhvarishvili, B. K. Preobrazhenskii, V. A. Romanov, and V. V. Tuchkevich, Zhur. Eksp. i Theoret. Fiz. 35, 1309 (1958), [translation: Soviet Phys. — JETP 35 (8), 914 (1959)]; L. T. Dillman, R. W. Henry, N. B. Gove, and R. A. Becker, Phys. Rev. 113, 635 (1959).

62. A. V. Pohm, W. E. Lewis, J. H. Talboy, and E. N. Jensen, Phys. Rev. 95, 1523 (1954).

63. R. L. Graham, J. L. Wolfson, and R. E. Bell, Can. J. Phys. 30, 459 (1952).

64. See Nuclear Data Sheets, National Academy of Sciences, National Research Council, 1958 (U. S. Government Printing Office, Washington, D. C.).

65. E. L. Chupp, J. W. M. DuMond, F. J. Gorgon, R. C. Jopson, and H. Mark as reported in D. Strominger, J. M. Hollander, and G. T. Seaborg, Revs. Modern Phys. 30, 585 (1958).

66. K. H. Lindenberger, Z. Physik 141, 476 (1955); H. Schüler and T. Schmidt, Naturwisschschaften 22, 838 (1934).

67. A. Y. Cabezas, I. P. K. Lindgren, and R. Marrus, Bull. Am. Phys. Soc. 5, 343 (1960).

68. A. H. Cooke and J. G. Park, Proc. Phys. Soc. (London) A69, 282 (1956); H. Schüler, J. Roig, and H. Korsching, Z. Physik 111, 165 (1938).